CHARACTERIZATION OF FAULT TOLERANT AND DUO-OUTPUT ACTIVE PIXEL SENSORS

by

Cory Gifford Jung
B.A.Sc. Simon Fraser University 2004

THESIS SUBMITTED IN PARTIAL FULFILLMENT OF
THE REQUIREMENTS FOR THE DEGREE OF
MASTER OF APPLIED SCIENCE

In the School
of
Engineering Science

Spring 2007

Approval

Name: **Cory Gifford Jung**

Degree: **Master of Applied Science**

Title of Thesis: **Characterization of Fault Tolerant and Duo-Output Active Pixel Sensors**

Examining Committee:

Chair: **Dr. Marinko Sarunic**
Assistant Professor

Dr. Glenn H. Chapman
Senior Supervisor
Professor

Dr. Ash M. Parameswaran
Supervisor
Professor

Karim S. Karim
Internal Examiner
Assistant Professor

Date Defended/Approved: April 4, 2007

Abstract

The Fault Tolerant Active Pixel Sensor (FTAPS) corrects for defects by operating two pixel halves in parallel and retaining half sensitivity when affected by a point defect. Photodiode and photogate FTAPS devices were fabricated in 0.35μm technology and behaved as expected with and without defects. The photodiode FTAPS was almost twice as sensitive as a standard Active Pixel Sensor (APS) and 0.18μm technology pixels were about half as sensitive as 0.35μm technology pixels. The photodiode FTAPS noise was calculated to be greater than a standard APS, however the FTAPS signal-to-noise ratio remained on par with the standard APS due to increased sensitivity. A detection algorithm was developed for identifying standard APS and FTAPS defects from statistical analysis of the images taken. A Duo-output Active Pixel Sensor (DAPS) performed background subtraction, however crosstalk from charge collection of the parasitic n+ diffusion degraded its performance.

Keywords: active pixel sensor; fault tolerance; background subtraction

Subject Terms: Digital imaging sensors

Dedication

To Leah, for your patience.

Acknowledgements

I would like to thank each of my thesis committee members, Glenn, Ash, and Karim, for putting in their time and effort to get me through my thesis. It has been a pleasure to work with each of you. Individually, I would like to thank:

Glenn, for your advice and stories.

Ash, for teaching and guiding me with a sense of humour.

Karim, for being a great example.

This thesis could not have been written without the help of my fellow graduate students in the "Sardine Can". My graduate experience would not have been the same without you. I will always remember the sushi lunches and entertaining conversations we had.

Lastly, I would like to thank my family, friends, and Leah for supporting me through my graduate work. I would not be where I am without each and every one of you.

Table of Contents

List of Figures

List of Tables

List of Acronyms

A/D – Analog-to-Digital

APS – Active Pixel Sensor

CCD – Charge-Coupled Device

CDS – Correlated Double Sampling

CIPA – Camera & Imaging Products Association

DAPS – Duo-output Active Pixel Sensor

DW – Double Width

DS – Double Sampling

FD – Floating Diffusion

FF – Fill Factor

FPN – Fixed Pattern Noise

FT – Fault Tolerant

FTAPS – Fault Tolerant Active Pixel Sensor

IC – Integrated Circuit

ISO – International Standards Organization

JPL – Jet Propulsion Labs

LIDAR – LIght Detection And Ranging

PDA – Personal Data Assistant

PG - Photogate

PPS – Passive Pixel Sensor

rms – root mean square

RS – Row Select

RST – Reset

SLR – Single Lens Reflex

SNR – Signal-to-Noise Ratio

TX - Transfer

3T – 3-Transistor

1. Introduction

The simple act of taking a picture has ensnared the interest of the human mind since the invention of photography. For whatever reason, the ability to capture a moment of time seems to appeal to people universally. Traditionally, pictures are captured with film. However, digital imaging sensors have emerged as a legitimate contender to replace film. While digital imaging sensors boast several advantages over film, they also face challenges that must be overcome if they are to equal the performance of film.

One challenge facing digital imaging sensors concerns resolution. The resolution of film cameras is still far better than the resolution of digital cameras. While research to improve the resolution of digital cameras is ongoing, the manufacturing yield of digital imagers limits the advances that can be made. In general, as the resolution of digital imagers is increased the number of defective sensors also increases. Consequently, the yield of the imager decreases. Furthermore, defects that occur in a digital imager will affect every picture it captures while a defect in a frame of film will only affect a single picture.

Most research on digital imaging sensors concentrates on methods of directly improving the performance of the sensor. This research takes a different tact by improving the functionality of the sensor to gain better performance. This thesis focuses on two digital imaging sensors with additional functionality: a pixel with fault tolerance that can recover from defects and a pixel with built-in background subtraction.

1.1. Digital Imaging Sensors

The field of imaging has undergone a dramatic change in the past decade due to the advent of digital imaging systems. Digital imagers offer several advantages that have allowed them to compete with film imagers in many applications. Most advantages of digital imagers are derived from their ability to easily interface with other digital systems. Microprocessors and other electronics are commonly used with digital imagers to process, store, transmit, and analyze images. For example, the microcontroller in a digital still camera performs post processing on captured images so it can display the images immediately after they are taken whereas film camera pictures must be developed first. As well, many of the processing options can be altered between shots, such as the International Standards Organization (ISO) of the imager, i.e. the sensitivity. For a film camera to get the equivalent effect, the film itself would have to be changed which is not practical on a shot-by-shot basis.

Ease of storage and transmission of digital images has also made a significant contribution to the growth of digital imaging. Digital memory devices are easier to maintain, are rewriteable, and are more compact than film. Developments in digital storage media have increased their capacity while reducing the cost per byte. It is not unusual for a relatively inexpensive memory card to store hundreds of high resolution (5 MegaPixel or larger) images. Furthermore, transmission of digital files has become easier than ever. There are a host of tools for distributing images, such as web pages, peer-to-peer programs, and e-mail.

To illustrate the cost savings of a digital camera, here is a simple example. For a film camera, the cost of a roll of film (24 pictures) and its development is about ~$15. For a digital camera, a typical memory card can store hundreds of picture for less than $100. More permanent storage of pictures is relatively inexpensive using DVDs

(less than a $1 for 4.7Gb) or a hard drive (less than $100 for 250Gb). Since pictures can be previewed, only the best are printed. As well, pictures are easily shared electronically so most people print very few of their digital pictures (less than 5%). Thus, the cost of a memory card and 250Gb hard drive is around $200 with the cost of printing pictures being negligible. For a film camera, $200 will cover the cost of about 13 rolls of film or 312 pictures. Since almost everyone shoots more than 300 pictures in the lifetime of the camera, taking pictures with a digital camera is cheaper than with a film camera.

Digital imaging has made an impact in many applications, from medical imaging to security. Still photography is a well-understood field where digital camera usage is now widespread. Table 1 shows data collected by the Camera & Imaging Products Association (CIPA) on the production of digital and film cameras produced from 2002-2005 [2]. Note the drastic decline in film cameras production while digital camera production increased from 23.4 million units in 2002 to 63.6 million units in 2005.

Table 1: Summary of digital and film cameras produced from 2002-2005

		Year (Production in millions of units)			
		2002	2003	2004	2005
Camera Type	Digital	23.4	43.4	59.4	63.6
	Film	23.1	15.6	9.7	5.1

A good example of a digital cameras have proven to be more efficient is in health care. Digital imagers have been implemented for diagnostic x-ray imaging. Traditional x-ray imaging using film is time consuming because of the time taken to develop each x-ray. Since different kinds of tissue require different exposure times to obtain good images, it is not uncommon for multiple x-rays to be taken to adjust the

exposure time. This magnifies the problem, as each x-ray must be developed to be viewed. A digital x-ray system eliminates the development time by immediately showing x-rays as they are taken. It is even possible to display an x-ray in real time. X-rays must often be stored for years as part of medical records. Storing x-rays in digital format is easier and more cost effective.

The advantages and potential of digital cameras is evident, however they still suffer some disadvantages compared to film cameras. The resolution, dynamic range, and colour of film are better than what digital image sensors have been able to achieve thus far. As well, the aforementioned issue of defects in digital image sensors is also a challenge for digital cameras. Defects in digital image sensors can develop during manufacturing or in the field. A defective pixel will affect every picture taken by a digital camera whereas a defect in a frame of film will affect that particular picture.

Despite these disadvantages, digital cameras are now prevalent in many applications. While many of the advantages of digital cameras result from interfacing the digital image sensors with other electronics, this would not be possible without the sensors themselves. Digital imaging sensors have come a long way since their invention.

1.2. Active Pixel Sensor History

Currently, there are two main digital imaging sensors: the Active Pixel Sensor (APS) and the Charge-Coupled Device (CCD). While both sensors were invented within two years of each other, the CCD garnered interest immediately and became the dominant digital imaging sensor. In the 1990's, interest in the APS was renewed and it now competes with the CCD in many applications.

In 1967, G. P. Weckler suggested operating photodiodes in a photon-flux integrating mode [5]. Incident light generates charges that are integrated on the capacitance of a reverse-biased photodiode. This was a key development for the APS as it commonly uses a photodiode for its light sensing element. Initially, G. P. Weckler used a load resistor to convert the photodiode output from current to voltage. In 1968, he reported a 100×100 element photodiode array [6]. Each element was essentially a Passive Pixel Sensor (PPS). A schematic of a PPS is shown in Figure 1.

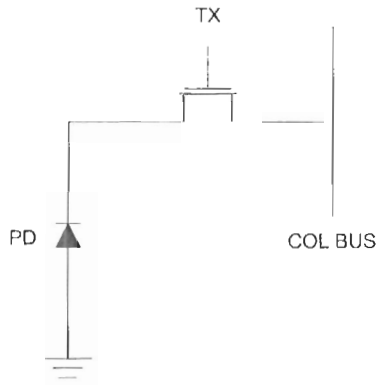

Figure 1: Passive pixel sensor schematic

Soon after the PPS was conceived, it was recognized that adding a buffer or amplifier to the pixel would improve its performance. P. J. W. Noble was the first to suggest using an in-pixel source follower transistor for readout buffering [7]. Later, any pixel with an "active" amplifier was termed an APS. S. G. Chamberlain analyzed the APS in more detail in 1969 [8]. While promising, the APS suffered from high Fixed Pattern Noise (FPN). At the time, fabrication of Integrated Circuit (IC) MOS devices was not as well developed. Significant variations in diode size, threshold voltage, and other device parameters were common which resulted in high FPN in APS arrays. An examination of FPN in APS devices was reported by P. W. Fry et al in 1970 [9].

As research on the APS was beginning, W. S. Boyle and G. E. Smith invented the CCD [10]. When it was conceived in 1970, the CCD was intended to be a serial

access memory device. However, the CCD soon focused development as an image sensor. Compared to the APS, CCD pixels had much lower FPN and were smaller as no in-pixel transistors were needed. Research on the APS was scarce for the next 20 years while the CCD came to dominate the digital imaging market. The CCD was used in camcorders, still cameras, scientific imaging, and many more applications.

Interest in the APS began to pick up again in the 1990's. While little work had been done directly on the APS, the CMOS fabrication process had undergone numerous improvements. As a CMOS-compatible device, these advances made the APS more viable for imaging. For example, smaller pixel layouts were possible as the minimum feature sizes of CMOS devices had shrunk. CCDs require multiple supply voltages, high power, and a specialized process to manufacture that is not compatible with the CMOS process. A CMOS imager is attractive as it requires only a single supply voltage, uses less power, and can be integrated with other CMOS circuitry such as Analog-to-Digital (A/D) converters.

In 1993, S. K. Mendis, S. E. Kemeny, and E. R. Fossum at Jet Propulsion Labs (JPL) kickstarted new interest in the APS by presenting a photogate APS [11]. In general, photogate pixels are larger than their photodiode counterparts because they require an additional transistor and extra control signals, however its architecture allows it to perform Correlated Double Sampling (CDS) which removes FPN from the output.

Today both APS and CCD technology share in the digital imaging market. APS cameras are frequently found in portable devices as an additional feature, such as Personal Data Assistants (PDAs) and cellular phones, where power consumption and size are at a premium. In the still camera market, less expensive, point-and-shoot cameras most often use CCD technology. Since CCD technology is more mature than

APS technology, it is better understood and less expensive to manufacture for lower-end cameras. High resolution, digital Single Lens Reflex (SLR) cameras feature both APS and CCD imagers. Generally, APS imagers are found in low power, low cost, small form factor applications. Both types of sensors are found in mid-range applications, however as the array size becomes larger CCD performance deteriorates unless they are cooled. This is why high resolution digital SLR cameras use APS arrays, but the most precise space imagers use cooled CCD imagers.

Research on the APS has steadily increased since the 1990's. Many aspects of the APS are being explored, such as its architecture and fabrication. In this thesis, increasing the functionality of the APS is the focus. Since defects in digital cameras degrade every picture that they take, a fault tolerant APS is examined that can correct for defects. In digital profiling, a laser illumination must be detected over the background illumination of the scene. Simple methods of removing the background illumination are insufficient, so a more complex solution is needed. An APS with built-in background subtraction was investigated for this application.

1.3. Fault Tolerant Active Pixel Sensor

1.3.1. Fault Tolerance in Digital Imaging

Incorporating fault tolerance is a common practice for the design of many electronic devices, such as digital memory, to increase their yield and reliability. While sharing the same regular, repeating array of elements like memory, fault tolerance is seldom considered for digital imaging arrays. The current practice is to calibrate an image sensor after manufacturing to locate all defective pixels in an imager. The locations of these defects are stored in a defect map. To correct for defective pixels, information from neighbouring pixels is used to interpolate for the defective pixels.

This can be acceptable in some applications if the defect rate is reasonably low, however the loss of even a single pixel in some applications, such as in mammography or space imaging, can be disastrous. A fault tolerant sensor that can correct for defects could improve the yield of digital imaging arrays at manufacturing time. Defects that develop once the imager is in the field are more troublesome as there are few techniques for recalibrating the sensor. Sometimes the imager can be sent back to the manufacturer to be recalibrated, but this is a time consuming method.

An imager operating in hard environments would benefit from fault tolerance. A common application of imagers is to operate them in harsh environments that would be dangerous for a human observer. Harsh environments increase the rate of defects that generate in an imager over time. As well, these imagers are often difficult or impossible to replace. A classic example is an imager sent into space to take pictures and transmit them back to Earth. The imager is irreplaceable and is subject to higher radiation in space that causes defects.

Fault tolerant digital imagers could alleviate problems with defects in the future. The trend in digital imaging towards higher resolution, pixel count, and imager area while shrinking pixel sizes has resulted in more dense imagers. As the complexity of digital imagers increases, the probability of defects occurring increases as well. Furthermore, the lifetime of digital cameras is growing. Consumers are unlikely to replace an expensive camera, such as a digital SLR after a short amount of time. The lifetime of a film SLR is commonly 20 years or longer without a significant reduction in performance. Some recent work that our lab group has been involved in has begun to investigate the growth of defects in imagers in the field [12].

1.3.2. Fault Tolerant Active Pixel Sensor Background

G. H. Chapman and Y. Audet examined the costs and benefits of adding fault tolerance to image sensors in 1999 [13]. They presented several implementations of fault tolerance, one of which was adding redundancy. Yield analysis showed that fault tolerance would improve the yield of an imager.

In 2001, the Fault Tolerant Active Pixel Sensor (FTAPS) design was presented and its operation was simulated [14]. The FTAPS design incorporated redundancy by splitting the photosensitive element in half and operating both halves in parallel. Figure 2 illustrates how the FTAPS would be split to add redundancy. Thus, if a point defect rendered either half of the pixel stuck high or stuck low, the other half would continue to operate with half the sensitivity. The defective pixel could easily be corrected for by doubling its output to get the correct signal. Combining redundant pixels with software correction increases the yield and lifetime of an APS array since it is very unlikely for both halves of a pixel to fail [15]. The cost of redundancy is the small area required for additional in-pixel transistors.

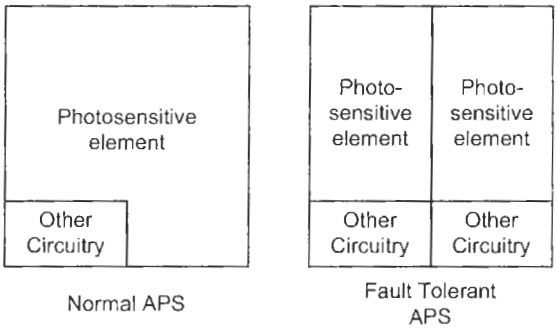

Figure 2: The fault tolerant APS concept

D. Y. H. Cheung, S. Djaja, and G. H. Chapman designed both photodiode and photogate FTAPS devices. ICs containing both types of pixels were fabricated in CMOS 0.18μm technology. Included in these ICs were photodiode FTAPS devices with intentional half stuck faults where half of the pixel was stuck low or stuck high.

In 2003-2004, D. Y. H. Cheung, S. Djaja, and G. H. Chapman presented experimental results that showed photodiode FTAPS devices with half stuck faults had approximately half the sensitivity of fault-free devices [16] [17]. Later in 2004, M. L. La Haye et al reported the photogate FTAPS behaved as expected, with defective pixels having half the sensitivity of defect-free pixels [18]. As well, FTAPS devices were found to be more sensitive than traditional APS devices.

In the past, some criticism of the FTAPS design has been voiced. While the FTAPS design when combined with software correction can correct for defects, finding and identifying the defects is another problem entirely. As well, K. Salama and A. Al-Yamani of Standford University presented a noise analysis of the photodiode FTAPS in 2005 [19]. They concluded that the performance of a FTAPS array with no faults would suffer from considerable degradation due to increased noise, particularly at low illumination levels. These issues will be addressed in this thesis.

1.3.3. Fault Tolerant Active Pixel Sensor Objectives

One of the main objectives of this thesis was to design, fabricate, and test FTAPS devices in CMOS 0.35µm technology. Testing of the FTAPS was split into three sets of experiments which are presented in Chapter 3. The first set determines the behaviour of FTAPS devices fabricated in 0.35µm technology with and without defects. Another series of tests examines the cause of increased sensitivity in FTAPS devices compared to traditional APS devices. Lastly, the performance of pixels fabricated in 0.18µm and 0.35µm technology are compared to investigate the effects of technology scaling. H. S. Wong suggested CMOS imagers using a standard CMOS process would have poorer performance as the devices are scaled down [20]. Chapter 4 addresses the issue of defect identification and Chapter 5 presents an alternative noise analysis of the photodiode FTAPS design. Each source of noise is

analyzed and the total noise of a traditional APS and FTAPS are calculated using device parameters obtained from HSpice simulations.

1.4. Duo-Output Active Pixel Sensor

1.4.1. Background Subtraction for Digital Profiling

Optical triangulation is a method of 3-D scanning used in several applications. Its advantages include having a simple structure, high resolution, long operating range, and non-contact measurements [21]. Figure 3 shows an example of the setup for 3-D scanning with optical triangulation.

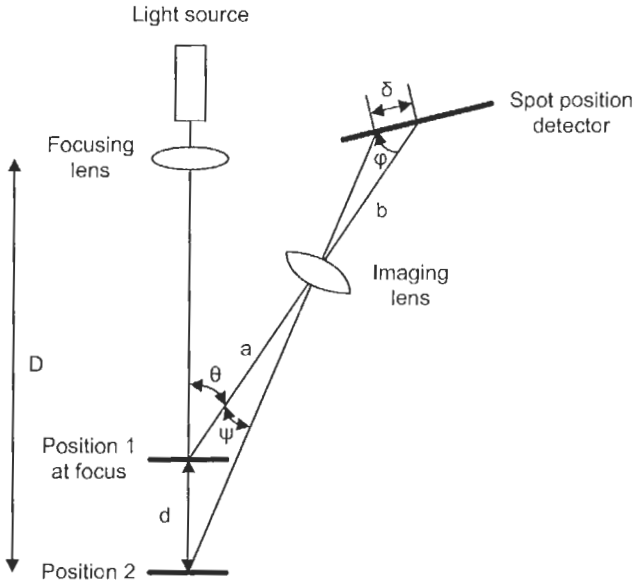

Figure 3: Setup for 3-D scanning by optical triangulation

The object to be scanned is illuminated with a light source, commonly a laser. The light reflects off the object and is detected by an imager. By locating the position of the peak illumination on the imager, the distance to the object can be calculated using triangulation. In Figure 3, as the depth of the object changes from Position 1 to Position 2, the location of the peak illumination moves a distance, δ.

A problem with 3-D scanning using optical triangulation is reduced accuracy due to ambient or background light. The detector does not distinguish between illumination from the light source and ambient light. Thus, ambient light is a source of "noise" in the system. Increasing the light power of the light source can reduce the effects of ambient light, however when the light source is a laser this is often undesirable. High laser powers can damage the object being illuminated and more safety precautions must be taken. Safe laser power levels are many times less than the usual background illumination levels. As mentioned previously, simple solutions for removing background illumination have been inadequate. The reflectivity over the surface of an object is generally not uniform. Thus at different points on the object, the both the background and laser illumination that is detected will differ based on the reflectivity at those points. Simple solutions such as subtracting a constant illumination level from the output cannot account for the changes in reflectivity. A detector with background subtraction to remove the ambient light from the output of the imager overcomes both of these problems to increase the accuracy of the scanning. The relative magnitude of the laser and background illumination levels is no longer an issue if the effect of the background is removed and changes in the background illumination due to variations in the object's reflectivity are also eliminated.

An APS with two readout circuits has been developed to perform background subtraction called the Duo-output Active Pixel Sensor (DAPS). The DAPS uses one readout circuit to measure the illumination of the scene with the light source on. This measurement includes the background illumination. Then the second readout circuit measures the illumination of the scene with the light source off. Since the second measurement only includes the background illumination, subtracting it from the first measurement removes the effect of the background illumination from the output.

While intended for background subtraction, the DAPS is also suitable for other applications. J. Ohta et al demonstrated that a DAPS array could be used for motion capture [22]. Range finding using LIght Detection And Ranging (LIDAR) is another application the DAPS could be used for. A LIDAR sensor similar to the DAPS has been reported by S. B. Gokturk et el [23]. As well, a LIDAR-based system could use depth information to selectively extract images. A high definition television camera has been developed by M. Kawakita et al that records depth information at video frame rates (i.e 30Hz) [24].

1.4.2. Duo-Output Active Pixel Sensor Background

The DAPS work presented in this thesis is a continuation of work done by D. Y. H. Cheung, S. Djaja, and G. H. Chapman. Photodiode and photogate DAPS devices were designed by D. Y. H. Cheung and S. Djaja and fabricated in CMOS 0.18µm technology. In 2005, D. Y. H. Cheung reported partial success in performing background subtraction with photodiode DAPS devices [25]. The performance of the photodiode DAPS was hindered by crosstalk between the readout circuits and leakage. He identified the cause of these problems to be a lack of shielding for the pixels. Light incident on the pixel affected the operation of in-pixel components resulting in the crosstalk and leakage he observed.

S. Djaja presented work on photogate DAPS devices fabricated in 0.18µm technology in 2006 [26]. He also had partial success in performing background subtraction with his devices. His main problem was poor sensitivity matching of the two readout circuits in a given DAPS caused by variations in the fabrication process. For ideal operation, the sensitivities of both readout circuits in a pixel should be matched; mismatches reduce the effective Signal-to-Noise Ratio (SNR) of the system.

Concurrent to the work done in our lab, another group independently was also working on the DAPS. The DAPS architecture was first reported in 2003 by J. Ohta et al [27]. They fabricated a 64×64 array of photogate DAPS devices in 0.6μm CMOS technology. This imager was used to demonstrated that the DAPS design could detect a modulated light source over a static background scene. Later in 2003, they used a DAPS array for motion capture by tracking a moving modulated light source through a series of pictures [22]. In 2006, K. Yamamoto et al presented an improved version of their DAPS fabricated in 0.35μm CMOS technology that can perform CDS to remove FPN [28].

1.4.3. Duo-Output Active Pixel Sensor Objectives

Since discovering that another group has been doing research on the DAPS design, our objectives for the DAPS have become more focused. While digital profiling is the main application we have targeted, many of the other applications mentioned in previous section require very precise removal of the background illumination. Three new DAPS designs were fabricated in 0.35μm technology in an attempt to improve the sensitivity matching of the readout circuits in a pixel and reduce the crosstalk from lack of shielding. These designs were tested to determine which has the best sensitivity matching and whether they are suitable for background subtraction. As well, the aspects of crosstalk and multiple integrations will be examined. Both sensitivity matching and crosstalk are issues that have not yet been addressed in detail and are essential for accurate removal of background illumination. The DAPS testing results are presented in Chapter 6.

1.5. Summary

The focus of this thesis is to examine two APS pixels with increased functionality. The FTAPS uses redundancy to increase the yield of a sensor at manufacturing time and improve its reliability over time. Expanding on FTAPS work done by D. Y. H. Cheung and S. Djaja, new FTAPS devices have been designed and fabricated to investigate the increased sensitivity of the FTAPS design and the effects of technology scaling. The issues of defect identification and noise for the FTAPS design will be addressed. A noise analysis is presented to determine the noise cost of incorporating fault tolerance.

The DAPS has two readout circuits to perform background subtraction for 3-D scanning. New DAPS designs have been fabricated with better sensitivity matching and less crosstalk. These DAPS designs were tested to determine which is the best for background subtraction.

Digital imaging is growing, with more and more film cameras replaced by digital ones. While not immediately embraced, the growth of digital imaging and improvements to the CMOS process has allowed the APS to flourish. Research on the APS has increased, resulting in new applications as well. This thesis focuses on two pixel designs with innovative functionality, however the basics of APS theory and operation are discussed before analyzing them in detail.

2. Theory and Operation of Active Pixel Sensors

A basic understanding of APS devices is needed to before design and analysis of more complex designs can be performed. An APS converts light into charge, charge into voltage, and voltage into an output. Each component, from the photosensitive element to the reset transistor, plays a crucial role in this conversion. To analyze the performance of different APS designs, an awareness of the standard performance measures of digital imaging sensors is needed. In particular, a deep understanding of noise sources is required for the noise analysis of the FTAPS that is presented later. Once the basic theory behind the APS is covered, the fundamentals of the FTAPS and DAPS will be described.

2.1. Detecting Light

The mechanism by which light energy is converted into electrical energy is called photo generation. Photons with sufficient energy can generate electron-hole pairs in a material. Figure 4 shows the typical band diagram for a semiconductor.

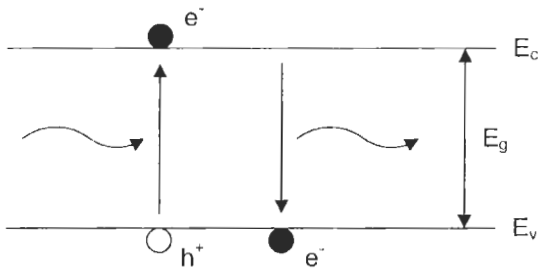

Figure 4: Photo generation and optical recombination

In a semiconductor, the photon must have energy greater than or equal to the bandgap energy E_g to excite an electron from the valance band E_v to the conduction

band E_c. The removal of the electron from the valance band creates a hole as well. The energy of a photon is

$$E = \frac{hc}{\lambda} \quad (1)$$

where h is Planck's constant, c is the speed of light, and λ is the wavelength of light. hc is ~1.2eV when λ is in μm. Thus, the bandgap energy of the material affects what wavelengths of light can generate an electron-hole pair. For example, the bandgap energy of silicon is 1.124eV.

For a CMOS imager, optical generation occurs in silicon. When light is incident on a silicon surface, some is reflected and some passes through to be absorbed below the surface. The equation that describes the absorption of light is

$$I(x) = I_0 e^{-\alpha x} \quad (2)$$

where I(x) is the light power at depth x, I_0 is the light power that enters at the surface of the silicon, x is the distance from the surface of the silicon, and α is the absorption coefficient. α is wavelength dependent due to the bandgap energy of the material. Absorbed photons must have energy greater than or equal to the bandgap energy. Since photons with higher energy have a greater probability of exciting an electron, they also are more easily absorbed. Recalling equation 1, the energy of a photon increases as the wavelength of the photon decreases. Thus, photons with shorter wavelengths are more easily absorbed. For example, blue light ($\lambda_{blue} \approx$ 470nm, $E_{blue} \approx$ 2.55eV) is absorbed more quickly and closer to the surface of silicon than red light ($\lambda_{red} \approx$ 670nm, $E_{red} \approx$ 1.79eV).

The quantum efficiency η of a material is another important parameter. Quantum efficiency is defined as the number of electron-hole pairs generated for every

absorbed electron [29]. Photons with much higher energies can create more than one electron-hole pair per photon, however silicon has a quantum efficiency of approximately 1 for light in the visible range.

The reverse process of photo generation is optical recombination. Figure 4 shows the process of recombination where an excited electron falls from the conduction band to the valance band, emitting a photon. The rate of recombination is proportional to the number of free carriers. Thus as more electron-hole pairs are generated, the rate of recombination increases. Since we want to measure the charge generated by optical generation, it is necessary to separate the holes and electrons to reduce recombination. Most commonly, an electric field is used to separate the negatively charged electrons and positively charged holes. This generates a photocurrent that can be measured to determine the intensity of light on the sensor. However, the photocurrent is very small for typical illumination levels, often on the pA scale. Thus, the sensor must be able to accumulate charge over time so that a larger signal can be read out.

2.2. Photodetectors

The two most common photodetectors employed by APS devices are photodiodes and photogates. Each applies an electric field to separate generated charges and each has a way of storing the generated charge over time.

2.2.1. Photodiode

APS devices most often use photodiodes as the photodetector. In CMOS technology, a diode is formed when a p-type semiconductor and n-type semiconductor interface is created, typically by diffusion or ion implantation. The concentration difference in carriers on the p and n sides cause them to diffuse which creates a depletion region

that has very few free carriers. The carriers leave behind ions which create an electric field that opposes further diffusion of carriers. Figure 5(a) depicts a diode at equilibrium where the diffusion current is equal to the drift current induced by the electric field so there is no net current.

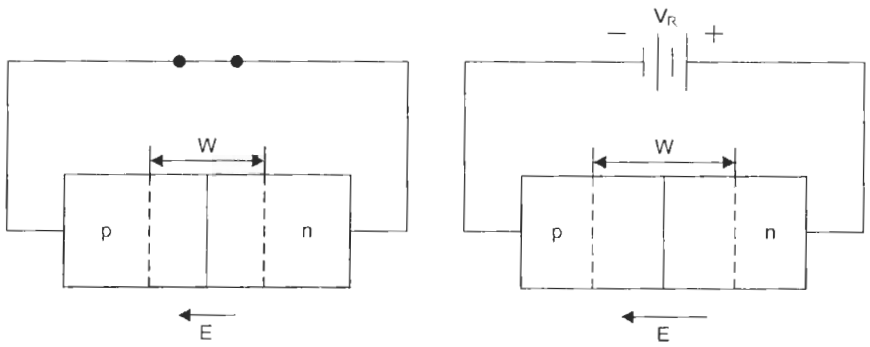

(a) (b)

Figure 5: Diodes under different conditions, (a) equilibrium, (b) reverse bias

When carriers are optically generated in the diode, carriers generated in the depletion region will be separated by the electric field and a photocurrent will result. As well, carrier generated outside of the depletion region can be collected if they diffuse to the region, however this is partially dependent on the diffusion length of the carrier. The diffusion length is the average distance a carrier travels before it recombines.

Since only carriers generated in or within a few diffusion lengths of the depletion region can be collected, increasing the width of the depletion region will improve the collection efficiency of the diode. As a result, photodiodes are often reverse biased to enlarge the depletion region as shown in Figure 5(b).

2.2.2. Photogate

Photogates, also called MOS capacitors, are also used as photodetectors. Many CCD imagers use MOS capacitors in their pixels. Figure 6 shows an example of a photogate in a p-type substrate.

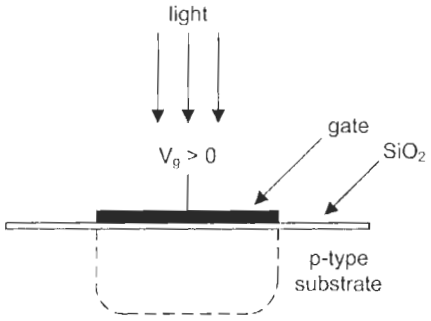

Figure 6: Photogate structure

When a positive voltage is applied to the gate of the photogate, it creates an electric field that repels holes. Once again, a depletion region is created where there are few free carriers. When carriers are optically generated in the depletion region, the electrons are collected and the holes will be expelled. As with the photodiode, carriers may also diffuse to the depletion region and be collected. Note that for a photogate to collect light efficiently, the gate material must be only weakly absorbing of light.

2.3. Active Pixel Sensor Operation

2.3.1. Photodiode Active Pixel Sensor Operation

The operation of an APS is dependent on its design. An APS will have a photodetector, usually a photodiode or photogate, and some active circuitry. The simplest APS is the 3-Transistor (3T) photodiode design. A schematic of a 3T photodiode APS is shown in Figure 7.

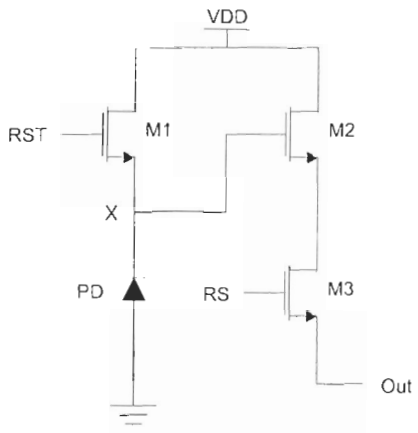

Figure 7: 3T photodiode APS schematic

Transistor M1 is the reset transistor, M2 is the amplifying transistor, M3 is the row transistor, and PD is the photodiode. The timing of the Reset (RST) and Row Select (RS) control signals in a typical photodiode exposure cycle is illustrated in Figure 8.

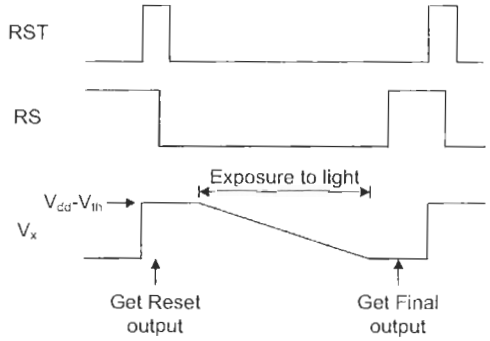

Figure 8: Typical photodiode APS exposure cycle

When RST goes high, the reset transistor turns on initializing the voltage at node X (V_x) to approximately $V_{DD} - V_{th}$ by precharging the gate of M2 and the photodiode. During an exposure, light generates photocurrent in the photodiode that discharges the voltage on node X. The charge is collected over time such that

$$Q_{col} = i_{photo} t_{exp} \tag{3}$$

where Q_{col} is the collected charge, i_{photo} is the photocurrent, and t_{exp} is the exposure duration. The charge is converted to voltage by the capacitance of node X:

$$V = \frac{Q_{col}}{C_X}. \quad (4)$$

C_X is the capacitance of node X which is primarily from the capacitance of the photodiode, but will include smaller sources as well such as the gate capacitance of the amp transistor. The photodiode capacitance is typically ~10 larger than the other sources of capacitance. The conversion of charge to voltage is referred to as the conversion gain. Most pixel designs will minimize C_X to maximize the conversion gain so that less charge must be collected to produce the same voltage.

The amp transistor acts as a buffer for the output. APS devices are usually voltage-mediated where a column bias transistor is connected to the output. Thus, the voltage at node X is reflected at the output. For a current-mediated APS, the gate voltage of the amp transistor (node X) determines the output current. The row transistor is for row addressing in an APS array. When the RS line is high, it allows the output to be read.

2.3.2. Photogate Active Pixel Sensor Operation

Photogate APS devices have an additional transistor that alters their operation slightly. A schematic of a photogate APS is shown in Figure 9. The reset transistor, amp transistor, and row select transistor are the same as for a 3T photodiode APS. A transfer gate controlled by control line TX has been added to facilitate the transfer of charge from the photogate to the floating diffusion or FD.

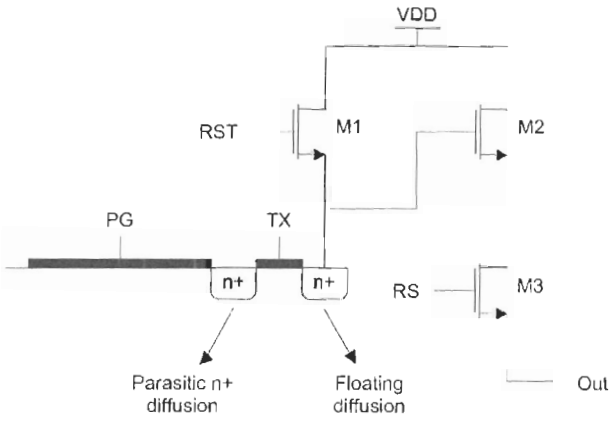

Figure 9: Photogate APS schematic

Figure 10 illustrates the control signal timing for a typical photogate APS integration cycle and Figure 11 shows how charges are transferred during the integration cycle.

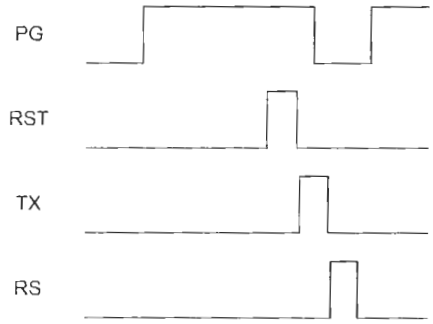

Figure 10: Typical photogate APS integration cycle

Initially, the PG, TX, and RST control lines are "off". The FD still contains charge from the previous output as shown in Figure 11(a). The integration cycle begins with the PG control line turning "on" to create a potential well for charge to be collected. Then the sensor is exposed to light and optical charge is collected under the photogate. Near the end of the exposure time, the RST control line is pulsed on to reset the voltage of the FD to $V_{DD} - V_{th}$, removing any previously stored charge as shown in Figure 11(c).

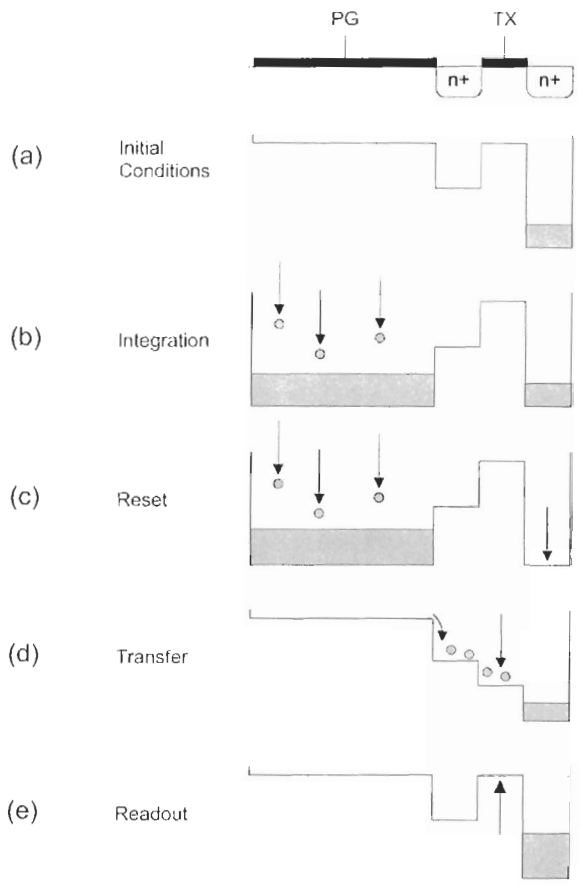

Figure 11: Charge transfer in a typical photogate APS integration cycle

The charge under the photogate is transferred to the FD by turning off the PG control line and turning on the TX control line. Turning off PG removes the electric field under the photogate so the charge is forced out. By turning on the TX control line, a path is provided for the charge to be transferred to the FD. Once the charge is fully transferred, the TX control line is turned off and the output can be readout.

Similar to the photodiode, the collected electrons will discharge the voltage at the FD (node X in the photodiode case). For the photogate, the relationship of equation (4) also holds true except that C_X is replaced by C_{FD}, the capacitance at the FD. C_{FD} includes the floating diffusion capacitance, the capacitance of from the gate of M2, and other parasitic capacitances. Since the capacitance of the diffusion is typically

the same magnitude as the other capacitances that form C_{FD}, C_{FD} is usually much smaller than the capacitance of a photodiode and thus smaller than C_X as well. Thus, photogate pixels generally have a higher conversion gains than photodiode pixels. Unfortunately, this advantage is eliminated because some incident photons are reflected or absorbed by the polysilicon gate, particularly photons with shorter wavelengths. Thus, photogates pixels will generate fewer carriers than a photodiode for the same light level.

2.4. Digital Image Sensor Performance Measures

To analyze the performance of digital imaging sensors, some standard performance measures are used. The Fill Factor (FF) of a pixel is a commonly referred to when considering its layout. The FF is the percentage of the pixel area that is photosensitive. For example, Figure 12 shows a block layout of a photodiode APS showing the photodiode area and the active circuitry area, such as transistors and control lines. The FF would be the percentage of the total pixel area that is the photodiode area. Generally, a high FF is desired to maximize the photosensitive area.

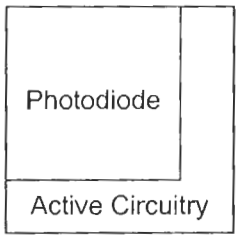

Figure 12: Block layout of a photodiode APS

Two digital image sensor performance measures that will be discussed in detail in this thesis are sensitivity and noise. The sensitivity is defined as the rate at which the output changes when the input light intensity is varied. Figure 13 illustrates an idealized output vs. input light intensity curve for a digital imaging sensor. The sensitivity of the sensor is the slope of the linear portion of the curve.

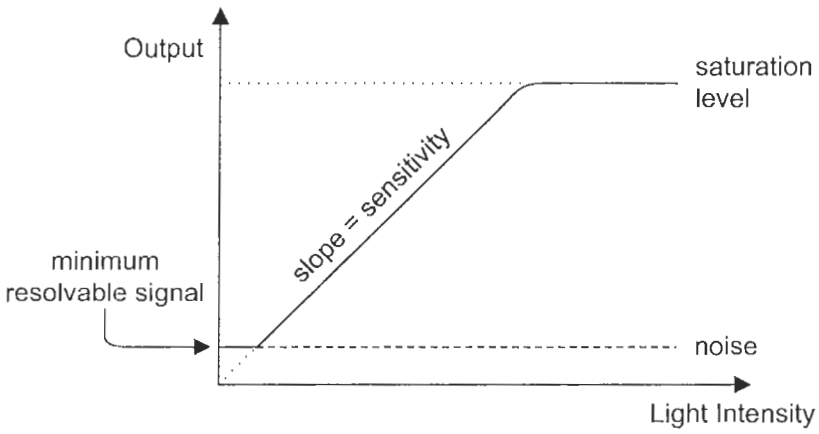

Figure 13: Idealized output vs. light intensity of a digital image sensor

A high sensitivity is usually desired for an imager, however the performance of an imager is limited by its noise. Assuming the dark current of the imager is small, the noise of an imager sets the minimum resolvable signal or the minimum output that can be detected by that imager. Thus, the signal-to-noise ratio, or the SNR, of a sensor is a more important parameter than its sensitivity. Also, the noise defines the dynamic range of a sensor, similar to the output swing, given as

$$dynamic\ range = \frac{saturation\ level}{minimum\ resolvable\ signal}. \qquad (5)$$

It should be clear that one should not examine the sensitivity of a sensor without also commenting on the noise.

2.5. Active Pixel Sensor Noise Sources

Shot noise, thermal noise, and flicker noise are the main sources of noise in APS circuits. Each of these noises is generated in a different way.

2.5.1. Shot Noise

Shot noise occurs as a result of the random generation of carriers and discrete nature of electrons. It manifests itself as random fluctuations of current. The shot noise can be calculated using the following equation

$$q_{shot} = \sqrt{\frac{I_{gen} t}{q_e}} \tag{6}$$

where q_{shot} is the shot noise in electrons, I_{gen} is the generated current, t is the time, and q_e is the charge of an electron.

There are two mechanisms that generate carriers, and thus current, in an APS. The most obvious mechanism is optical generation. Photocurrent generated by light is subject to shot noise. Thus, photocurrent shot noise is unavoidable unless we generate less current, which is undesirable. The photocurrent shot noise is also illumination dependent and sets the maximum possible SNR for the sensor. In practice, the photocurrent shot noise is not usually the limiting factor due to other larger noise sources.

The other mechanism affected by shot noise is thermal generation of carriers in the depletion region, resulting in dark current. Dark current is much lower than the photocurrent in most situations, so the dark current shot noise is smaller as well. The same techniques that reduce dark current will also reduce dark current shot noise, such as reducing the size of the depletion region and removing the collection area away from the surface.

2.5.2. Thermal Noise

Thermal noise arises from thermal agitation of electric charge in conductors [31]. It is a white noise such that the noise power is constant over all frequencies. For a resistor, the thermal noise is

$$v_{therm} = \sqrt{4kTRN_{BW}} \tag{7}$$

where v_{therm} is the root mean square (rms) voltage thermal noise, k is Boltzmann's constant in joules per Kelvin, T is the temperature in Kelvin, R is the resistance in ohms, and N_{BW} is the noise equivalent bandwidth. The thermal noise can be modelled as a voltage source in series with the resistor. The noise equivalent bandwidth is the equivalent bandwidth of a filter if it was an ideal filter, i.e. zero gain in the stop band. Since the thermal noise does cover all frequencies, the noise equivalent bandwidth limits the amount of thermal noise. For a simple RC circuit, the noise equivalent bandwidth can be expressed as

$$N_{BW} = \frac{\pi}{2} f_o = \frac{1}{4RC}. \tag{8}$$

where f_0 is the bandwidth of the RC circuit in radians.

2.5.3. Flicker Noise

Flicker noise is a result of conductivity fluctuations that occur at a junction due to traps. Unlike thermal noise, it is not constant over all frequencies. The flicker noise has a 1/f dependence, thus it can be dominant at low frequencies. At higher frequencies, the thermal noise dominates. The flicker noise rms current i_{flick} is related to the DC current and equivalent noise bandwidth by

$$i_{flick} \propto I_{DC} \sqrt{\frac{N_{BW}}{f}} \tag{9}$$

where I_{DC} is the dc current and f is the frequency.

In an APS, trapping and de-trapping of electrons mainly occurs at the Si-SiO_2 interface leading to flicker noise. To minimize the flicker noise in transistors, reducing the device area or using a buried channel device will reduce the area of the Si-SiO_2 interface. Unfortunately, we often do not have access to buried channel devices and transistors are already minimum geometry to maximize the FF of the pixels.

2.5.4. Referred Noise

Noise is generated by many components in an APS circuit. The noise is usually generated at different places in the circuit and may also have different units, so it is difficult to compare the overall effect of each noise source. Thus, each noise source is referred, usually to the input or output of the circuit. To refer each noise source, they must be converted to reflect their effect at the referred point. This method allows the noise from each source to be added to determine the total noise and to compare the relative sizes of each noise source at the referred point.

2.6. Fault Tolerant Active Pixel Sensor Theory

The FTAPS is designed to operate like a traditional APS when there are no defects. The photosensitive area, whether it is a photodiode or photogate, is split in half and all of the transistors are duplicated so that each half is operated in parallel. Figure 14 shows the schematic of a photodiode FTAPS.

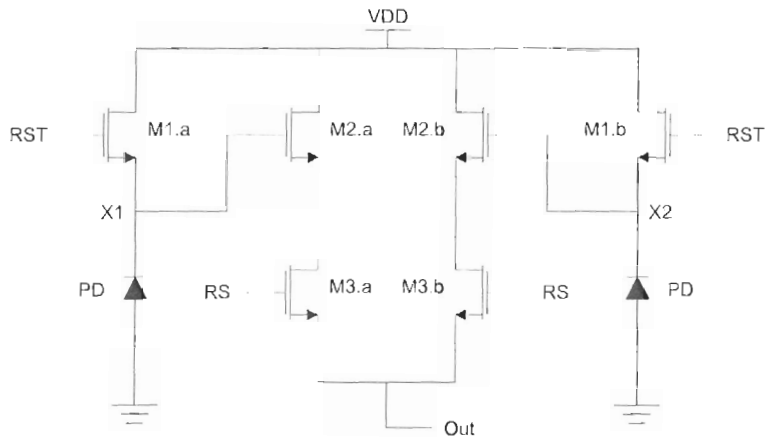

Figure 14: Photodiode FTAPS schematic

The total photosensitive area of a FTAPS would be the same as a traditional APS. However, a cost of incorporating fault tolerance is a reduction in FF due to the additional transistors. It is possible to use a single row select transistor, combining M3.a and M3.b, so that only two transistors must be added. The cost in area of incorporating the fault tolerant design has been calculated to be less than 10% [14].

It should be noted that the output of each FTAPS half is combined after the row select transistors. Unlike most APS circuits, the FTAPS output must be current-mediated instead of voltage-mediated so that the output of each FTAPS half is summed at the output. Most APS circuits are voltage-mediated because their response is more linear than a current-mediated APS. Thus, the linearity of a FTAPS will be worse than a traditional APS which can lead to increased FPN. Again, this is a cost of incorporating fault tolerance.

2.6.1. Fault Tolerant Active Pixel Sensor Defect States

The most common defects that occur in ICs that do not render an entire chip defective are point defects. Point defects are small and only affect a small area of the IC. A short in metal lines or a faulty via are examples of electrical point defects.

Normally an electrical fault in an APS results in a "stuck" fault at its output where the output is stuck at V at V_{DD} (stuck high) or stuck at V_{SS} (stuck low). Since image sensors rely on optical input, they are also susceptible to optical defects. For example, an APS which was covered by a piece of dust or unetched piece of metal would always have a "dark" output. It is important to recognize that the APS can be affected by both electrical and optical point defects. The FTAPS uses redundancy to retain partial functionality in the presence of a point defect. The concept is that if there is a point defect in one half of a FTAPS, the other half will continue to operate normally.

There are seven pixel states considered in Table 2. For an FTAPS, each half is either defect-free or good (G), stuck high (H), stuck low (L), or hot. A stuck high pixel is considered to be a "bright" pixel and a stuck low pixel is considered to be a "dark" pixel. Note that an electrical stuck high defect will normally result in a "dark" pixel, thus the distinction is necessary.

Table 2: The output and method of correction for each FTAPS pixel state

Pixel State	Output	Correction
GG	mx_{in}	Not needed
GL	$½mx_{in}$	Multiply by 2
GH	$½mx_{in}$ + offset	Remove offset and multiply by 2
LH	offset	Interpolation
HH	V_{DD}	Interpolation
LL	V_{SS}	Interpolation
Hot	-	Interpolation or calibration

A defect-free pixel is denoted GG, where both halves of the FTAPS are good. The output of the pixel is the nominal sensitivity of an FTAPS, m, multiplied by the input illumination, x_{in}. A half stuck low pixel GL, or a pixel one half of the FTAPS is stuck

low, has an output with only half the sensitivity of a nominal FTAPS. To correct the output of a GL pixel, the output should be multiplied by two. Similar to a GL pixel is a half stuck high pixel GH. Since half of the pixel is stuck high, this results in an output which has half the sensitivity of a nominal FTAPS with an offset. Correcting the output of this pixel requires removing the offset and then multiplying the output by two.

The remaining defects cannot be corrected for so their output must be interpolated using information from neighbouring pixels. LH, HH, and LL are pixels with multiple stuck defects such that both halves of an FTAPS have been rendered unusable. In each of these cases, the pixel output will be stuck at some value so there can be no recovery of the output.

The last defect type is the "hot" pixel. Some pixels have a defect that causes them to have an exposure duration dependent component to their output. The output of a hot pixel may include an offset as well. As a result, the output of a hot pixel is not given in Table 2 since its behaviour is complex. Possible causes of a hot defect include excessive dark current or a leaky storage node. If one or both halves of a FTAPS are hot, the simplest correction method is to interpolate for the pixel output. Another possible correction method is to subtract the effect of the exposure duration dependent component of the output. However, this would require a complex calibration and would reduce the dynamic range of the pixel. In this case, a FTAPS which was half hot would be at an advantage compared to a hot standard APS. Since half of the pixel output would not suffer from the effects of the hot defect, the FTAPS would maintain at least half of its output swing regardless of how long the exposure duration was.

While it may seem like the FTAPS cannot correct for many of the defect types in Table 2, the premise of the FTAPS is to correct for the most common defects. Fabrication of ICs has advanced to the point that a defect rate on the order of 1/100000 or 1/1000000 defects per pixel is reasonable. Since the defect rate is quite low it is uncommon for a pixel to be defective, though it is not unlikely for several pixels to have a single point defect in an entire array of pixels. The single defect cases GL and GH are easily corrected for. However, it is very rare for a pixel to have *two* point defects that would render both halves of a FTAPS faulty, as in the cases of HL, HH, and LL. For example, using a defect rate p of 1/100000 point defects per pixel, the probability of getting of having two defects in a single pixel would be p^2 or $1/10^{10}$ using simple binomial probability. Since most digital cameras have less than 10 Megapixels (10^7), very few cameras would have a HL, HH, or LL defect in them.

The FTAPS can correct for the common defects of GH and GL with interpolation used for the rare cases of HL, HH, and LL. Hot pixels could potentially be corrected as well, as was stated previously. However, interpolation for a hot pixel output is more likely to be implemented.

2.7. Duo-Output Active Pixel Sensor Theory

The DAPS utilizes a unique pixel design that allows background subtraction to be performed. Essentially, two readout circuits are connected to the same photodetector so that a single pixel has two outputs. A schematic of the photogate DAPS is shown in Figure 15.

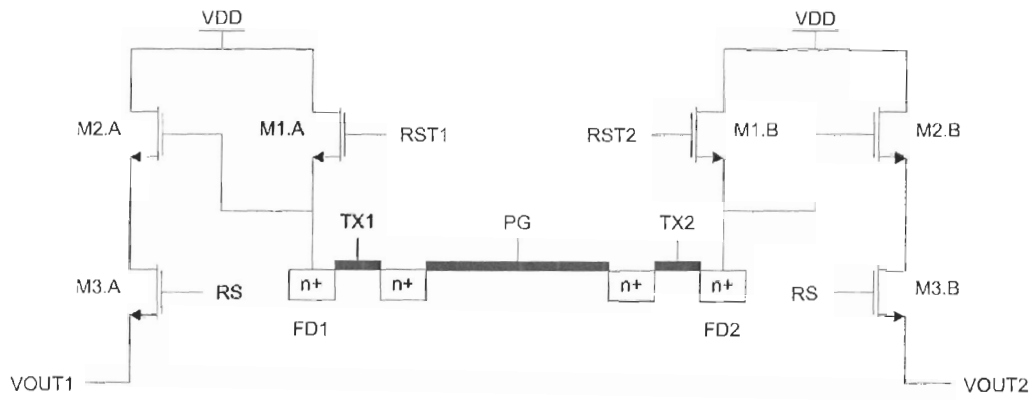

Figure 15: Photogate DAPS schematic

Each transistor is duplicated forming two readout circuits. Additional control lines are needed for RST2 and TX2, however RST2 can often be connected to RST1 so only a single reset line is needed. The outputs VOUT1 and VOUT2 are connected to column transistors that are biased to provide a voltage-mediated output. Charge collected under the photogate during an exposure is transferred to the floating diffusions FD1 and FD2.

Recalling Figure 3 showing the setup for optical triangulation, it is desired to measure the intensity of the light source, however any measurement will also include the background light. The DAPS removes the background signal from its output by taking two exposures. The light source will be "on" in the first exposure and "off" in the second exposure. Thus, the light source is "modulated" so that it goes on and off at an intended frequency and duty cycle. Figure 16 shows how charge is collected and transferred during a typical transfer cycle and Figure 17 shows the timing of a typical integration cycle.

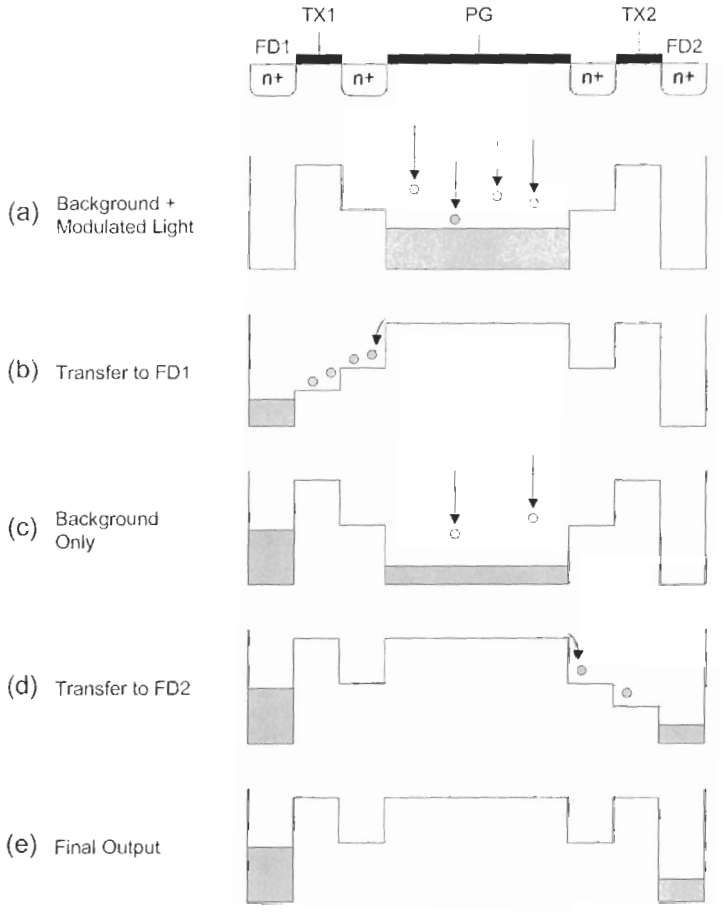

Figure 16: Transfer cycle of a photogate DAPS

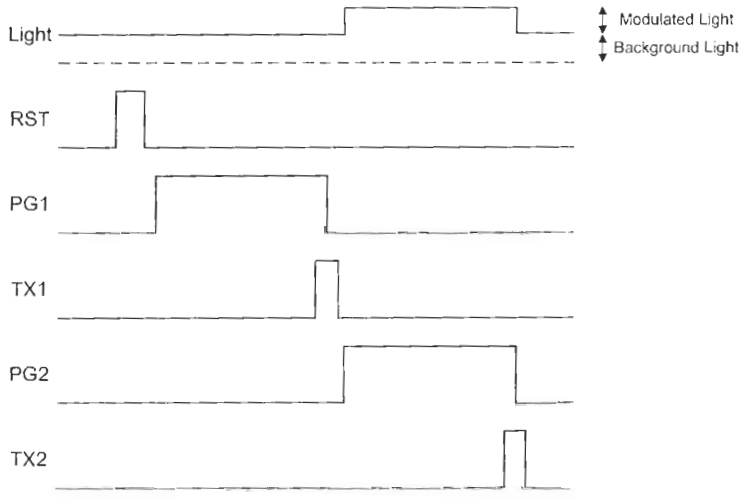

Figure 17: Typical integration cycle of a photogate DAPS

In the first exposure, charge is generated due to both the modulated light source and the background light. These charges are transferred and stored in FD1. In the second exposure, the modulated light source is off and only the background light is measured. The charge generated in the second exposure is transferred to FD2. Since VOUT2 is a measurement of the background light only, it is subtracted from VOUT1 to yield a measurement of the modulated light source. The subtraction can be done in hardware or in post-processing of the sensor output.

An advantage of the photogate DAPS is the ability to perform multiple exposures without resetting the pixel. This is an important feature when it is desired to modulate the light source at a high frequency. In these circumstances, the exposure time must necessarily be short and the output will likely be small as well. The transfer cycle in Figure 16 can be repeated several times without resetting the floating diffusions to get a larger output which is easier to measure. A photodiode DAPS is unable to perform multiple exposures due to the nature of its transfer.

2.8. Overview

Electron-hole pairs can be generated when light of sufficient energy is incident on a semiconductor. APS devices use photodiodes and photogate to generate electric fields so that the holes and electrons are separated, allowing them to be measured. The capacitance at the gate of the amp transistor determines the conversion gain and converts the charge to a voltage. This voltage determines the output of the APS, whether the output is voltage or current-mediated.

The FTAPS and DAPS include additional in-pixel circuitry to implement their functionality. The FTAPS operates two halves of a pixel in parallel so that if a point

defect renders one half defective, the other half will continue to operate. Thus, the pixel will maintain half its sensitivity which can be corrected in post-processing.

The DAPS uses two readout circuits to perform two exposures. In the first exposure, a modulated light source is on and, in the second, the light source is off. By subtracting the output of the first exposure from the second, the background signal is removed leaving only the output due to the modulated light source. Now that the basics of APS operation have been covered, the remainder of the thesis will concentrate on more in-depth analysis of the FTAPS and DAPS.

3. Fault Tolerant Active Pixel Sensor Testing

The FTAPS has been designed to recover from single point defects that occur during manufacturing and over time. Three sets of experiments were done on FTAPS devices to characterize their behaviour. The first set of experiments were to confirm that the FTAPS concept is viable for pixels fabricated in CMOS 0.35µm technology. Previous testing of FTAPS devices was only on pixels fabricated in CMOS 0.18µm technology [25] [26]. The fault tolerant concept was tested by comparing the sensitivity of defect-free FTAPS devices with FTAPS device with intentional, built-in stuck defects.

Previous work on the FTAPS suggested that it had higher sensitivity than a standard APS [18]. The second set of experiments were done to identify possible sources of increased sensitivity for current-mediated APS devices. The sensitivity three pixel designs were compared: the defect-free FTAPS devices, the standard APS design, and a variation of the standard APS design.

In the last set of experiments the sensitivity of pixels fabricated in 0.35µm technology were compared to pixels fabricated in 0.18µm technology. The 0.35µm CMOS technology used was a 4-metal, double poly (no silicide) process as opposed to the 6-metal, single poly (with silicide) process used for 0.18µm technology. The goal of this testing was to examine the impact of the technology scaling on APS designs fabricated in standard CMOS technologies.

3.1. Active Pixel Sensor Layouts

The pixel layouts were designed carefully to make sensitivity comparisons between pixel designs as simple as possible. Only the necessary changes were made between pixel layout to minimize the factors that could affect pixel performance. Figure 18 and Figure 19 show the layout of a standard photodiode APS and the layout of a photodiode FTAPS. Each pixel is 16μm×12μm and the photodiode areas are the same size, less the area required to split the photodiodes in the FTAPS layout. As well, all transistors are minimum length and width. By ensuring that the photodetector area is the same for each pixel design, it is simpler to make sensitivity comparisons. For a given input light energy density, each pixel design will absorb approximately the same amount of energy. Note that all pixels tested this thesis are metal shielded with metal-4 to cover everything but the photodetector area, however the shielding is not shown in the figures.

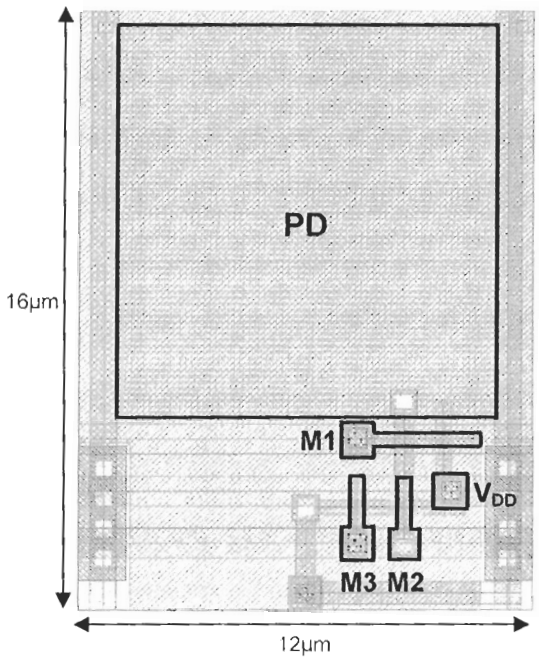

Figure 18: Standard photodiode APS layout

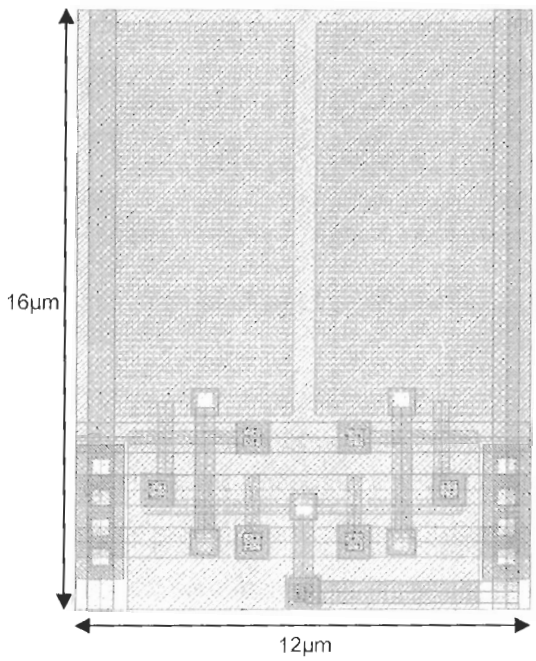

Figure 19: Photodiode FTAPS layout

FTAPS were designed with intentional half stuck defects so that the behaviour of the FTAPS could be tested with a known defect applied to it. A half stuck low and half stuck high FTAPS were designed. The layouts of the half stuck low and half stuck high photodiode FTAPS are illustrated in Figure 20 and Figure 21. Note the locations where the photodiode has been tied to V_{DD} or V_{SS}.

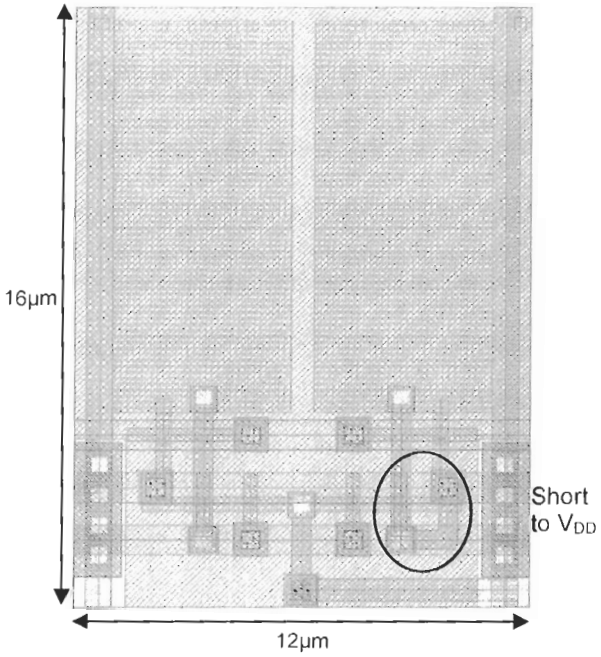

Figure 20: Photodiode FTAPS layout with half stuck low defect

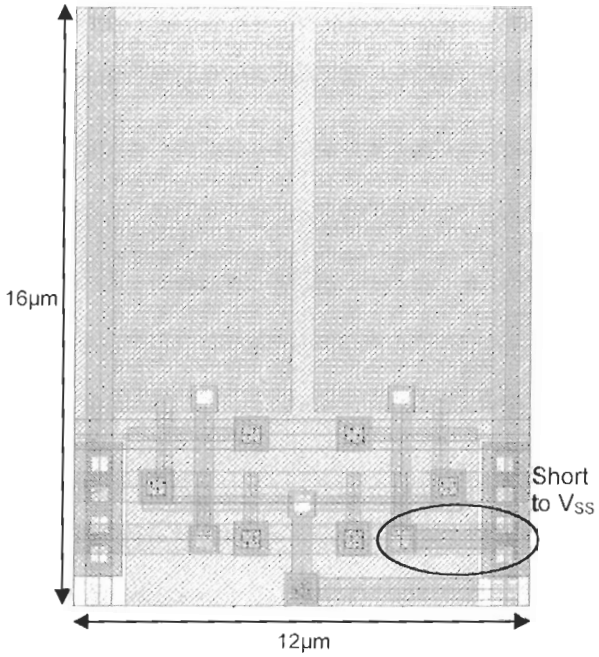

Figure 21: Photodiode FTAPS layout with half stuck high defect

Previous modelling work suggested that a standard photodiode APS with a wider amp transistor and row transistor would have increased sensitivity, similar to that of the FTAPS design. HSpice simulations indicated that by doubling the width of the amp transistor and row transistor, the sensitivity of the pixel would approximately double. The layout of the standard APS was altered to double the width of the amp and row transistors. This pixel design is called the Double Width (DW) APS in this thesis.

In all, five pixel photodiode designs are tested: the standard APS, the defect-free FTAPS, the half stuck high FTAPS, the half stuck low FTAPS, and the DW APS. For each photodiode APS design, a photogate variation was also made with the same

concepts in mind. Figure 22 - Figure 25 show the layouts of the standard and fault tolerant photogate pixels.

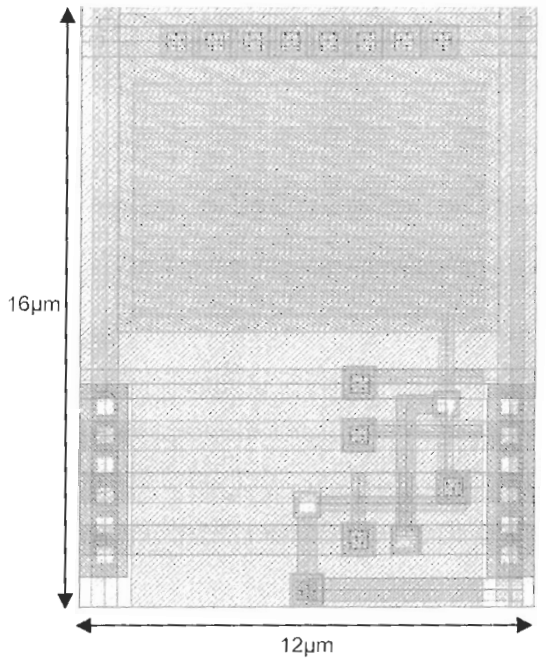

Figure 22: Standard photogate APS layout

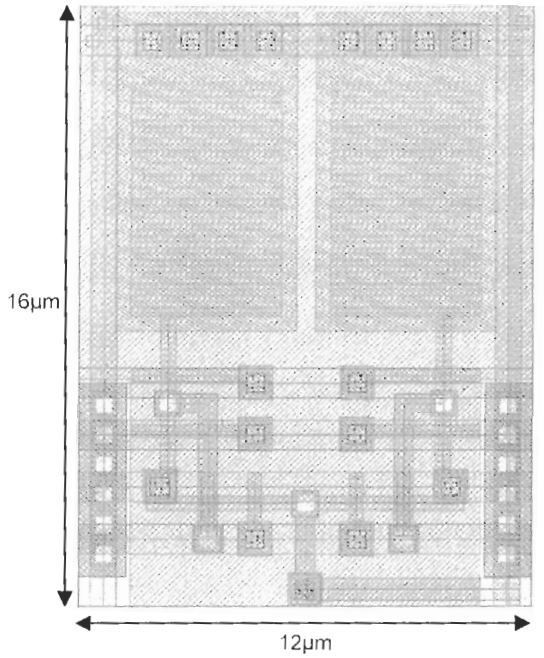

Figure 23: Photogate FTAPS layout

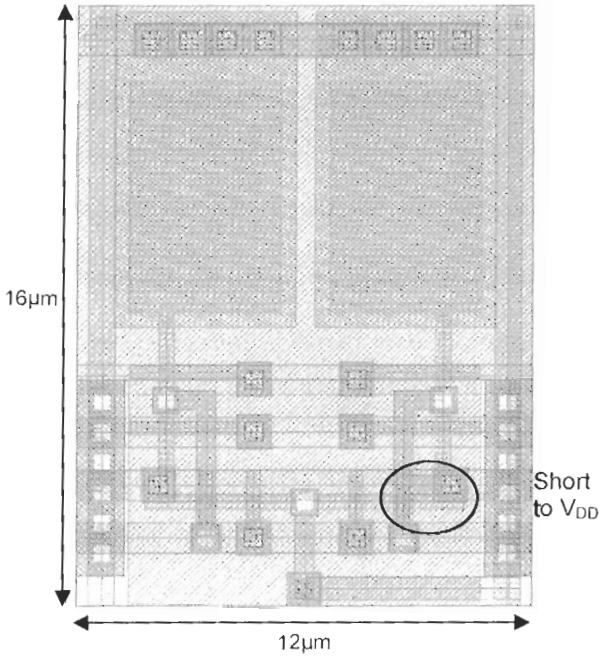

Figure 24: Photogate FTAPS layout with half stuck high defect

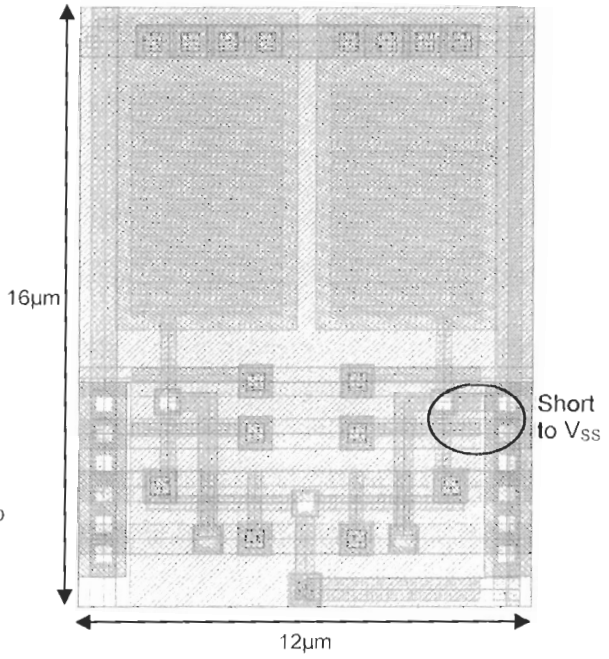

Figure 25: Photogate FTAPS layout with half stuck low defect

The layouts of the photodiode and photogate DW APS designs are shown in Figure 26 and Figure 27.

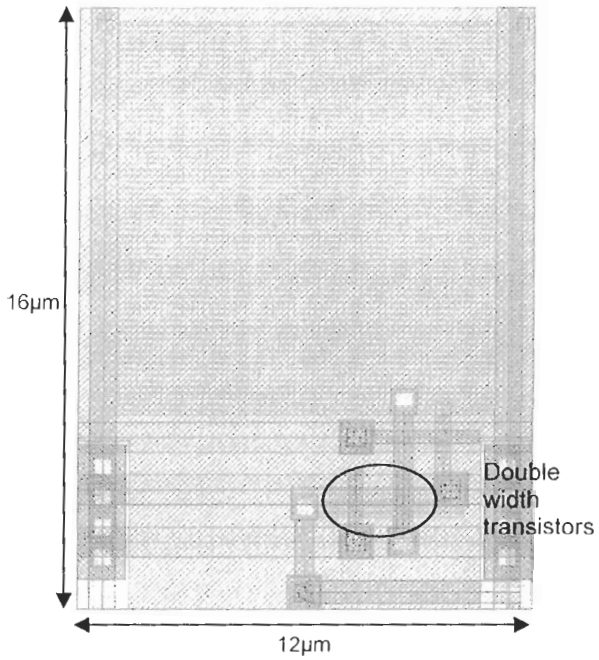

Figure 26: Photodiode double width APS layout

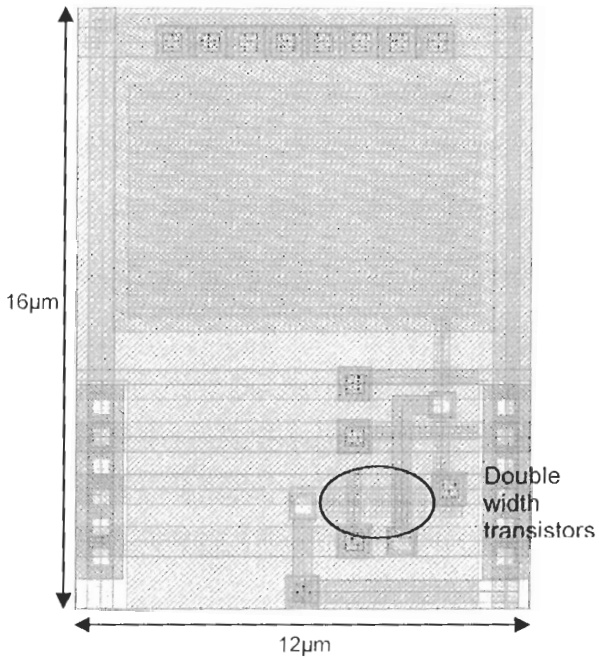

Figure 27: Photogate double width APS layout

3.2. Experimental Setup

The apparatus for the APS testing was designed to test APS devices with consistency and accuracy. A diagram and picture of the experimental setup are shown in Figure 28 and Figure 29. An array of four red LEDs was used to illuminate the pixels as their output power is easily controlled and they have a known output spectrum. All of the pixels are illuminated at once, so the illumination is required to be uniform across the entire 2024µm×2024µm area of the chip. To achieve uniform illumination over the chip area, a diffuser was used to disperse the LED light. The APS chip is mounted on a breadboard which is affixed to a piece of plastic to prevent unwanted movement. Spacers are used to connect the pieces of the setup together and to maintain consistent positioning of each component.

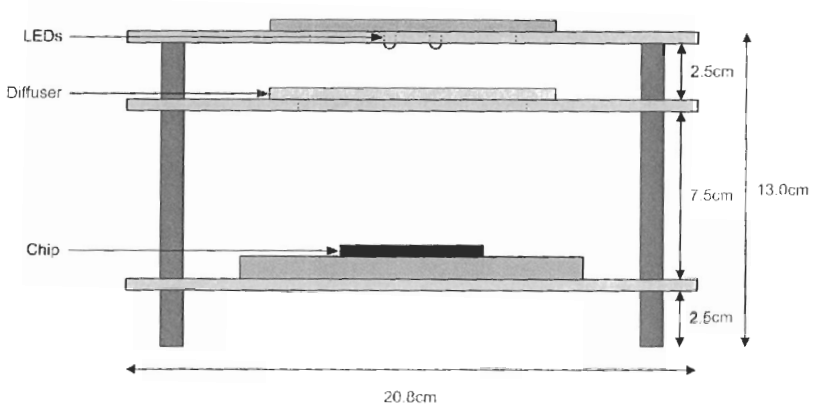

Figure 28: Diagram of the experimental setup

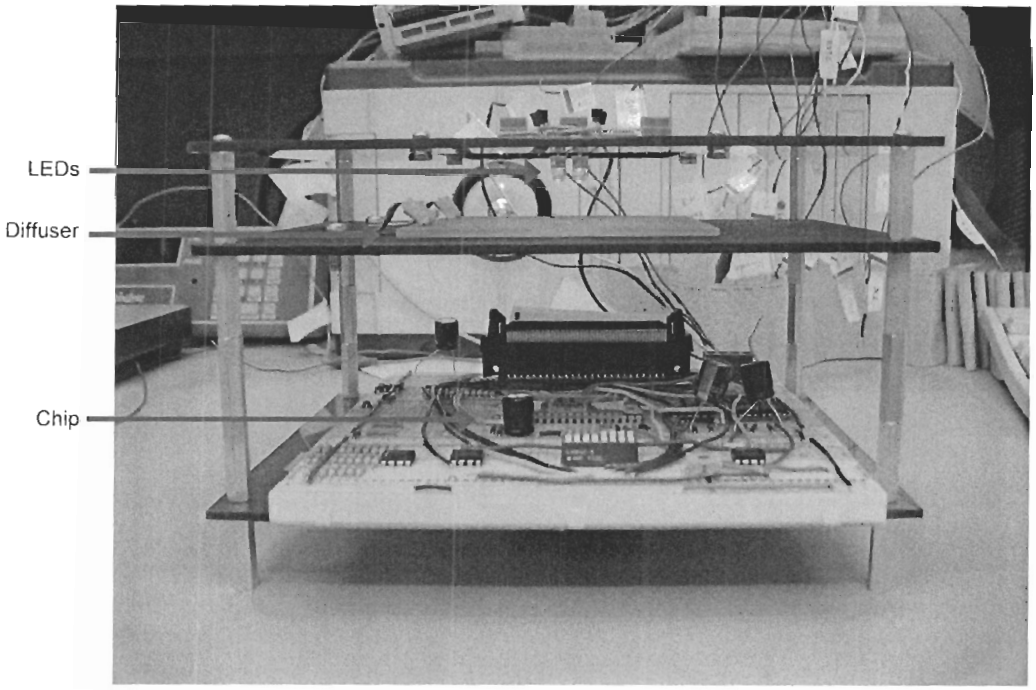

Figure 29: Picture of the experimental setup

Power, column select, row select, and the control signals are provided by a PC running LabVIEW. Figure 30 shows a system diagram of the experimental setup illustrating how the PC is connected to the APS chip. Two data acquisition card have several analog and digital outputs that are used for control signals. LabVIEW software controls the timing and amplitude of these outputs.

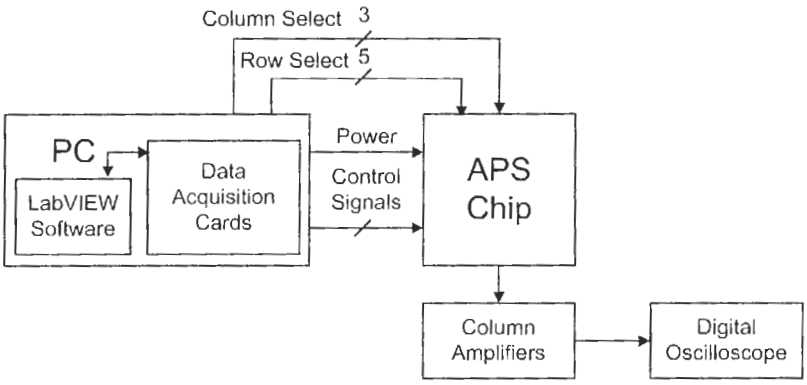

Figure 30: System diagram of experimental setup

To control the output of the LEDs, LabVIEW varies the voltage of the LED control signal. This voltage is converted to current with operational amplifiers to power the LEDs. Calibrating the light power density of the LEDs was done by positioning a light power meter at the same position the APS chip was during testing. While varying the LED control signal, the light power detected by the meter was recorded. This data was used to create a calibration curve of the light power density vs. voltage of the LED control signal.

The external circuitry, such as the operational amplifiers, was powered by a power supply. The output of the APS chip was captured with an oscilloscope and transferred to a PC for analysis.

3.3. Column Amplifiers

Since the FTAPS can only be operated as a current-mediated device, all of the pixels tested in this chapter were operated in this manner for consistency. However, the oscilloscope is not able to detect current signals, so the current output was converted to voltage for data capture. Column amplifiers were used as current-to-voltage converters.

A TLC2744A quad operational amplifier was used to implement four column amplifiers external from the APS chip. Figure 31 shows the schematic of a column amplifier. With a 27kΩ resistor in the feedback path, the conversion gain of the column amp was 27000V/A with the output of a pixel measured at Vout.

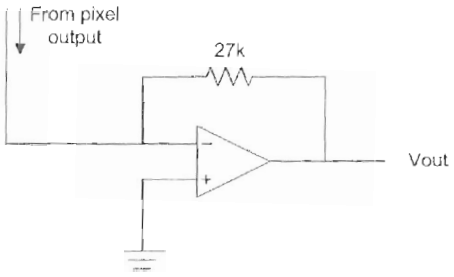

Figure 31: Column amplifier schematic

3.4. Control Signal Timing

The parameters of the control signals, such as duty cycle, frequency, and amplitude, were important factors in all of the APS testing. For the photodiode APS devices, there are only two controls signals: pixel Reset and LED illumination. The frequency of the Reset line dictates the cycle or exposure time so the Reset line is the more important of the two signals. The frequency of the Reset line was set so that the highest LED light energy densities (or highest LED control voltages) would saturate the pixel while maintaining several illuminations that did not saturate the pixel. The duty cycle of the Reset line must be large enough to completely reset the pixel, regardless of the final output of the pixel. The amplitude of the Reset line was always set to toggle between 0V (off) to 3.3V (on) to ensure the photodiode was reset as completely and quickly as possible.

The LED control signal was varied from 0V to 7V in 0.25V step increments. The duty cycle and phase were adjusted so that the LED would only be on when Reset was off to simulate a shuttered system. The output of the pixels is sampled at two points.

The Reset voltage is sampled shortly after the Reset line turns off and the Readout voltage is sampled shortly before the Reset line turns on. The LED was kept off during the sampling times.

The control signal timing for photodiode APS testing is illustrated in Figure 32. The Reset line frequency was 66.67Hz and the dotted lines indicate the times where the Reset voltage and final Readout voltage were acquired. Double Sampling (DS) was implemented, as the Reset voltage is acquired after the Readout voltage. Variations and noise between individual measurements was minimized by setting the oscilloscope to average the captured data.

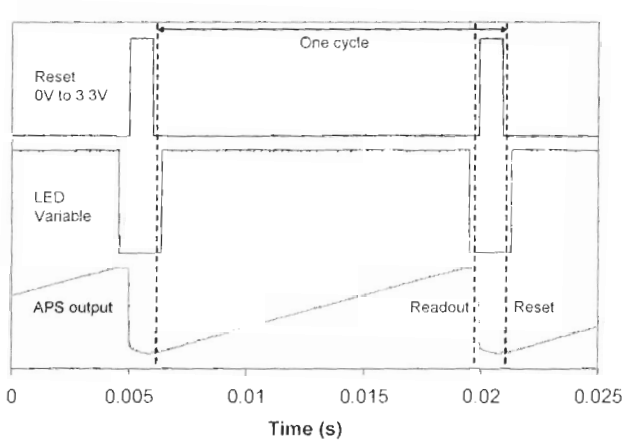

Figure 32: Control signal timing for photodiode APS testing

The timing for the photogate APS testing was slightly more complicated as there are two additional control signals: Photogate (PG) and Transfer (TX). Once again starting with the Reset line, its frequency was adjusted to ensure that only the higher LED energies would saturate the pixel output. Unlike the photodiode, the Float Diffusion (FD) node of photogate pixels (node X in the photodiode case, see Figure 7) is separate from the photodetector. Thus, it is possible to keep the FD node reset until charge from the photogate is transferred via the transfer gate. This prevents undesirable effects such as charge leaking off the FD or stray illumination

discharging the FD. Thus, a long Reset line duty cycle is used to reset the FD for most of a cycle.

The amplitude of the PG line was set to toggle from 0V (off) to 3.3V (on) for maximum collection and transfer efficiency. The phase and duty cycle of the PG line were set to maximize the collection time of the photogate. The PG line must be timed with the TX line to transfer charge from the photogate to the FD as in Figure 11. Thus, PG turns off after TX turns on and stays off until the pixel is reset again.

Once PG goes on, the LED line will go on to provide the illumination for the exposure cycle. The LEDs remain on until transfer of charge to the FD is about to begin.

The TX line was timed to facilitate the transfer of charge. The amplitude of the TX line was set to oscillate from -0.75V (off) to 1.65V (on). The off voltage of -0.75V was used instead of 0V to prevent charge from leaking through the transfer gate. The on voltage of 1.65V was set to one half of V_{DD} to provide the necessary potential wells for charge transfer. As well, it was necessary to reset the potential of the parasitic n+ diffusion of the photogate pixels (see Figure 9). If the parasitic n+ diffusion is not reset, charge builds up in it that adversely affects the pixel performance. This was more noticeable for longer cycle times as it resulted in a higher dark current signal which reduced the output swing of the pixel. Resetting the parasitic n+ diffusion was achieved by turning both Reset and TX on.

Figure 33 shows the control signal timing for photogate APS testing with a Reset frequency of 125Hz. The standard APS and DW APS were tested at 125Hz while the FTAPS designs were tested at 75Hz. Once again, the dotted lines indicate when the Reset and Readout voltages are acquired. For the photogate pixels, the Reset voltage

is acquired before the Readout voltage, thus correlated double sampling is implemented.

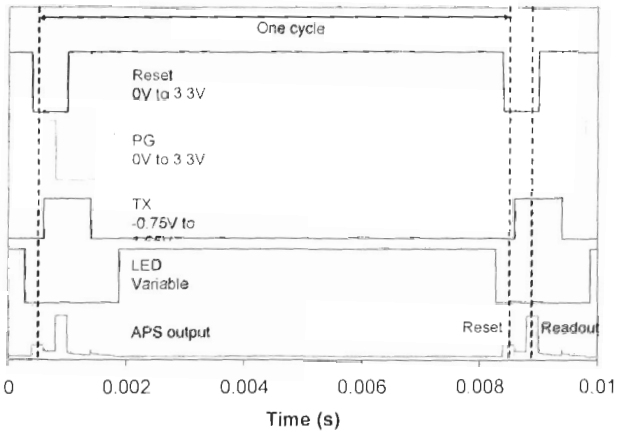

Figure 33: Control signal timing for photogate APS testing

The procedure for testing both the photodiode and photogate pixels was to vary the LED voltage from 0V to 7V in 0.25V step increments, capturing the output waveform of the pixel for each LED voltage. This data is used to plot the output voltage vs. the input light energy density, i.e. the output characteristics of the pixel, for analysis.

3.5. Active Pixel Sensor Analysis

The performance of each APS design was compared by analyzing the captured data to determine particular performance measures such as the sensitivity and output swing of a pixel. A specific procedure was followed to produce the output characteristics of each pixel. The desired performance measures were derived from the output characteristics.

For each LED voltage, a pixel's output waveform has been captured with an oscilloscope. The Reset voltage and Readout voltage were acquired from each waveform. From a basic standpoint, subtracting the Readout voltage from the Reset voltage yields the pixel output at a particular input level. However, the pixel will have

some non-zero output even when there is no illumination, i.e. when the LED voltage is 0V. This "dark output" is the result of dark current and leakage in the pixel. Since it is desired to remove the dark output from the pixel output, the final output value is the Readout voltage less the Reset voltage and dark output. This results in a list of pixel outputs for each LED voltage tested.

Now, each LED voltage must be converted to its equivalent light energy density by using the LED calibration curve of the light power density vs. LED voltage (see Section 3.2). The power density is then converted to energy density by factoring in the duration that the LEDs are on. Finally, the output voltage of a pixel can be plotted vs. the light energy density. A sample graph of the output characteristics of a standard photodiode APS is shown in Figure 34.

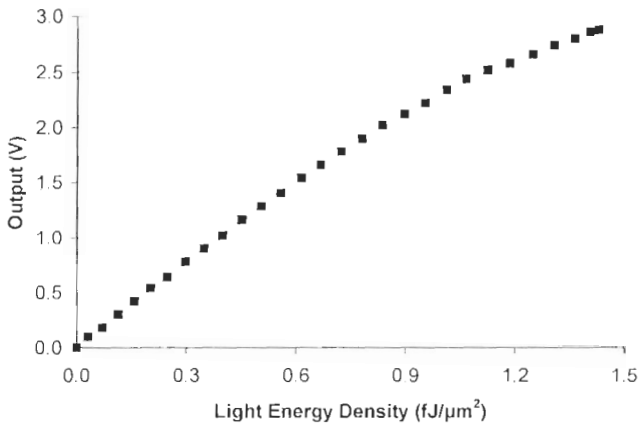

Figure 34: Sample output characteristic of a standard photodiode APS

The three main performance measures that are examined for FTAPS testing are the sensitivity, output voltage swing, and input saturation level of the pixel. These measures are depicted in the idealized output characteristics shown in Figure 35.

Of these measures, the sensitivity is analyzed the most. As defined in Section 2.4, the sensitivity is the rate at which the output changes when the input light intensity

is varied. In relation to the output characteristics of a pixel, the sensitivity is the slope of the curve. Thus, to obtain the sensitivity of a pixel, regression analysis is used to fit a line to the most linear portion of its output curve. This is illustrated in Figure 34 as the line fitted to the output curve.

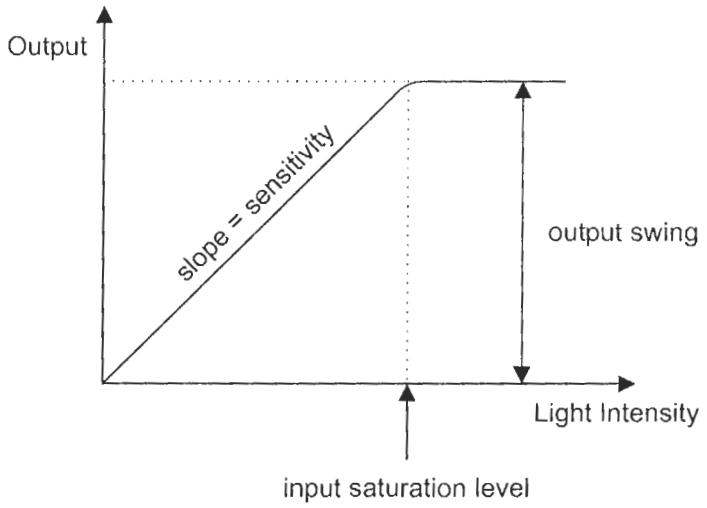

Figure 35: Idealized output characteristics of a pixel showing sensitivity, output swing, and input saturation level

The output swing and input saturation level of a pixel are easy to determine from the output characteristics. Since the minimum output is set to 0V when there is no illumination, the output swing is simply the maximum output voltage the pixel achieves. The input saturation level is the minimum input energy density that is required to saturate the pixel for the cycle time tested. Thus, the minimum input that saturates the pixel output is the input saturation level.

3.6. Test Results of Fault Tolerant Active Pixel Sensors

3.6.1. Analysis of Fault Tolerant Concept in 0.35µm Technology

Testing of the fault tolerant pixels, with and without defects, was done for both photodiode and photogate designs. The sensitivity of the defect-free pixels was compared to pixels with built-in half stuck defects. From theory and previous testing,

the fault tolerant concept would be considered successful if the sensitivity of the half stuck defective pixels was approximately half the sensitivity of the defect-free pixels.

For each pixel design, nine pixels were tested to determine their sensitivity, output swing, and input saturation level. Beginning with the photodiode FTAPS pixels, Table 3 shows a summary of the photodiode FTAPS test results. The half stuck low FTAPS and the half stuck high FTAPS have a large disparity in their performances as their sensitivity, output swing, and input saturation level are different. This is also illustrated in Figure 36 which shows the output characteristics of a defect-free FTAPS, a half stuck low FTAPS, and a half stuck high FTAPS.

Table 3: Summary of photodiode FTAPS test results

	Sensitivity ($V/fJ/\mu m^2$)		Mean Output Swing (V)	Mean Input Saturation Level ($fJ/\mu m^2$)
	Mean	**Standard Deviation**		
Defect-free FTAPS	4.72	0.142	5.35	1.43
Half stuck low FTAPS	2.52	0.096	2.80	1.41
Half stuck high FTAPS	1.50	0.071	1.19	0.78

The half stuck low photodiode FTAPS behaves as expected. Its sensitivity and output swing are approximately half that of the defect-free FTAPS (sensitivity: 53.4%, output swing: 52.4%) and its input saturation level is almost the same (98.7%). However, the half stuck high photodiode FTAPS performs much more poorly. Its sensitivity is only 31.8% of the defect-free FTAPS, its output swing is 22.3%, and its input saturation level is degraded to 55.0%. For each pixel type, the sensitivity of the nine pixels tested were consistent, as indicated by the relatively low standard deviations.

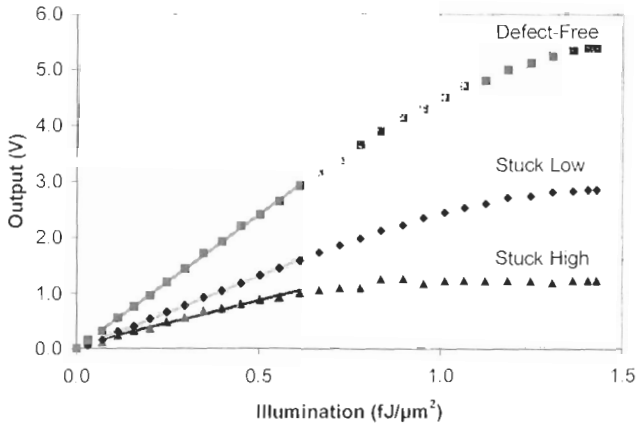

Figure 36: Sample output characteristics of photodiode FTAPS designs

The cause of the unexpected behaviour for the half stuck high photodiode FTAPS can be observed in the output waveforms captured in testing. Figure 37 shows the output waveforms of a defect-free photodiode FTAPS and half stuck high photodiode FTAPS. The waveform shows the output of the pixels during reset with an input light density of 0.556fJ/μm^2.

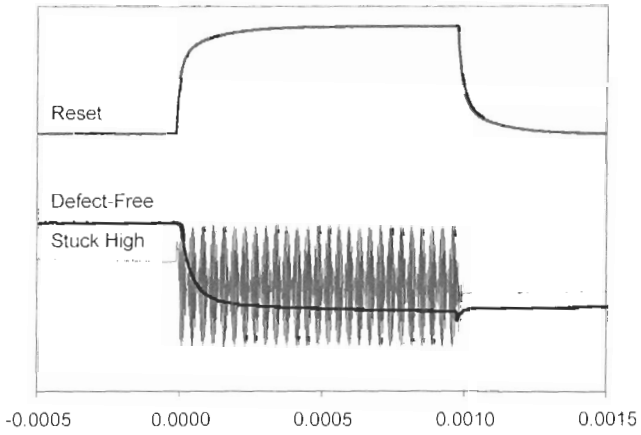

Figure 37: Output waveforms of defect-free photodiode FTAPS and half stuck high photodiode FTAPS during reset

During reset, a race condition occurs in the half stuck high photodiode FTAPS. Figure 38 shows a schematic of the photodiode FTAPS with node X2 tied to ground to create a half stuck high defect. Thus, when the RST line is high the reset transistor tries to

pull the voltage of X2 to $V_{DD} - V_{th}$. However, since node X2 is tied to ground, a race condition occurs which degrades the output of the pixel.

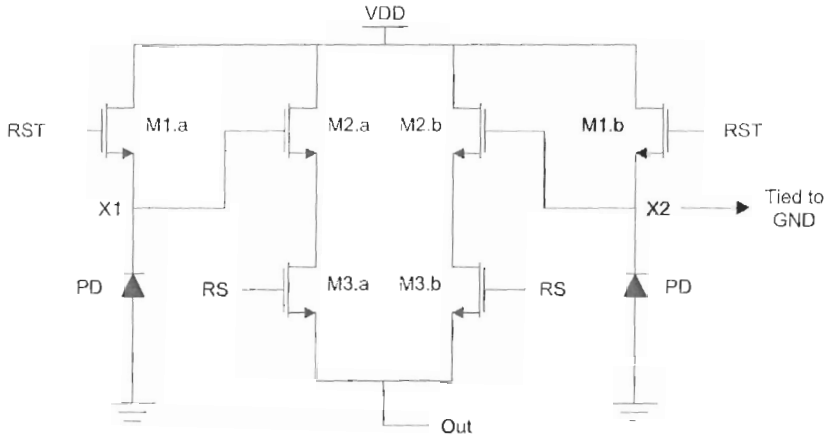

Figure 38: Schematic of photodiode FTAPS showing how half stuck high defect is built-in

Previous tests on half stuck high photodiode FTAPS devices fabricated in 0.18µm did not have a problem with a race condition during reset [25]. Therefore, the race condition must be a result of a design problem in the APS chip tested or the change to 0.35µm technology. A possible cause of the race condition is the layout of the half stuck high photodiode FTAPS array. The half stuck high pixels are arranged in an 8×8 array. Since these pixels are in very close proximity, the current drain that results from all 64 of these pixels trying to draw a high current during reset could cause the poor performance of the half stuck high photodiode pixels. In the previously tested chip, half stuck high pixels were arranged in several smaller arrays of 4×1 so the current drain in a particular area would not be as large. Further investigation is needed to pinpoint the cause of the half stuck high FTAPS race condition problem. A possible new design could have a small resistance from the photodiode to ground instead of a short to see if that would avoid the race condition.

The photogate FTAPS devices were better behaved than their photodiode counterparts. Table 4 gives a summary of the photogate FTAPS results.

Table 4: Summary of photogate FTAPS test results

	Sensitivity (V/fJ/μm²)		Mean Output Swing (V)	Mean Input Saturation Level (fJ/μm²)
	Mean	Standard Deviation		
Defect-free FTAPS	6.81	0.613	4.54	1.05
Half stuck low FTAPS	3.36	0.260	2.52	1.02
Half stuck high FTAPS	2.89	0.221	2.01	0.96

The half stuck photogate pixels behave similarly, although the half stuck high pixel has slightly poorer performance. The output characteristics of a defect-free, a half stuck low, and a half stuck high photogate FTAPS illustrated in Figure 39 show much improvement over the photodiode FTAPS output characteristics.

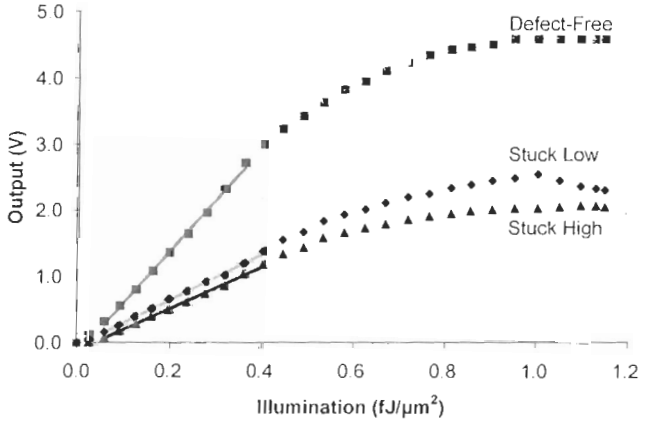

Figure 39: Sample output characteristics of photogate FTAPS designs

The half stuck low photogate FTAPS behaves as expected. Its sensitivity and output swing are approximately half that of a defect-free FTAPS (sensitivity: 49.3%, output swing: 55.4%) and its input saturation level is almost the same (97.6%). The half stuck high photogate FTAPS performs almost as well. Its sensitivity and output voltage swing are slightly less than half that of a defect-free FTAPS (sensitivity:

42.4%, output swing: 44.2%) and its input saturation level is similar as well (91.3%). The sensitivity of the half stuck low photogate FTAPS was very close to the expected sensitivity (50% of a defect-free FTAPS) and well within the expected error of the experiment. The half stuck high photogate FTAPS was slightly less than the expected sensitivity which cannot be completely explained by experimental error. However, the consistency of the sensitivity would still allow correction to be done though the output would have to be multiplied by more than two.

While the half stuck high photogate FTAPS has slightly worse performance than the half stuck low pixel, it does not have the same problem with a race condition during reset that the photodiode version has. This suggests that the problem is not caused by the fabrication technology, rather the current drain of the half stuck photodiode pixel array is too great. While the photogate FTAPS designs are also grouped in arrays of 8×8, they have less capacitance at the gate of their amp transistors which means they draw less current during reset.

To summarize the fault tolerant concept testing results,

Table 5 shows the half stuck pixel performance when compared to the defect-free cases. The half stuck low photodiode FTAPS and both half stuck photogate FTAPS devices behaved as expected. Their sensitivities and output swings were approximately half that of a defect-free pixel and their input saturation levels were about the same. The half stuck high photodiode FTAPS had poorer performance than expected due to a race condition that occurred when the pixel was reset. This is likely a result of the chip layout, but could also be caused by the change to 0.35μm technology.

Table 5: Half stuck pixel performance in comparison to the defect-free pixels

		Compared to defect-free FTAPS		
		Sensitivity (%)	**Output Swing (%)**	**Input Saturation Level (%)**
Photodiode	Half stuck low	53.4	52.4	98.7
	Half stuck high	31.8	22.3	55.0
Photogate	Half stuck low	49.3	55.4	97.6
	Half stuck high	42.4	44.2	91.3

3.6.2. Analysis of Fault Tolerant Active Pixel Sensor Sensitivity

The standard APS, defect-free FTAPS, and DW APS were tested to determine their sensitivity, output swing, and input saturation level. The performance measures of each pixel design were compared to identify possible methods of increasing the sensitivity of an APS, and more specifically, to gain a better understanding of why the FTAPS design may have better sensitivity than a standard APS of the same size.

For the photodiode pixels, both the DW APS and FTAPS exhibited enhanced performance compared to the standard design. The DW APS and FTAPS exhibit very similar behaviour, as seen in Figure 40 which shows sample output characteristics of each pixel design.

In Table 6, which shows a summary of the photodiode APS test results, the sensitivity and output swing of the DW APS and FTAPS are both clearly larger than that of the standard APS. Compared to the standard photodiode APS, the DW APS and FTAPS have almost double the sensitivity (DW: 192%, FT: 186%), double the output swing (DW: 184%, FT: 184%), and nearly identical input saturation level (DW: 99.2%, FT: 100%). Since the standard deviation of each pixel type's sensitivity

were relatively small, the experimental error should not be significant in these results.

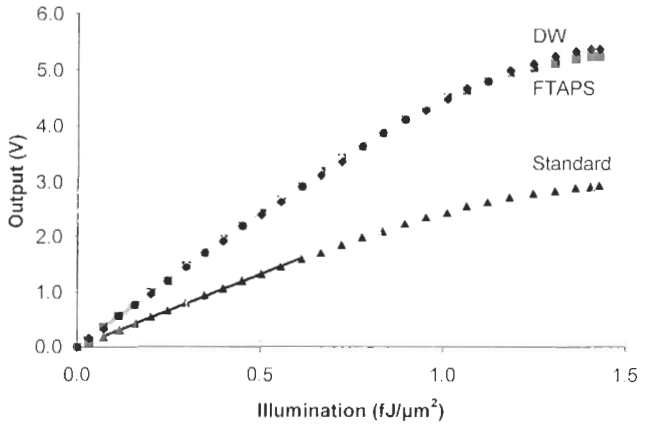

Figure 40: Sample output characteristics of photodiode standard APS, FTAPS, and DW APS designs

Table 6: Summary of photodiode standard APS, DW APS, and FTAPS test results

	Sensitivity (V/fJ/μm²)		Mean Output Swing (V)	Mean Input Saturation Level (fJ/μm²)
	Mean	Standard Deviation		
Standard APS	2.54	0.049	2.91	1.43
DW APS	4.87	0.125	5.37	1.41
FTAPS	4.72	0.142	5.35	1.43

For the photogate pixels, both the DW APS and FTAPS also exhibited enhanced performance. However, only the DW APS had increased sensitivity. Sample output characteristics of each photogate design are shown in Figure 41. Each pixel design clearly behaves differently.

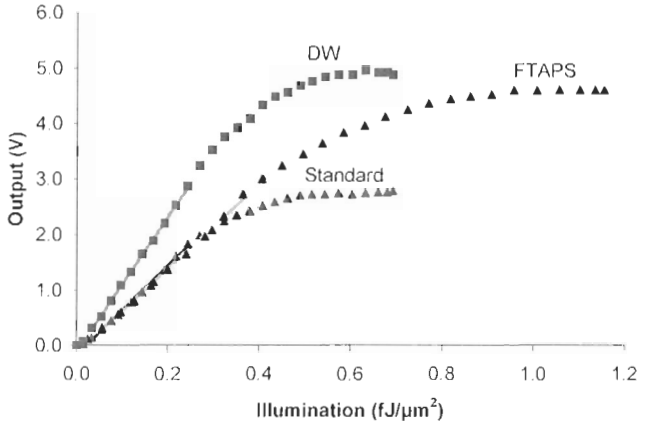

Figure 41: Sample output characteristics of photogate standard APS, FTAPS, and DW APS designs

Table 7 shows a summary of the photogate test results. The DW photogate APS performed best, with an increased sensitivity (164%) over the standard pixel, almost double output swing (188%), and similar input saturation level (108%). The FTAPS had no increase in sensitivity compared to the standard pixel (99.0%), and an increased output swing and input saturation level (output swing: 172%, input saturation level: 187%).

Table 7: Summary of photogate standard APS, DW APS, and FTAPS test results

	Sensitivity (V/fJ/μm²)		Mean Output Swing (V)	Mean Input Saturation Level (fJ/μm²)
	Mean	Standard Deviation		
Standard APS	6.87	0.66	2.63	0.561
DW APS	11.29	0.87	4.92	0.607
FTAPS	6.81	0.61	4.54	1.049

To more easily analyze the test results, the performance of the DW APS and FTAPS are directly compared to the standard APS performance in Table 8. It is clear from these results that since the photogate FTAPS sensitivity is no better than for a standard photogate APS, the fault tolerant design does not inherently increase the sensitivity of a pixel.

Table 8: DW APS and FTAPS performance in comparison with standard APS performance

		Compared to standard APS		
		Sensitivity (%)	**Output Swing (%)**	**Input Saturation Level (%)**
Photodiode	DW APS	192	184	99.2
	FTAPS	186	184	100
Photogate	DW APS	164	188	108
	FTAPS	99.0	172	187

To better understand the FTAPS behaviour, an explanation of the DW behaviour is needed. The photodiode and photogate DW APS devices both exhibited increased sensitivity and output swing. Since the only difference between the DW APS devices and standard APS devices are the widths of the amp transistor and row transistor, it is evident that the changes made to these devices affect the sensitivity of the APS. Increasing the width of the amp and row transistors increases their current driving ability. In particular, increasing the width of the amp transistor in the DW APS increases its transconductance g_m. Thus, a change in voltage at the gate of the amp transistor will have a greater effect on the output current for a DW APS than for a standard APS. This results in an increase in sensitivity and output swing without a change in the input saturation level. However, it is not clear why the photodiode DW APS sensitivity increases by 192% and the photogate DW APS sensitivity increases by 164%. More experimentation is needed to discover why the sensitivity of the photodiode and photogate pixels increase at different rates.

To explain the behaviour of the FTAPS devices, recall that the conversion gain of a pixel is highly dependent on the capacitance at the gate of the amp transistor. In a photodiode pixel, that capacitance mostly consists of the capacitance of the

photodiode itself. The photodiode FTAPS splits the photodetector area in half so that two photodiodes can be operated in parallel as in Figure 42.

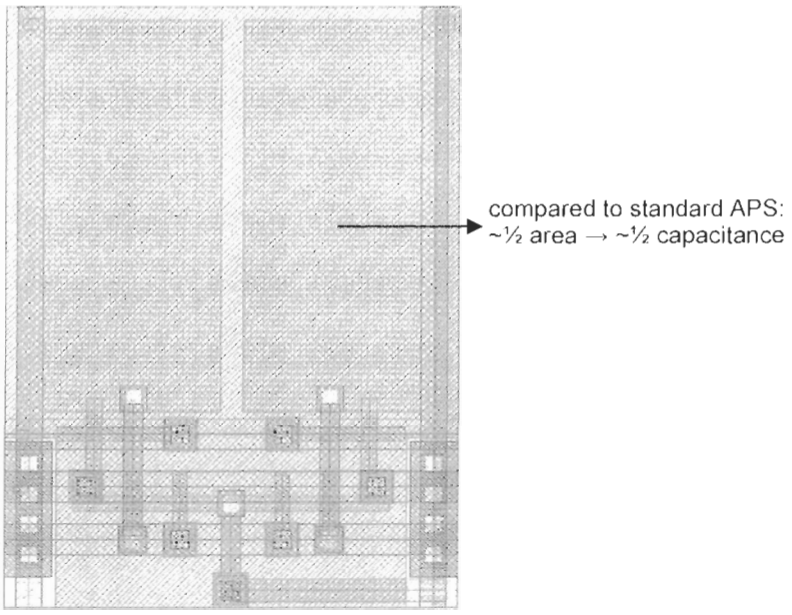

Figure 42: Photodiode FTAPS layout comparing area and capacitance of one photodiode half to standard APS photodiode

Since these photodiodes have approximately half the area, they also have approximately half the capacitance, ignoring edge effects. Recalling equation (4), if C_X is reduced by half, the conversion gain doubles. So while one half of a photodiode FTAPS only collects about half the light that a standard APS would collect, it has approximately the same overall sensitivity due to the increase in conversion gain. Since the FTAPS operates two photodiodes halves in parallel with their outputs being added, its sensitivity and output swing should be approximately double that of a standard APS while maintaining the same input saturation level. So while the photodiode FTAPS acts similarly to the photodiode DW APS, its behaviour is caused by a completely different mechanism.

In photogate pixels, the gate of the amp transistor is isolated from the photogate itself. Thus, splitting the photogate in half has no effect on the capacitance at the

gate of the amp transistor. Therefore, the conversion gain is the same for the FTAPS and standard APS. Each photogate FTAPS half is half as sensitive as a standard APS since they only collect about half the light so overall both pixels have the same sensitivity. However, the photogate FTAPS has increased output swing and input saturation level which is not explained by the previous analysis. For a photogate pixel, an increase in the input saturation level is the result of either an increased photogate well capacity or an increase in the capacitance of the FD. In this instance, the photogate FTAPS has roughly the same well capacity as the standard pixel. Thus, the increased input saturation level must be from an increase in the FD capacitance. A larger FD capacitance requires more charge to discharge it. In the photogate FTAPS, the FD is the same area as the FD in the standard APS. Thus, the FD area of the photogate FTAPS is effectively double that of a standard APS. Twice as much charge is needed to discharge the FD causing the input saturation level and output swing to double. This behaviour is confirmed by the results in Table 8 which shows an increase in input saturation level (187%) and output swing (172%) for the photogate FTAPS.

To summarize this analysis, the FTAPS design is not inherently more sensitive than a standard pixel. The photodiode FTAPS has greater sensitivity and output swing as it has a higher conversion gain than a standard APS. The photogate FTAPS does not exhibit enhanced sensitivity, however it has greater output swing and input saturation level as a result of an effective doubling of its FD area. The sensitivity and output swing of the DW APS designs doubled due to the increased transconductance of the double width amp transistor and row transistor. Thus, increased sensitivity for current-mediated pixels can be achieved by either increasing the conversion gain of a pixel or increasing the transconductance of the transistors in the output branch.

3.6.3. Analysis of Active Pixel Sensors in 0.35μm and 0.18μm Technology

A standard photodiode APS and photodiode FTAPS were tested from the previous APS chip fabricated in 0.18μm technology and designed by D. Y. H. Cheung. These pixels were tested to compare the performance of pixels in two different technologies and to confirm that the photodiode FTAPS has greater sensitivity than a standard APS. Unlike the pixels designed in 0.35μm, the 0.18μm pixels are different sizes. However, since the input is in terms of energy density the size should not affect the results significantly. Testing was done to determine the sensitivity, output swing, and input saturation level of each pixel design as in previous testing. Table 9 shows the results of testing the 0.18μm pixels with the 0.35μm photodiode APS test results for comparison. Nine pixels of each design were tested.

Table 9: Summary of photodiode APS test results for 0.35μm and 0.18μm technology

	Sensitivity (V/fJ/μm^2)		Mean Output Swing (V)	Mean Input Saturation Level (fJ/μm^2)
	Mean	Standard Deviation		
Standard APS (0.18μm)	1.22	0.080	1.43	1.46
FTAPS (0.18μm)	2.52	0.201	2.64	1.37
Standard APS (0.35μm)	2.54	0.049	2.91	1.43
FTAPS (0.35μm)	4.72	0.142	5.35	1.43

As expected from the previous section's analysis, the 0.18μm FTAPS has approximately double the sensitivity and output swing (sensitivity: 206%, output swing: 185%) of the standard pixel and a similar input saturation level (93.9%).

As predicted by H. S. Wong [20], the 0.18μm pixels are less sensitive than the 0.35μm. Both 0.18μm pixels are approximately half as sensitive per unit area as

their 0.35µm counterparts (standard APS: 48.1%, FTAPS: 53.3%). As CMOS technology scales down, several factors can affect the performance of digital imaging sensors. These factors include: higher substrate doping, increased number of layers, shallower junction depths, and increased edge capacitance. In conclusion, while it is not clear what the cause is, photodiode pixels are less sensitive when fabricated in a standard 0.18µm CMOS process than in a 0.35µm CMOS process.

3.7. Testing Summary of Fault Tolerant Active Pixel Sensors

Three sets of tests were done on FTAPS devices. The first set tested the fault tolerant concept for 0.35µm pixels, the second set examined the mechanisms for increased sensitivity in FTAPS devices, and the last set compared the sensitivity of pixels fabricated in 0.18µm CMOS technology with pixels fabricated in 0.35µm CMOS technology.

FTAPS pixels were designed with and without defects built-in to test the fault tolerant concept for 0.35µm pixels. Each of the defective pixels behaved as expected, except for the half stuck high photodiode FTAPS. A race condition that occurred during reset resulted in poorer performance than expected.

Tests to compare the performance of the standard APS to the DW APS and FTAPS indicated that the fault tolerant design does not inherently increase the sensitivity of the pixel. The photodiode FTAPS achieves higher sensitivity because splitting the photodiode in half increases the conversion gain of each pixel half. As a result, each half of a photodiode FTAPS has the same sensitivity as a standard APS. When the outputs of each half are added, the overall sensitivity of the photodiode FTAPS approximately doubles. Since the conversion gain of the photogate FTAPS is the same as the standard APS conversion gain, its sensitivity is also the same. However,

an increase in its effective FD area results in a larger input saturation level and output swing. The DW APS pixels exhibited higher sensitivity and output swing because the double width amp and row transistor have high transconductance.

Tests on pixels fabricated in 0.18µm CMOS technology confirmed that photodiode FTAPS devices have higher sensitivity and voltage swing than standard pixels. Compared to pixels fabricated in a standard 0.35µm CMOS technology, the 0.18µm pixels were approximately half as sensitive.

Future work on the FTAPS should focus on how hot pixel defects could be corrected with this design. Recent study in this area has indicated that the most prevalent defects that occurs in the field are hot pixels. Thus, the behaviour of a FTAPS with a hot defect should be examined. If the FTAPS can recover from hot defects, its utility would be enhanced.

Now that the behaviour of the FTAPS has been characterized, the problem of defect identification will be addressed. Even though a defective FTAPS can be corrected for, its defect state must be identified first. The next chapter describes a method for identifying defective FTAPS.

4. On-Line Defect Identification Algorithm

One of the major criticisms of the FTAPS in the past has been that in order to correct for a defective pixel, both the location and type of defect must be identified. After an imager is manufactured, a factory calibration is often used to determine the location and type of each defective pixel so that they can be corrected for. With an FTAPS imager, the main difference would be that instead of having to interpolate the values of single defect pixels, their outputs could still be used with some correction. However, it is more difficult to identify pixels that become defective in the field.

To locate defective pixels, an imager could be sent back to the factory for re-calibration, however this is a time consuming process. A more efficient method would be to calibrate the imager in the field. A factory calibration examines the response of pixels to uniform light fields to characterize each pixel. Unfortunately, these uniform illuminations cannot be duplicated in the field without adding significant cost to the imager.

Some algorithms have been reported that identify defective pixels by analyzing a sequence of images taken normally in the field. Y. Tan and T. Acharya used sequential probability ratio testing and compared the difference between a pixel's output and the average output of its neighbouring pixels [32]. Their method was successful in finding defects, however it was also susceptible to falsely identifying defect free pixels as being faulty, otherwise known as false positives. Using a slightly different method, B. Jin et el compared the difference between a pixel's output and the average output of its neighbouring pixels with a threshold to determine if a pixel

is faulty [33]. They demonstrated that their method could potentially find and repair defective pixels in an imager, but the method has not been simulated or implemented.

To address the issue of identifying defects in the field, our research group presented an on-line defect identification algorithm [34] that can locate the pixel types described in Table 2. The following section describes this algorithm in detail.

4.1. On-Line Defect Identification Algorithm

In 2005, our research group reported an algorithm for on-line defect identification that uses statistics of the image over a sequence of normally taken images to identify defective pixels [34]. Consider the simple case of a pixel with a stuck low defect. In a single picture, if a pixel is dark it could be a stuck low pixel or a good pixel that happens to be dark in that picture. However, if a pixel is dark in a series of pictures, it is more likely that the pixel is stuck low rather than good. Thus, the on-line defect identification algorithm uses image data combined with statistics to determine pixel types. The following section describes the details of the algorithm.

For a series of T images, the pixel output at a given location (i,j) forms a set of samples $Y = y^{(0)}, y^{(1)},..., y^{(T)}$. For every possible defect state D, the set of samples Y is used as data with Bayesian inferences to calculate the likelihood a pixel is of that defect state. The Bayesian inference is expressed mathematically as

$$P(D \mid Y) = \frac{P(Y \mid D)P(D)}{\sum_{D' \in \{all\ D\}} P(Y \mid D')P(D')} \tag{10}$$

where $P(D|Y)$ is the likelihood that the pixel is defect type D given the set of samples Y. $P(Y|D)$ is a measure of how well the set of samples Y fits the behaviour of defect

state D which is obtained from a statistical metric from the image data and $P(D)$ is the *a priori* probability that the pixel is defect state D without any additional data. For example, $P(D)$ could be based on manufacturing data concerning the probability of defect type D. The denominator of equation 10 is a normalizing factor which scales $P(D|Y)$ based on the likelihood of the pixel being one of the other defect states.

Here is an example to illustrate how equation (10) is implemented. For a particular pixel, the probability of its pixel state being HH is to be calculated given a set of pixel outputs, i.e. $P(HH|Y)$. While $P(Y|HH)$ is given as a single probability in equation (10), a more practical implementation is to calculate $P(y^{(i)}|\mathrm{HH})$ for each pixel output $y^{(i)}$ in the set Y. If a pixel's output range is defined to be from 0 (min) to 1 (max), the output of a HH pixel is always 1. Thus, the probability of $P(y^{(i)}|\mathrm{HH})$ is

$$P\left(y^{(i)} \mid HH\right) = \begin{cases} 1, & y^{(i)} = 1 \\ 0, & otherwise \end{cases}.$$

The probability of a pixel being one of the other pixel states for a particular pixel output $y^{(i)}$ is given in Table 10. These probabilities are based on the expected behaviour of the pixel in each state as given in Table 2.

Table 10: Probability equations for the FTAPS pixel states given a pixel output $y^{(i)}$

Pixel State *CD*	$P(y^{(i)}\|CD)$
GG	$P\left(y^{(i)}\right)$
LL	$\begin{cases} 1, & y^{(i)} = 0 \\ 0, & otherwise \end{cases}$
HL	$\begin{cases} 1, & y^{(i)} = 0.5 \\ 0, & otherwise \end{cases}$
GL	$P\left(2y^{(i)}\right)$
GH	$P\left(2y^{(i)} - 1\right)$

Lastly, the *a priori* probability $P(HH)$ could be taken as the probability of a pixel being HH after manufacturing. For this example, assume $P(HH)=0.01$ for simplicity (which is unrealistically high). Ignoring the normalizing factor, it is evident that if the pixel is HH the probability $P(HH|Y)$ will approach 1 as the number of pixel outputs in the set Y increases. If the pixel is some other pixel type, if any of the pixel outputs is not V_{DD} then $P(HH|Y)$ will be 0.

4.2. Defect Identification Algorithm Simulation

The defect identification algorithm was evaluated by performing Monte Carlo simulations. A flowchart illustrating the procedure followed by the simulation is given in Figure 43. First, the location of all simulated defects is assigned. Each defect is also assigned a defect state from the set $\{GG, GL, GH, LH, HH, LL\}$ whose defect model is based on its output behaviour as given in the *Output* column of Table 2.

Next, the simulated defects are applied to the set of images to be analyzed. The set of images is taken from an image bank of regularly taken images that we consider to have no defects. The pixel outputs of the simulated defects are modified based on the defect model. For example, the pixel output of a HH pixel would be modified to always be the maximum possible pixel output.

In Step 3, the *a priori* probability $P(D)$ for every pixel is initialized for each defect state. Step 4 to Step 9 form a loop to iteratively calculate $P(D|Y)$ for each defect state at each pixel location. Since processing data from the entire image set at once would be computationally demanding, a single picture is considered at a time. In Step 4, the next image is loaded for analysis. Based on its image information, a probability density function $P_E(e)$ for a metric is calculated. Various metrics can be used, which will be described later.

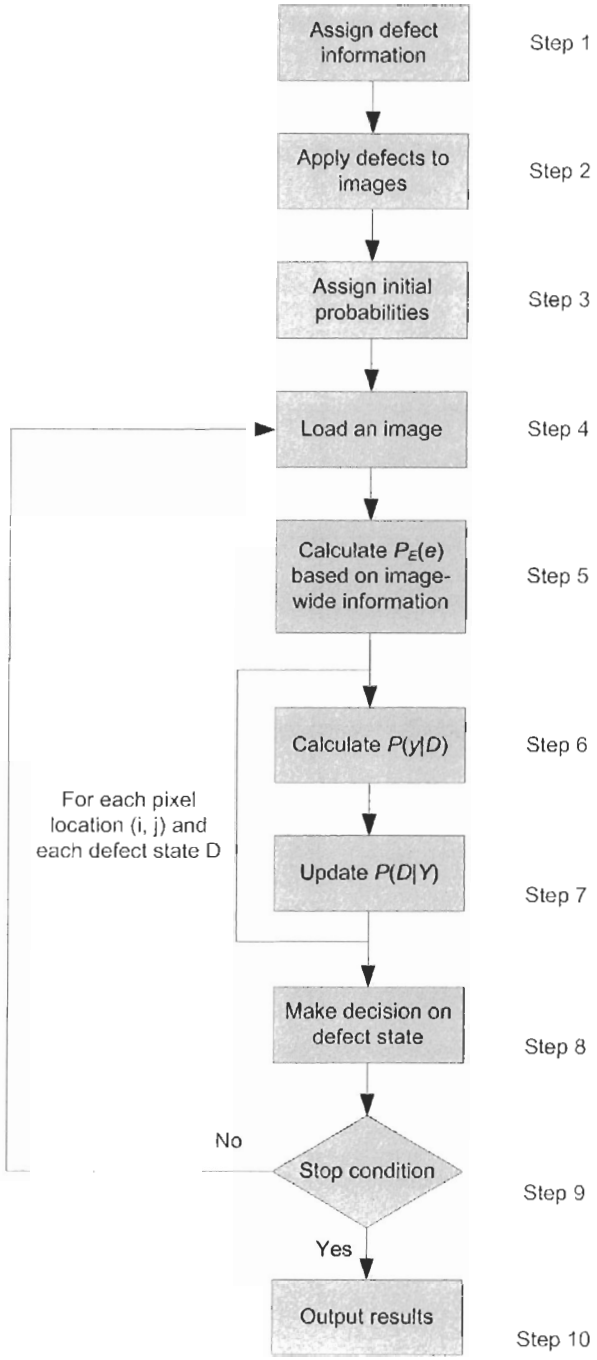

Figure 43: Defect identification simulation flow chart

Next, $P_E(e)$ and the metric are used to calculate how well a particular defect state fits the data. Then $P(D|Y)$ is evaluated which is used in subsequent iterations as the *a priori* probability, replacing $P(D)$. Thus, the *a priori* probability for iteration k will be the $P(D|Y)$ calculated in iteration $(k\text{-}1)$. Steps 6 and 7 are repeated for each defect

type and all pixel locations. In Step 8, a decision is made on the defect state of each pixel. One method of assigning defect states is to choose the most probable defect state for the pixel. Finally, the simulation checks to see if it should finish. If the stop condition is met, the simulation concludes by outputting the results. Otherwise, the simulation will loop back to Step 4 so that another image will be analyzed. One possible stop condition is to conclude the simulation when a certain number of images have been analyzed.

As mentioned in Step 5, $P_E(e)$ must be calculated so that $P(y|D)$ can be determined in Step 6. Two implementations that have been tested extensively are the image statistics method and the interpolation method. The image histogram, which is the distribution of pixel outputs in an image, is used as $P_E(e)$ in the image statistics method. The pixel output is the metric so the image statistics method considers the likelihood of a pixel having a particular output. For example, Figure 44 shows an image histogram of a picture where the minimum pixel value is 0 and the maximum pixel value is 255.

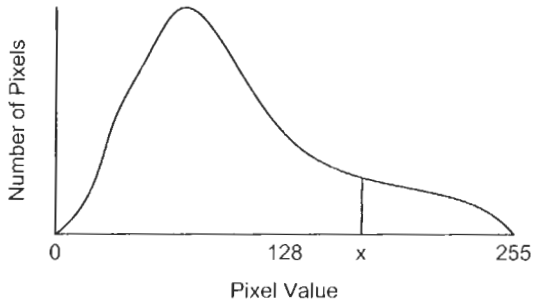

Figure 44: Sample image histogram

The likelihood of a pixel having a value of x is the number of pixels with the value of x divided by the total pixels. Also, usually very few have values of 0 or 255, so pixels which are consistently 0 or 255 are simple to identify as LL and HH.

When calculating $P(y|D)$, $P_E(e)$ is modified according to the defect state. Figure 45 shows the ideal pixel response of GG, GL, and GH pixels. The output of GG pixels can vary from 0 to 255, GL pixels from 0 to 128 , and GH pixels from 128 to 255. Thus, if the sample histogram in Figure 44 is modified for the GL defect, the histogram would look like Figure 46.

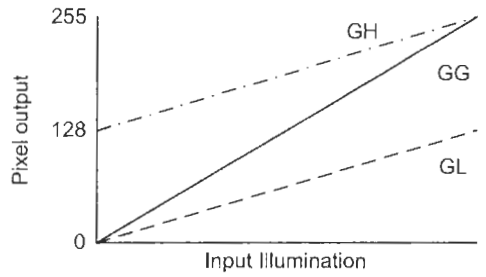

Figure 45: Ideal pixel response of GG, GL, and GH pixels

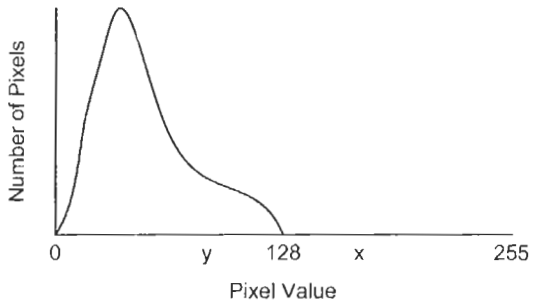

Figure 46: Sample histogram from Figure 44 modified for a GL

Now, if a pixel had value x, there would be no chance of it being a GL pixel. Its range is outside the 0 to 128 stated previously. However, a pixel with a value of y would have some probability of being a GL pixel, as well as a GG pixel.

A better technique is to use an interpolation algorithm to estimate what the output of each pixel should be. In this case, the metric becomes the interpolation error which is the error between the interpolated output and the actual output. To generate the $P_E(e)$ for the interpolation method, the interpolation error is calculated for all of the

pixels in an image. The distribution of the interpolation error becomes the probability density function $P_E(e)$.

4.3. Defect Identification Simulation Results

The preliminary results of the defect identification algorithm were presented in [34]. The image histogram was used as $P_E(e)$ and two defect models were tested. The "simple" defect model, simulated a conventional APS or CCD imager having the set of pixel states $\{G, H, L\}$. In the FTAPS defect model, the set of possible FTAPS pixel states $\{GG, GL, GH, LH, HH, LL\}$ were simulated. A 5% defect rate was used for the "simple" defect model and a 0.5% defect rate was used for the FTAPS defect model. These defect rates are both unrealistically high, however to glean useful information from the simulations it was easier to use a higher defect rate so that each defect state was well represented.

A bank of 398 pictures was used as the image bank for the simulations. The image bank was deemed to be typical of a set of pictures an amateur photographer might take. Figure 47 shows a sample picture taken from the test bank before and after artificial defects were applied. A random set of images was chosen from the image bank for each simulation iteration with 100 iterations run in total for each set of test parameters. To reduce the time taken to run each simulation, 1 Megapixel images were used. As well, a "dark field" or was used for the first image of each iteration. A dark field is an all-dark picture which could be produced by taking a picture with the lens cap of the camera on. This is not an unreasonable image to include since no special equipment is needed to produce a dark field image with a digital camera.

(a) Original picture

(b) Picture with defects applied

Figure 47: Sample picture before (a) and after (b) defects are applied

From Figure 43, the "stop condition" for a simulation iteration was when each defect was identified with a 99% confidence threshold. If the 99% confidence threshold was not reached after all 398 pictures in the image bank had been loaded the algorithm

was deemed to have failed. The number of images taken to satisfy the stop condition was used to compare the performance of each simulation run.

The simple defect model was tested first to simulate a conventional digital camera where the set pixel states is $\{G, H, L\}$. The results of the simulation are illustrated in Figure 48. The defect identification algorithm only needed 3.45 pictures on average and no more than 20 pictures to correctly identify all defects with no false positives. These results suggest that the on-line defect identification algorithm is suitable for identifying defects in conventional digital camera systems.

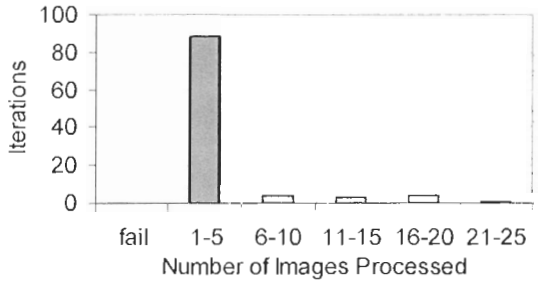

Defect Model	Average	Standard Deviation	Fail
Simple	3.45	3.91	0

Figure 48: Convergence rate of defect identification algorithm on simple defect model

Next, the more complicated FTAPS defect model was tested to simulate a camera system using an FTAPS array. From Figure 49, it is evident that the FTAPS defect model took much longer to identify all the defects. To correctly identify all defective pixels with no false positives, it took 114 pictures on average and up to a maximum of 240 pictures. The FTAPS defect model took much longer to identify all defects because the GH and GL pixels have more complicated behaviour than HH and LL pixels. GH and GL pixels respond to changes in illumination while HH, HL, and LL pixels always have a fixed value.

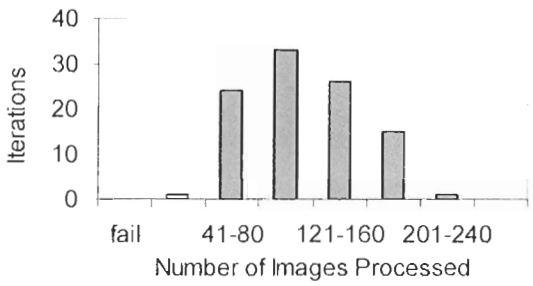

Defect Model	Average	Standard Deviation	Fail
FTAPS	114.13	41.05	0

Figure 49: Convergence rate of defect identification algorithm on FTAPS defect model

The fact that it could take up to 240 pictures or perhaps more to identify all defects for the FTAPS model is of concern. However, while 240 pictures may seem like a lot, a photographer could easily take that many pictures over the course of a couple months. Furthermore, it is important to note that the algorithm did not fail even once in 100 iterations and there were no false positives. This work suggested that the on-line defect identification algorithm could be used to identify defects of a camera in the field. Building on this work, J. Dudas et el continued developing the defect identification algorithm and were able identify all FTAPS defects within 50 pictures in each simulation in [35].

4.4. On-Line Defect Identification Algorithm Summary

Due to criticisms of the FTAPS design that defects must be identified before they can be corrected for, an on-line defect identification algorithm was proposed to solve this problem. The algorithm uses statistics of the image over a sequence of normally taken images combined with Bayesian inferences to identify defective pixels. To test the validity of the algorithm, Monte Carlo simulations were run using a simple defect model and a FTAPS defect model. All defects were identified with no false positives for 100 iterations with both defect models. The simple defect model converged in 3.45 pictures on average. Since the simple defect model mimics a conventional

digital camera, the on-line defect algorithm is suitable for finding stuck defects in current digital cameras. The FTAPS defect model took 114.13 pictures on average to converge as a result of the increased complexity of GH and GL defects. This preliminary work is a proof-of-concept for the on-line defect identification algorithm that addresses the issue of identifying FTAPS defects.

5. Fault Tolerant Active Pixel Sensor Noise Analysis

While the FTAPS has the ability to partially recover from defects, there are tradeoffs to adding fault tolerance. The most obvious tradeoff is a reduction in the pixel's Fill Factor (FF) due to the addition of transistors. Another issue to consider is the addition of noise in the system. It is expected that the noise in the system will increase, since the additional transistors will contribute to the noise. However, it is not clear how significantly the system's overall performance will be affected.

K. Salama et el suggested that the noise added by the FTAPS design is significant, particularly at low illumination levels [19]. The FTAPS was re-analyzed in [36] by C. Jung et el and they concluded that the additional noise added by the FTAPS design was negligible at all but the lowest illumination levels. These noise analyses were both done for photodiode FTAPS designs. The analysis by C. Jung et el also assumed that the designs would be fabricated in 0.18µm CMOS fabrication technology.

In this chapter, the noise of a photodiode FTAPS design in 0.35µm CMOS technology is compared and contrasted with the noise of a standard APS design. Since most of the APS testing presented in this thesis deals with devices fabricated in 0.35µm devices, it is appropriate to analyze the noise for this technology. It uses model files for 0.35µm devices and corrects some minor errors made in the analysis presented in [36].

5.1. Active Pixel Sensor Noise Analysis Background

For the noise analysis of the APS designs, the focus is on in-pixel noise. The noise generated by sampling of the APS output was neglected for simplicity. However, to model the test setup that was used as closely as possible, the column amplifiers used to convert the current output to a voltage (see Figure 31) were included in the analysis.

For comparison, the noise of a standard APS and a FTAPS were analyzed. The analysis of both pixels is similar and overlaps in several instances. The specific circuits that were analyzed are shown in Figure 50.

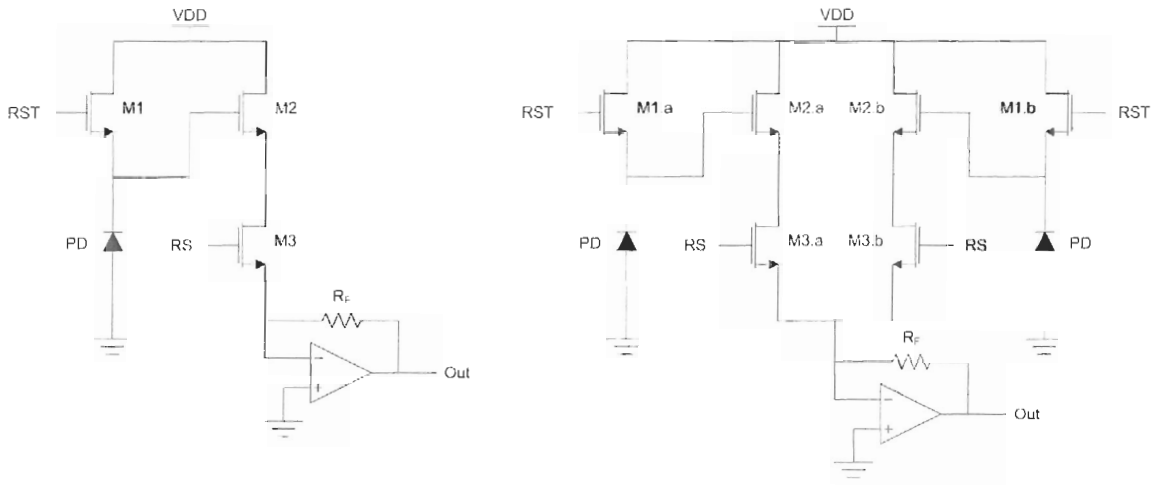

Figure 50: Schematics of photodiode APS designs for noise analysis (a) standard APS, (b) FTAPS

Each of the noise sources discussed in Section 2.5, shot noise, thermal noise, and flicker noise, were considered in the noise analysis. In most analyses, the noise is referred to the input or output of the pixel. Since the FTAPS has two photodiodes, and thus two inputs, the noise was output referred.

The analysis began by determining equations for the noise contributed by each circuit component. These equations were used to derive expressions for the total noise produced by a standard APS and a FTAPS. Then the total noise of each APS design was calculated qualitatively using parameter values derived from HSpice simulations, device datasheets, and experimental data. Finally, the calculated noise of the standard APS and FTAPS were compared and analyzed.

5.2. Noise Analysis of Active Pixel Sensor Components

5.2.1. Photodiode

Three sources of noise are present at the photodiode of an APS device. Photocurrent shot noise is noise that results from the optical generation of carriers. From equation (6), the photocurrent shot noise in electrons is

$$q_{t,ph} = \sqrt{\frac{I_{ph} T_{exp}}{q_e}} \tag{11}$$

where I_{ph} is the photocurrent, T_{exp} is the exposure time, and q_e is the charge of an electron.

The dark current that results from thermally generated carriers in the photodiode also produces a shot noise. The equation for dark current shot noise in electrons is

$$q_{t,dk} = \sqrt{\frac{I_{dk} T_{exp}}{q_e}} \tag{12}$$

where I_{dk} is the dark current.

Lastly, when an APS is reset, the capacitance at the gate of the amp transistor is charged to the reset level. This results in a thermal noise that is often referred to as the reset noise of a pixel. The reset noise in electrons is

$$q_{t,reset} = \frac{\sqrt{kTC_{PD}}}{q_e} \tag{13}$$

where k is Boltzmann's constant, T is the temperature, and C_{PD} is the capacitance of the photodiode. Since the photocurrent shot noise, dark current shot noise, and reset noise are generated at the gate of the amp transistor, they were output referred later in the analysis.

5.2.2. Amplifying Transistor

The transistors in an APS circuit produce both thermal noise and flicker noise. Dağerli et el used simulation-oriented MOSFET noise models to calculate the thermal and flicker noise of transistors in CMOS image sensors [37]. Their technique was used in the noise analysis of the standard APS and FTAPS as well.

First, the small signal model of the standard APS was analyzed for simplicity. The schematic of the standard photodiode APS shown in Figure 7 was converted to its small signal model shown in Figure 51.

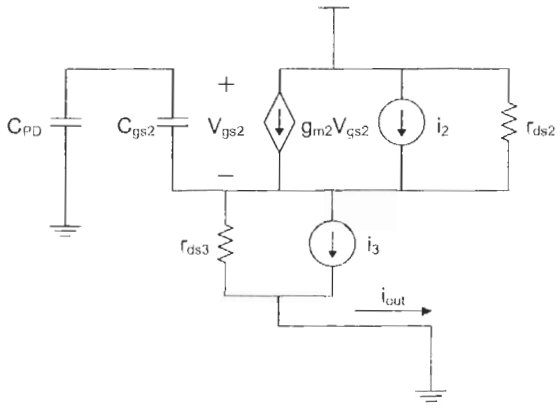

Figure 51: Small signal model of a photodiode APS

The amp transistor M2 normally operates in the linear region, so it was modelled by its gate-source capacitance (C_{gs2}), a voltage-controlled current source connected from drain to source ($g_{m2}V_{gs2}$), and its drain-source resistance (r_{ds2}). Noise produced

by the amp transistor was represented by a current source connected from its drain to source (i_2). The row transistor M3 normally operates in the saturation region, so it was modelled differently from the amp transistor. The small signal model of the row transistor consisted of only its drain-source resistance (r_{ds3}) with its noise modelled as a current source connected from its drain to source (i_3).

From the small signal model, the output noise current due to amp transistor noise is

$$i_{out2} = \frac{i_2}{s\frac{r_{ds3}C_{gs2}C_{PD}}{C_{gs2}+C_{PD}} + \frac{g_{m2}r_{ds3}C_{PD}}{C_{gs2}+C_{PD}} + \frac{r_{ds3}}{r_{ds2}} + 1}. \tag{14}$$

Re-arranging equation (14), gave a simpler expression for i_{out2}:

$$i_{out2} = k_2 \frac{i_2}{1+sk_2} \tag{15}$$

where

$$k_2 = \frac{r_{ds2}(C_{gs2}+C_{PD})}{g_{m2}r_{ds2}r_{ds3}C_{PD} + (C_{gs2}+C_{PD})(r_{ds2}+r_{ds3})}. \tag{16}$$

Note that $1/k_2$ is the pole of i_{out2}. The output noise current is converted to voltage by the column amplifier, so the mean square output noise is given by

$$\overline{V_o^2} = \int_0^\infty \left| i_{out} R_F \right|^2 df. \tag{17}$$

where R_F is the feedback resistance of the column amplifier.

Next, expressions for the thermal noise and flicker noise were substituted for i_2. In the simulation-oriented models employed by Dağerli et el, the thermal noise produced by a transistor in the linear region is

$$i_{2,t} = \sqrt{\frac{8}{3} kTg_{m2}} \,. \tag{18}$$

To calculate the thermal noise of the amp transistor seen at the output of the circuit, the integral in equation (17) was simplified by noting that the noise bandwidth of the operational amplifier N_{BW} was smaller than the pole of i_{out2}. This simplified the integral so the mean square output thermal noise of the amp transistor is

$$\overline{V_{o2,t}^2} = k_2^2 i_{2,t}^2 R_F^2 N_{BW} \,. \tag{19}$$

Then, substituting equation (18) into equation (19) yields the final expression for the mean square output thermal noise of the amp transistor:

$$\overline{V_{o2,t}^2} = \frac{8}{3} kTg_{m2} k_2^2 R_F^2 N_{BW} \,. \tag{20}$$

To estimate the flicker noise, an empirical model was used. The model is not accurate under all conditions, but is suitable as an estimate. The flicker noise of a transistor is modelled as

$$i_f = \sqrt{\frac{K_F I_{ds}^{A_F}}{C_{ox} L_{eff}^2 f^{E_F}}} \tag{21}$$

where K_F, A_F, and E_F are flicker noise constants in HSpice models, I_{ds} is the drain-to-source current, C_{ox} is the oxide capacitance for the process technology, L_{eff} is the effective length of the transistor, and f is the frequency of the observation time. In the BSIM3 0.35µm model file for NMOS transistors, A_F and E_F are equal to one or close to one, so equation (21) was simplified to

$$i_f = \sqrt{\frac{K_F I_{ds}}{C_{ox} L_{eff}^2 f}} \,. \tag{22}$$

Equation (22) was substituted into equation (15) to get the flicker noise generated in the amp transistor. The resulting expression was then substituted into equation (17) so the mean square output flicker noise of the amp transistor is

$$\overline{V_{o2f}^2} = k_2^2 R_F^2 \frac{K_F I_{ds3}}{C_{ox} L_{eff}^2} \int_0^{\infty} \frac{1}{f\left(1 + f^2 / f_0^2\right)} df \,. \tag{23}$$

where f_s is the frequency of observation time, i.e. the time taken to sample the Readout and Reset voltages in an exposure cycle. The closed form solution of the integral is

$$\int_{f_s}^{\infty} \frac{1}{f\left(1 + f^2 / f_0^2\right)} df = \frac{1}{2} ln\left(1 + \frac{f_0^2}{f_s^2}\right). \tag{24}$$

so the final expression for the mean square output flicker noise of the amp transistor is

$$\overline{V_{o2,f}^2} = \frac{k_2^2 R_F^2}{2} \frac{K_F I_{ds3}}{C_{ox} L_{eff}^2} \ln\left(1 + \frac{N_{BW}^2}{f_s^2}\right) \tag{25}$$

5.2.3. Row Transistor

Just like the amp transistor, the row transistor produces both thermal and flicker noise. From the small signal circuit in Figure 51, the output noise current due to row transistor noise is

$$i_{out3} = \frac{i_3 r_{ds3}\left(s\frac{C_{gs2}C_{PD}}{C_{gs2}+C_{PD}} + g_{ds2} + \frac{g_{m2}C_{PD}}{C_{gs2}+C_{PD}}\right)}{r_{ds3}\left(s\frac{C_{gs2}C_{PD}}{C_{gs2}+C_{PD}} + g_{ds2} + \frac{g_{m2}C_{PD}}{C_{gs2}+C_{PD}}\right) + 1}. \tag{26}$$

Since $C_{PD} >> C_{gs2}$, Equation (26) was simplified to

$$i_{out3} = \frac{sC_{gs2} + g_{m2} + g_{ds2}}{sC_{gs2} + g_{m2} + g_{ds2} + g_{ds3}} i_3 . \qquad (27)$$

Using simulation-oriented models for the thermal noise of the row transistor in saturation was

$$i_{3,t} = \sqrt{4kTg_{ds3}} . \qquad (28)$$

Since the pole and zero in equation (27) are again larger than the noise bandwidth of the operational amplifier, substituting equation (27) into equation (17) yields

$$\overline{V_{o3,t}^2} = \frac{g_{m2} + g_{ds2}}{g_{m2} + g_{ds2} + g_{ds3}} i_{3,t}^2 R_F^2 N_{BW} . \qquad (29)$$

The final expression for the mean square thermal noise of the row transistor is derived by simply substituting for $i_{3,t}$:

$$\overline{V_{o3,t}^2} = 4kTg_{ds3}\left(\frac{g_{m2} + g_{ds2}}{g_{m2} + g_{ds2} + g_{ds3}}\right)^2 R_F^2 N_{BW} . \qquad (30)$$

The flicker noise generated by the row transistor uses the same model described in equation (22). Using the same method used to calculate the mean square flicker noise of the amp transistor for the row transistor, yields

$$\overline{V_{o3,f}^2} = \left(\frac{g_{m2} + g_{ds2}}{g_{m2} + g_{ds2} + g_{ds3}}\right) R_F^2 \frac{K_F I_{ds3}}{C_{ox} L_{eff}^2} \int_0^\infty \frac{1}{f\left(1 + f^2 / f_0^2\right)} df . \qquad (31)$$

Lastly, evaluating the integral results in the mean square flicker noise of the row transistor as

$$\overline{V_{o3,f}^2} = \left(\frac{g_{m2} + g_{ds2}}{g_{m2} + g_{ds2} + g_{ds3}}\right) \frac{R_F^2}{2} \frac{K_F I_{ds3}}{C_{ox} L_{eff}^2} \ln\left(1 + \frac{N_{BW}^2}{f_s^2}\right) . \qquad (32)$$

5.2.4. Feedback Resistor

The feedback resistor used in the column amplifier generates thermal noise. The expression for the mean square feedback resistor thermal noise is similar to equation (7):

$$\overline{V_{o,R_F}^2} = 4kTR_F N_{BW} \tag{33}$$

5.2.5. Operational Amplifier

The operational amplifier used for the column amplifiers is a low noise amplifier, so only the noise voltage was considered. The output noise voltage from the operational amplifier is

$$V_{o,op} = V_{op}\left(1 + \frac{R_F}{R_{APS}}\right). \tag{34}$$

R_{APS} is the resistance of the APS that is seen at the input of the operational amplifier. From the small signal circuit in Figure 51, for a standard APS

$$R_{APS,st} = r_{ds3} + \frac{\left(C_{gs2} + C_{PD}\right) r_{ds2}}{r_{ds2}C_{PD}\left(g_{m2} + sC_{gs2}\right) + C_{gs2} + C_{PD}}. \tag{35}$$

Equation (35) is simplified by disregarding the sC_{gs2} term since $g_{m2} >> sC_{gs2}$. The simplified expression for R_{APS} is

$$R_{APS,st} = r_{ds3} + \frac{\left(C_{gs2} + C_{PD}\right) r_{ds2}}{g_{m2}r_{ds2}C_{PD} + C_{gs2} + C_{PD}}. \tag{36}$$

The expression for R_{APS} for the FTAPS is slightly different due to the additional circuitry in the design. Since the FTAPS operates two half pixels in parallel, the resistance seen by the operational amplifier for an FTAPS is the resistance of the two half pixels in parallel:

$$R_{APS,ft} = \frac{1}{2}\left(r_{ds3} + \frac{\left(C_{gs2} + C_{PD}\right) r_{ds2}}{g_{m2} r_{ds2} C_{PD} + C_{gs2} + C_{PD}} \right). \tag{37}$$

Also, note that the photodiode capacitance used in equation (36) will differ from that used in equation (37).

From equation (34), the output mean square noise of the operational amplifier is

$$\overline{V_{o,op}^2} = \int_0^{\infty} \left| V_{op}^2 \left(1 + \frac{R_F}{R_{APS}} \right)^2 \right| df \,. \tag{38}$$

For thermal noise, V_{op} is the thermal noise density of the amplifier v_t. Thus, the output mean square thermal noise of the operational amplifier is

$$\overline{V_{o,op,t}^2} = v_t^2 \left(1 + \frac{R_F}{R_{APS}} \right)^2 . \tag{39}$$

For flicker noise, V_{op} is

$$V_{op} = v_t \sqrt{\frac{f_{ce}}{f}} \tag{40}$$

where f_{ce} is the noise corner frequency of the operational amplifier. Substituting for V_{op} in equation (38) and solving the integral yields the output mean square flicker noise of the operational amplifier:

$$\overline{V_{o,op,f}^2} = \frac{v_t^2 f_{ce}}{2} \left(1 + \frac{R_F}{R_{APS}} \right)^2 ln\left(1 + \frac{N_{BW}^2}{f_s^2} \right). \tag{41}$$

5.3. Total Noise of Active Pixel Sensor Designs

The total mean square noise of each APS design was derived by summing each of the noise components. However, the equations for photocurrent shot noise, dark

current shot noise, and reset noise given in equations (11), (12), and (13) are in terms of noise charge at the gate of the amp transistor. These noise sources must be output referred before summing all of the noises. The noise charge at the gate of the amp transistor is converted to voltage by the capacitance at that node, primarily consisting of the capacitance of the photodiode. The transconductance of the amp transistor converts the voltage at its gate to the drain-source current that flows through the amp transistor and row transistor. The amp transistor is operated as a common source amplifier with the row transistor acting as a source resistance. Finally, the current is converted to voltage by the column amplifier. The noise charge is converted to mean square output noise by

$$\overline{V_o^2} = \left(\frac{A_v q_t q_e R_F}{C_{PD}} \right)^2 \tag{42}$$

where

$$A_v = \frac{g_{m2}}{1 + g_{m2} r_{ds3}} \tag{43}$$

which is the gain of a source degenerated common source amplifier. Thus, the mean square output photocurrent shot noise is

$$\overline{V_{o,ph}^2} = \left(\frac{g_{m2} q_{t,ph} q_e R_F}{(1 + g_{m2} r_{ds3}) C_{PD}} \right)^2, \tag{44}$$

the mean square output dark current shot noise is

$$\overline{V_{o,dk}^2} = \left(\frac{g_{m2} q_{t,dk} q_e R_F}{(1 + g_{m2} r_{ds3}) C_{PD}} \right)^2, \tag{45}$$

and the mean square output reset noise is

$$\overline{V_{o,rst}^2} = \left(\frac{g_{m2} q_{t,rst} q_e R_F}{(1 + g_{m2} r_{ds3}) C_{PD}} \right)^2. \tag{46}$$

Summing all of the noise sources for a standard APS yields the total mean square noise:

$$\overline{V_{o,tot,st}^2} = \overline{V_{o,ph}^2} + \overline{V_{o,dk}^2} + \overline{V_{o,rst}^2} + \overline{V_{o2,t}^2} + \overline{V_{o2,f}^2} + \overline{V_{o3,t}^2} + \overline{V_{o3,f}^2} + \overline{V_{o,R_F}^2} + \overline{V_{o,op,t}^2} + \overline{V_{o,op,f}^2} \quad (47)$$

The expression for the total mean square noise of the FTAPS is very similar to that of the standard APS. The main difference is that many of the noise sources are doubled, since the FTAPS operates two pixel halves in parallel. Photocurrent shot noise, dark current shot noise, reset noise, and transistor noises are all doubled. However, the magnitudes of the respective noises for the FTAPS differ from the standard pixel. For example, the photodiode capacitance C_{PD} of the FTAPS is about half as large as C_{PD} for the standard APS, which greatly impacts many of the noises. The total mean square noise of the FTAPS is

$$\overline{V_{o,tot,ft}^2} = 2\overline{V_{o,ph}^2} + 2\overline{V_{o,dk}^2} + 2\overline{V_{o,rst}^2} + 2\overline{V_{o2,t}^2} + 2\overline{V_{o2,f}^2} + 2\overline{V_{o3,t}^2} + 2\overline{V_{o3,f}^2} + \overline{V_{o,R_F}^2} + \overline{V_{o,op,t}^2} + \overline{V_{o,op,f}^2} \quad (48)$$

5.4. Noise Analysis Parameter Values

Before the noise of the standard APS and FTAPS could be qualitatively evaluated, the values of all of the component parameters were determined using component datasheets, experimental data, and HSpice simulation.

The operational amplifier used for the column amplifiers was the TLC2274 – a low noise quad operational amplifier. The datasheet for the TLC2274 provided the noise bandwidth, corner frequency, and thermal noise density of the amplifier.

The dark current of the pixels was determined experimentally using the technique reported by I. Shcherback et el [38]. The signal of a standard APS was measured after a long cycle time with no illumination. The dark current density wass then given by

$$dark\ current\ density = \frac{C_{PD}}{A_{PD}} \times \frac{\Delta V}{\Delta t}. \tag{49}$$

where A_{PD} is the area of the photodiode, ΔV is the change in the output voltage, and Δt is the cycle time.

HSpice was used to estimate most of the remaining circuit parameters, particularly the small signal values. Several DC point simulations of the APS circuit were done to extract the parameters of the circuit for different illumination levels. The noise of the APS designs was evaluated for three conditions:

- dark – no illumination
- average – illumination level that produces half of maximum output
- saturation – illumination level that saturates the pixel output

The small signal parameters of the transistors were extracted from these simulations. Some parameters were also taken from the model file such as the oxide capacitance C_{ox}.

The last source of parameter values were the experiments themselves. From the timing of the control signals, parameters such as the exposure time T_{exp} were taken. All of the parameter values used in the noise analysis are shown in Table 11, Table 12, and Table 13. The parameters in Table 11 are illumination independent whereas Table 12 and Table 13 show parameter values that vary with the illumination conditions. These parameter values were used to calculate the contribution of each noise source and the total noise of each APS design.

Table 11: Illumination independent parameter values for APS noise analysis

Parameter	Variable	Design	Value
Noise bandwidth [Hz]	N_{BW}	Both	1.0E+06
Corner frequency [Hz]	f_{ce}	Both	1.0E+03
Thermal noise density [V]	v_t	Both	2.846E-07
Feedback resistance [Ω]	R_F	Both	2.7E+04
Exposure time [s]	T_{exp}	Both	1.32E-02
Observation frequency [Hz]	f_s	Both	6.67E+02
Oxide capacitance [F/m^2]	C_{ox}	Both	4.604E-03
Effective transistor length [m]	L_{eff}	Both	2.7E-07
Flicker noise coefficient	K_F	Both	1.00E-24
Photodiode capacitance [F]	C_{PD}	Standard	4.177E-14
		Fault tolerant	8.296E-14
Dark current [A]	I_{dk}	Standard	1.18E-14
		Fault tolerant	5.90E-15

Table 12: Photocurrent for dark, average, and saturation illumination conditions

		Dark	Average	Saturation
Photocurrent I_{ph} [A]	Standard	0	5.00E-12	1.20E-11
	Fault tolerant	0	2.50E-12	6.00E-12

Table 13: Small signal transistor parameters under dark, average, and saturation illumination conditions

Transistor	Parameter	Dark	Average	Saturation
Amp	g_{m2} [A/V]	1.187E-04	1.029E-04	3.259E-06
	g_{ds2} [A/V]	3.586E-06	2.909E-06	4.001E-08
	r_{ds2} [Ω]	2.789E+05	3.438E+05	2.499E+07
	C_{gs2} [F]	5.202E-16	5.159E-16	2.499E-17
	I_{ds2} [A]	9.269E-05	4.037E-05	1.426E-07
Row	g_{ds3} [A/V]	2.768E-04	3.204E-04	3.526E-04
	r_{ds3} [Ω]	3.613E+03	3.131E+03	2.836E+03
	I_{ds3} [A]	9.269E-05	4.037E-05	1.426E-07

5.5. Noise Comparison of the Standard Active Pixel Sensor and Fault Tolerant Active Pixel Sensor

Using the equations derived in Section 5.2 and the parameter values determined in the Section 5.4, the noise of the standard APS and FTAPS designs were calculated. A summary of the mean square noise generated by each source is shown in Table 14.

From Table 14, it is evident that the mean square noise generated at the photodiode of a FTAPS is approximately twice as large as in the standard APS. Furthermore, the mean square photocurrent shot noise, dark current shot noise, and reset noise listed in the table is only for one half of a FTAPS. Since there are two photodiodes in a fault tolerant pixel, these noises were doubled again.

Noise generated by the amp transistor, row transistor, and feedback resistor are the same for both the standard APS and FTAPS. As with the photodiode noises, the transistor noise listed in Table 14 is for one half of a FTAPS. The noise generated by the operational amplifier is slightly larger in the FTAPS than in the standard APS. The resistance of the APS seen from the input of the operational amplifier R_{APS} is smaller in the FTAPS case which results in higher noise.

The dominant noise source for all illumination conditions transistor flicker noise. In particular, the amp transistor mean square noise is at least an order of magnitude larger than any other noise source. An ideal APS is photocurrent shot noise limited, where the photocurrent shot noise is the dominant noise source for most illumination levels. This analysis shows that electronic noise, in the form of transistor flicker noise, dominates at all illumination levels for the standard APS and FTAPS fabricated in 0.35μm technology.

Table 14: Summary of the mean square noise of each source for the standard APS and FTAPS

Component	Noise Type	Illumination	Standard (V^2)	Fault tolerant (V^2)
Photodiode	Photocurrent shot ($\overline{V_{o,ph}^2}$)	Dark	0	0
		Average	6.788E-06	1.338E-05
		Saturation	2.799E-08	5.518E-08
	Dark current shot ($\overline{V_{o,dk}^2}$)	Dark	1.815E-08	3.578E-08
		Average	1.595E-08	3.146E-08
		Saturation	2.741E-11	5.405E-11
	Reset ($\overline{V_{o,rst}^2}$)	Dark	2.510E-07	4.984E-07
		Average	2.206E-07	4.382E-07
		Saturation	3.790E-10	7.527E-10
Amp Transistor	Thermal ($\overline{V_{o2,t}^2}$)	All	4.692E-10	4.692E-10
	Flicker ($\overline{V_{o2,f}^2}$)	Dark	8.343E-04	8.343E-04
		Average	3.633E-04	3.633E-04
		Saturation	1.284E-06	1.284E-06
Row Transistor	Thermal ($\overline{V_{o3,t}^2}$)	All	2.383E-10	2.383E-10
	Flicker ($\overline{V_{o3,f}^2}$)	Dark	9.077E-05	9.077E-05
		Average	3.953E-05	3.953E-05
		Saturation	1.397E-07	1.397E-07
Feedback Resistor	Thermal ($\overline{V_{o,R_F}^2}$)	All	4.469E-10	4.469E-10
Operational Amplifier	Thermal ($\overline{V_{o,op,t}^2}$)	All	7.977E-07	2.239E-06
	Flicker ($\overline{V_{o,op,f}^2}$)	All	5.834E-09	1.637E-08

Equation (46) and (47) were used to calculate the total noise of each APS design. Table 15 lists the total mean square noise and total noise for the standard APS and FTAPS under the dark, average, and saturation illumination conditions.

Table 15: Summary of the total noise for the standard APS and FTAPS

	Illumination	Standard	Fault Tolerant	Noise Ratio (FT: Standard)
Total Mean Square Noise [V^2]	Dark	9.262E-04	1.853E-03	2.001
	Average	4.107E-04	8.357E-04	2.035
	Saturation	2.257E-06	5.216E-06	2.311
Total Noise [V]	Dark	3.043E-02	4.305E-02	1.415
	Average	2.027E-02	2.891E-02	1.426
	Saturation	1.502E-03	2.284E-03	1.520

As there are two amp transistors and row transistors in the FTAPS, the mean square transistor flicker noise in a FTAPS is double that of a standard APS. Since the flicker noise is the dominant noise source, the total mean square noise of a FTAPS is also approximately double that of a standard APS. The result is the total noise of a FTAPS is greater than the noise of a standard APS by approximately the square root of two. However, this is not the worst case scenario.

In other process technologies, it is likely that the transistor flicker noise would not be the dominant noise source. The worst-case scenario is if one of the photodiode noises were dominant. If that were the case, the total mean square noise of a FTAPS would be quadruple that of a standard APS leading to twice as much total noise. This is a likely situation as the photocurrent shot noise was found to be the dominant noise source in APS devices fabricated in 0.18μm CMOS technology [36].

The overall performance of the photodiode FTAPS does not suffer due to increased noise because its sensitivity also increases by approximately two, as stated in Chapter 3. In the worst case, where photodiode noise is dominant, the noise and

sensitivity of the FTAPS are both doubled in comparison with the standard APS. Thus, the SNR of the FTAPS is the same as a standard APS. In the instances where the flicker noise is dominant, the noise of the FTAPS only increases by a factor of the square root of two. In this case, the SNR of the FTAPS is actually better than that of the standard APS by a factor of the square root of two.

While the SNR was not calculated in this work, a modified mean square noise was calculated for the FTAPS to illustrate the effect of increased sensitivity. The total mean square noise of the FTAPS was divided by two to simulate the effect of a two times increase in sensitivity on the FTAPS SNR. Table 16 shows the modified FTAPS mean square noise and the noise ratio compared to the standard APS. In each case, the noise ratio as close to one, which validates the argument that the overall performance of the photodiode FTAPS. The increased sensitivity of the photodiode FTAPS compensates for the increased noise in the FTAPS SNR.

Table 16: Comparison of standard APS total mean square noise and FTAPS modified total mean square noise

	Illumination	Standard	Fault Tolerant (modified)	Noise Ratio (FT: Standard)
Total Mean Square Noise [V^2]	Dark	9.262e-04	9.267e-04	1.001
	Average	4.107e-04	4.179e-04	1.017
	Saturation	2.257e-06	2.608e-06	1.156

5.6. Noise Analysis Conclusion

The noise of the standard photodiode APS and photodiode FTAPS was analyzed and compared. Sources of shot noise, thermal noise, and flicker noise were identified in each APS component and equations were derived to describe the behaviour of each noise source. The noises were output referred so that they could be summed together to determine the total noise of each APS design. HSpice simulations,

component datasheets, and experimental data were used to determine the parameter values in the noise analysis so that the noise of each source could be calculated quantitatively.

The noise of each source was calculated for dark, average, and saturation illumination conditions. The dominant noise source for pixels fabricated in 0.35μm CMOS technology was transistor flicker noise for all illumination conditions. After totalling the noise of each APS design, the noise of the FTAPS was larger by the square root of two. In the worst-case scenario where a photodiode noise is dominant, the noise of the FTAPS is twice as large as the standard APS. Since the sensitivity of the photodiode FTAPS is approximately twice as large as for the standard APS, the SNR of the FTAPS is greater by the square root of two when the transistor flicker noise dominates and is the same as a standard APS when a photodiode noise dominates.

6. Duo-output Active Pixel Sensors

The DAPS has the potential to be used for background subtraction and LIDAR. One of the main requirements of these applications is the sensitivity of the readout circuits in a DAPS must be reasonably matched. A mismatch in sensitivity results in a "noise" in the output when background subtraction is performed. Since each DAPS has two readout circuits, variations in the fabrication process can cause the sensitivities of these circuits to differ. This is a common problem encountered with APS arrays and is considered a type of FPN.

After testing a previous design of the photogate DAPS fabricated in 0.18μm CMOS technology, S. Djaja noted that the sensitivity of the readout circuits in a given DAPS were poorly matched [26]. He also suggested some methods of improving the sensitivity matching of the DAPS readout circuits.

Three DAPS designs were fabricated that incorporated some of S. Djaja's suggestions in an attempt to improve the sensitivity matching of the sensor. Initial testing focused on determining which design's readout circuits that were best matched. Once the design with the best sensitivity matching was identified, the background subtraction capabilities of the sensor were tested. Lastly, the issue of crosstalk was examined.

6.1. Duo-Output Active Pixel Sensor Layouts

The DAPS layouts that were fabricated in 0.35μm technology incorporated two suggestions given by S. Djaja. The first suggestion was to reduce the effect of

process variations by laying out the readout circuitry on the same side of the pixel so that they would be closer together. In previous DAPS designs, the readout circuitry was oriented on opposite sides of the pixel.

The second suggestion involved the parasitic n+ diffusions of the DAPS. As shown in Figure 9, the parasitic n+ diffusion is the diffusion that lies between the photogate and the transfer gate of the pixel. Instead of trying to match the sizes of the parasitic n+ diffusions in the readout circuits, it was proposed that the diffusions of both readout circuits be joined. Since the parasitic n+ diffusion would be shared, matching of the diffusion would not be needed. This approach was also taken by J. Ohta et el in their DAPS design [27].

Three DAPS layouts were designed that utilized these suggestions. The first design, DAPS-separate (see Figure 52), had readout circuits on the same side of the pixel and separate parasitic n+ diffusions. Another design, DAPS-joined (see Figure 53), combined both of S. Djaja's suggestions and had readout circuits on the same side of the pixel with a joined parasitic n+ diffusion. Both of these pixels are 16μm×12μm in dimensions.

The last DAPS design, DAPS-opposite (see Figure 54), had readout circuits on the opposite sides of the pixel with a joined parasitic n+ diffusion. A fourth DAPS layout was designed with readout circuits on opposite sides of the pixel and separate parasitic n+ diffusions, but an error rendered these pixels unusable. Though it is shown lying on its side, its dimensions are 24μm×12μm. As with previous APS layouts, these pixels were metal shielded so that only the photogates were subject to illumination.

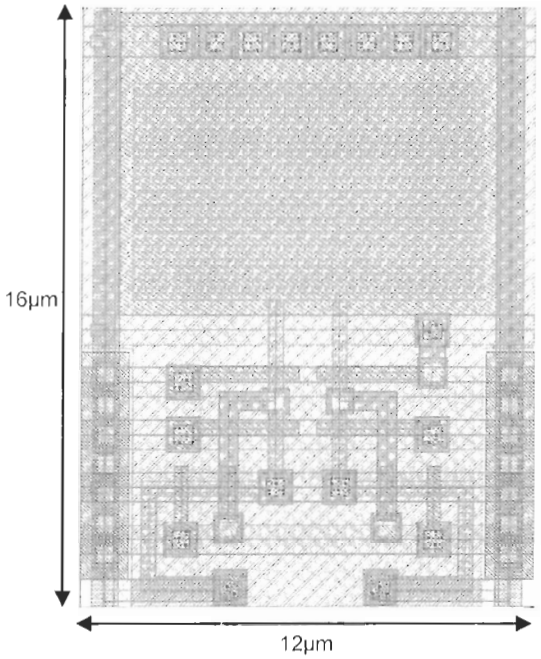

Figure 52: DAPS layout with readout circuits on the same side and separate parasitic n+ diffusions (DAPS-separate)

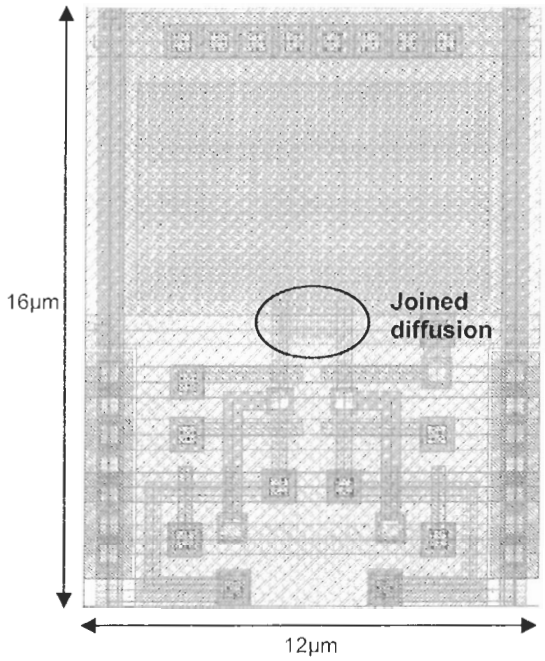

Figure 53: DAPS layout with readout circuits on the same side and a joined parasitic n+ diffusion (DAPS-joined)

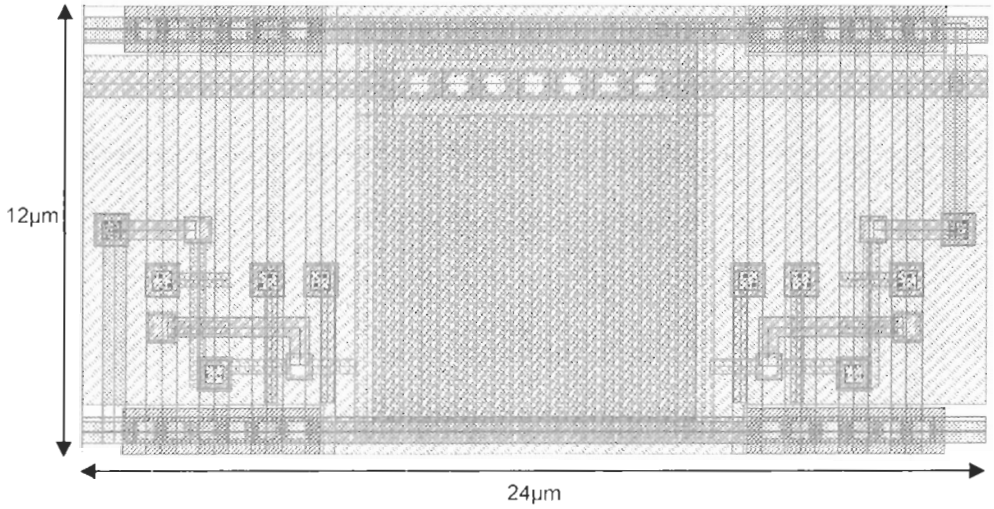

Figure 54: DAPS layout with readout circuits on opposite sides and a joined parasitic n+ diffusion (DAPS-opposite)

From these layouts, note that the parasitic n+ diffusion must be made larger to join the parasitic n+ diffusions. While the parasitic n+ diffusion area is only marginally larger for the DAPS-joined design, the diffusion in the DAPS-opposite design surrounds the photogate and is significantly larger.

6.2. Duo-Output Active Pixel Sensor Test Plan

The initial test plan for the DAPS designs involved two stages. In the first stage, each of the three DAPS designs was tested to determine which design had the best readout circuit sensitivity matching. A mismatch in readout circuit sensitivities would manifest as a "noise" when performing background subtraction. For example, if both readout circuits captured the same illumination and they were mismatched in sensitivity, subtracting the background would result in a non-zero answer which would not be desired. Thus, the ideal DAPS design would have matched readout circuit sensitivities to maximize the effective SNR of the background subtraction output. Note that a calibration may be able to reduce the effect of a sensitivity mismatch, however a relatively low sensitivity deviation is still desired.

The second stage of testing was to test the background subtraction performance of the DAPS. Only the design with the best sensitivity matching was tested. The background subtraction capabilities of the DAPS were tested at several background illumination levels to determine the performance of the technique and to identify areas of improvement.

After completing the second stage of testing, crosstalk between the output circuits of a DAPS was found to be significant. Based on this evidence another set of experiments was performed in an attempt to determine the cause of the crosstalk.

As with the FTAPS testing, the DAPS testing was performed using the test setup described in Section 3.2. The control signal timing that was used will be described in later sections. However unlike the FTAPS devices, the DAPS devices were operated in voltage mode. Instead of employing an operational amplifier (shown in Figure 31), a column bias transistor was used to convert the current in the output branch to a

voltage output. Figure 55 shows a schematic of an APS output branch with the column bias trasnsistor. Also, improvements to the test program allowed more automated testing of the pixels. As a result, a greater number of pixels could be tested in a shorter amount of time. To handle the increased amount of data, Matlab was used to process the experimental data.

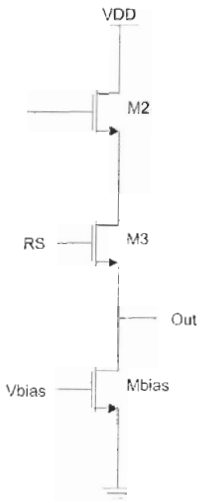

Figure 55: Output branch of APS showing column bias transistor

6.3. Duo-Output Active Pixel Sensor Sensitivity Testing

The DAPS sensitivity matching testing was performed similarly to the FTAPS sensitivity testing. The output of the DAPS was recorded for varying levels of illumination. By plotting the output characteristics of the pixel, the sensitivity of the pixel was found from the slope of the output curve. The sensitivity of each DAPS design was analyzed to determine which DAPS had the best sensitivity matching.

6.3.1. Duo-Output Active Pixel Sensor Sensitivity Control Signal Timing

The control signals for the DAPS were set up similarly to the control signals used for the photogate testing in Section 3.4. The main difference from the previous photogate control signals is the inclusion of the TX2 control line. Since both readout circuits must be tested, the control signal timing for the DAPS alternates between

transferring charge with TX1 and TX2. The timing of the control signals used for DAPS-separate and DAPS-joined sensitivity testing is illustrated in Figure 56.

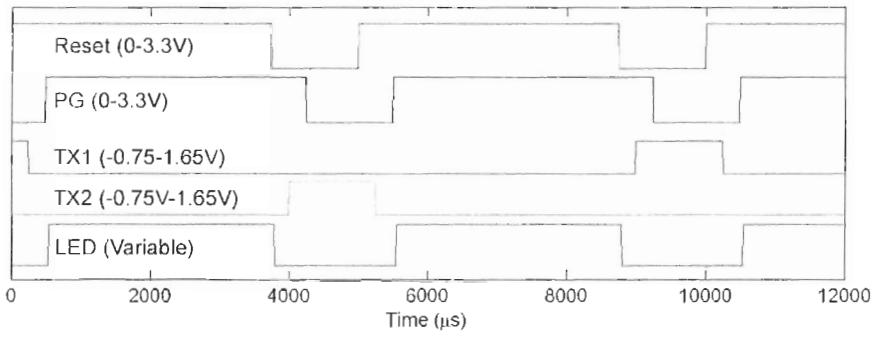

Figure 56: DAPS-separate and DAPS-joined sensitivity testing control signals

The frequency of the Reset control line was 100Hz and the LED voltage was varied from 0 to 7V in 0.25V increments. The DAPS-opposite design required different control signal timing as there was significant delay during charge transfer. To accommodate for the delay, the transfer time was extended by increasing the duty cycle of the TX control lines. The timing of the control signals used for DAPS-opposite sensitivity testing is illustrated in Figure 57. The frequency of the Reset control line was 80Hz and again the LED voltage was varied from 0 to 7V in 0.25V increments.

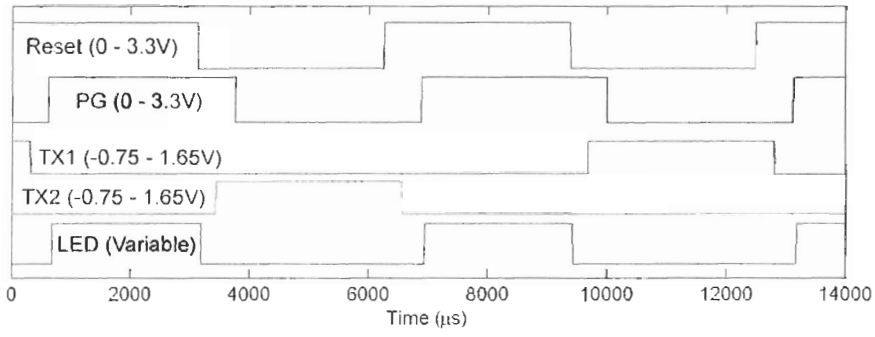

Figure 57: DAPS-opposite sensitivity testing control signals

6.3.2. Duo-Output Active Pixel Sensor Sensitivity Test Results

The output of the DAPS devices was extracted from the output waveforms. The output waveform of the DAPS was captured ten times for each illumination level. A

single set of output waveforms for a DAPS-separate device is shown in Figure 58. A single waveform is plotted for each illumination level tested. Note that two outputs are shown, corresponding to the two DAPS readout circuits. The readout circuit associated with TX1 was called Channel 1 and the readout circuit associated with TX2 was called Channel 2. CDS was employed for this testing; the reset and readout times are indicated with dashed lines. For each illumination level, the difference of the reset value and readout value, i.e. the CDS output, was determined in each of the ten output waveforms captured. The average of these CDS output values was used to plot the output characteristics of the pixel.

Contrast the output waveforms of the DAPS-separate design with the output waveforms of a DAPS-opposite design shown in Figure 59. Clearly, the DAPS-opposite design is slower at transferring charge from the parasitic n+ diffusion to the FD. The larger area of the parasitic n+ diffusion in the DAPS-opposite design means that the diffusion also has a larger capacitance. The larger capacitance of the parasitic n+ diffusion is the likely cause of the slow transfer rate of the DAPS-opposite design. For ideal transfer, the capacitance of the parasitic n+ diffusion should be minimized. Therefore, increasing the size of the parasitic n+ diffusion to form a shared diffusion in a DAPS is detrimental to charge transfer efficiency.

From the output waveforms, the output characteristics of each pixel were plotted and a piecewise linear fit of each curve was calculated to determine the sensitivity of each readout circuit. A sample of the output characteristics of each DAPS design is illustrated in Figure 60 – Figure 62. From inspection of these figures, the DAPS-separate design appears to have the best sensitivity matching for its readout circuits. Further analysis later in this section will confirm this observation.

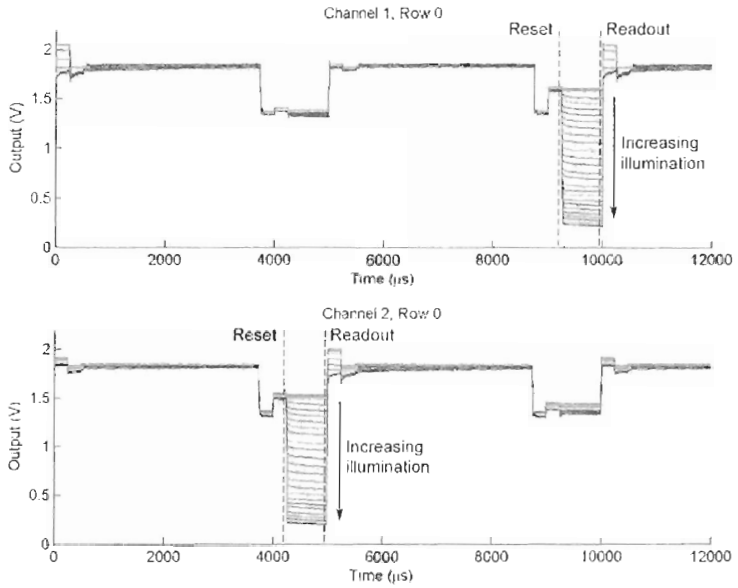

Figure 58: Sample sensitivity testing DAPS-separate output waveforms

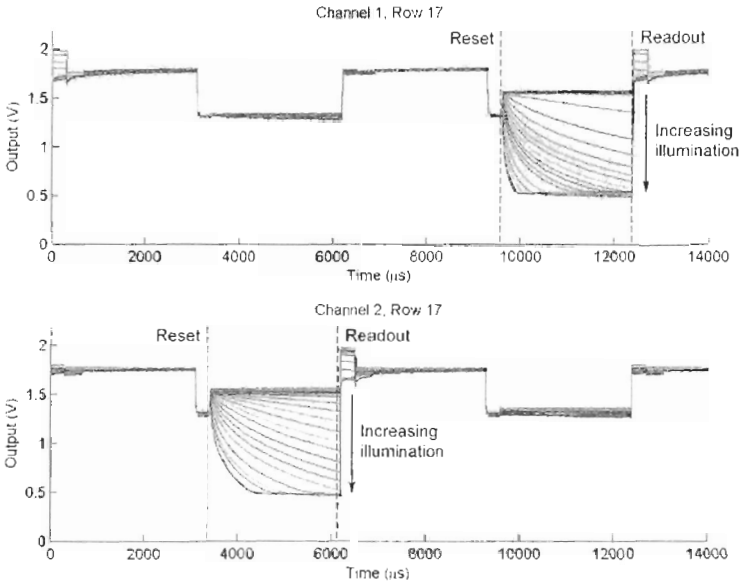

Figure 59: Sample DAPS-opposite output waveforms for sensitivity testing

As well, it is evident from Figure 60 – Figure 62 that there is a range of low illuminations where the sensor has little or no sensitivity. This behaviour is undesirable as it limits the usable range of input illumination levels. The range of illuminations is smallest in the DAPS-separate design and largest in the DAPS-

opposite design suggesting that a larger parasitic n+ diffusion increases the range of low illuminations where the sensor has little or no sensitivity.

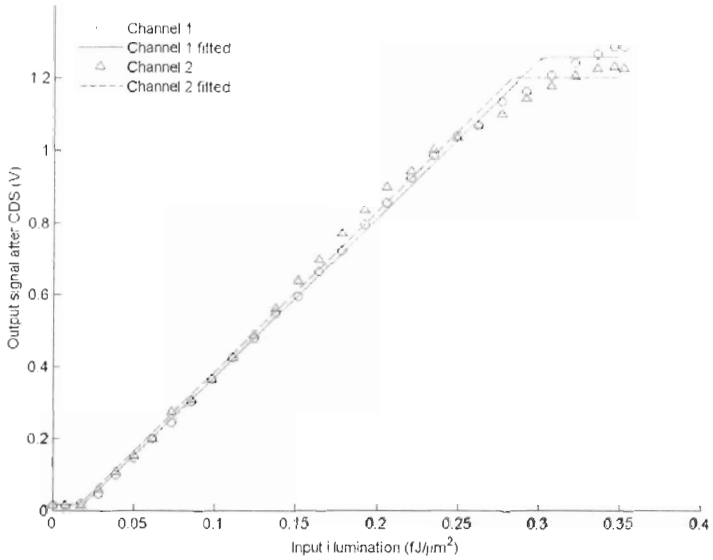

Figure 60: Sample sensitivity testing DAPS-separate output characteristics

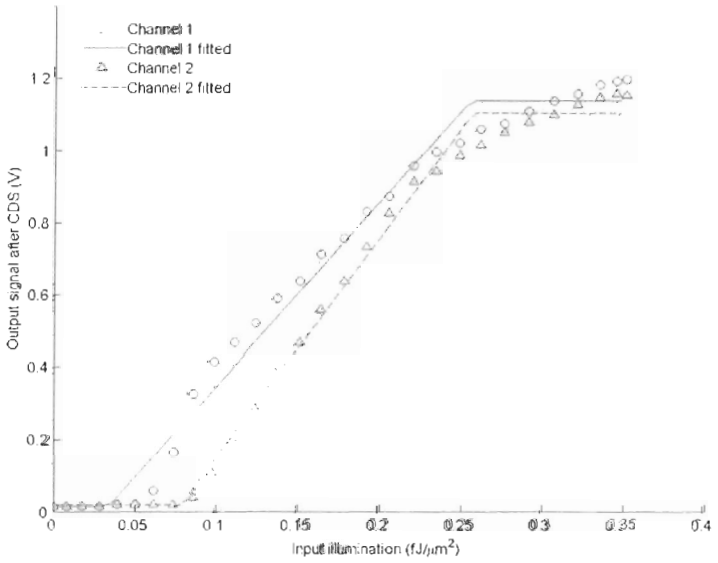

Figure 61: Sample sensitivity testing DAPS-joined output characteristics

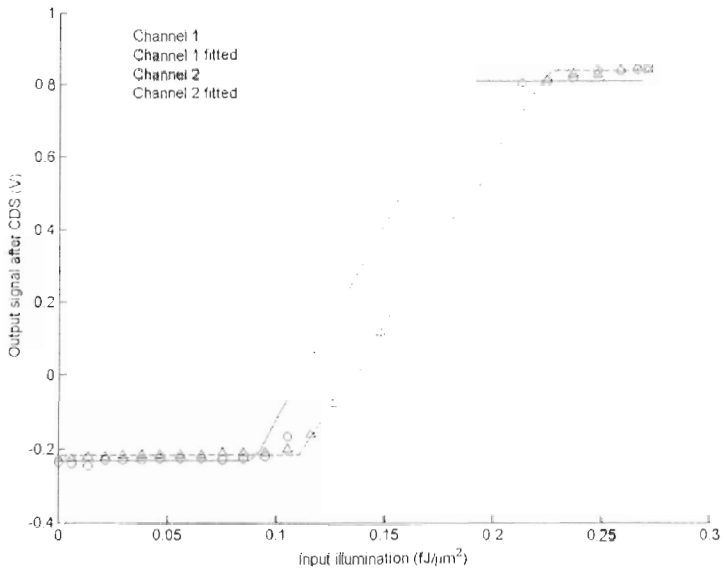

Figure 62: Sample sensitivity testing DAPS-opposite output characteristics

The reason for this behaviour at low illumination levels is the parasitic n+ diffusion must be filled to some extent before charge is transferred to the FD. A larger parasitic n+ diffusion requires more charge to fill it, increasing the range of illuminations that the DAPS is unresponsive. To mitigate this effect, the parasitic n+ diffusion area should be minimized.

In their DAPS design, J. Ohta et el introduced a NMOS transistor between the parasitic n+ diffusion and ground to reset the diffusion, much like how the diffusion was reset in our experiments. When they reset the parasitic n+ diffusion, they observed the same lack of output for low illuminations. Later, the same research group found that they could partially eliminate this problem by pre-charging the diffusion to some potential between V_{SS} and V_{DD} [22]. While this was partially successful, the addition of a transistor for each parasitic n+ diffusion reduces FF and increases the complexity of the control signal timing. As well, an intermediate gate voltage (between V_{DD} and V_{SS}) for these transistors is needed for ideal performance.

Six DAPS-separate pixels, six DAPS-joined pixels, and five DAPS-opposite pixels were tested. To quantify the sensitivity matching of a pixel, a deviation % was defined. The deviation % was calculated as

$$Deviation\ \% = \frac{|Sens_1 - Sens_2|}{\min(Sens_1, Sens_2)} \times 100\% \quad (50)$$

where $Sens_1$ is the sensitivity of Channel 1 and $Sens_2$ is the sensitivity of Channel 2. Thus, a low deviation % corresponds to a well matched readout circuits. Table 17 shows the sensitivity of Channel 1 and 2 of each tested DAPS pixel as well the deviation %.

Table 17: Summary of DAPS sensitivity testing

		Sensitivity (V/fJ/μm²)		
Design	**Pixel**	**Channel 1**	**Channel 2**	**Deviation %**
DAPS-separate	1	4.95	5.31	7.39
	2	4.64	4.63	0.31
	3	4.39	4.44	1.26
	4	4.37	4.53	3.59
	5	4.64	4.59	1.04
	6	4.32	4.50	4.13
DAPS-joined	1	5.05	6.26	23.90
	2	5.06	6.09	20.30
	3	5.44	6.11	12.44
	4	5.08	6.21	22.34
	5	5.46	6.18	13.22
	6	5.52	6.25	13.19
DAPS-opposite	1	16.07	9.22	74.26
	2	10.84	9.24	17.31
	3	6.90	8.78	27.21
	4	11.93	8.67	37.57
	5	10.99	8.46	29.82

The DAPS-separate design clearly had the best matching of the three designs. Its average matching % was 2.95% while the average matching % of the DAPS-joined and DAPS-opposite designs were 17.57% and 37.23% respectively. Thus, the best sensitivity matching is achieved by minimizing the area of the parasitic n+ diffusion.

6.3.3. Duo-Output Active Pixel Sensor Sensitivity Testing Conclusion

The DAPS-separate, DAPS-joined, and DAPS-opposite designs were tested to determine which had the best sensitivity matching. Pixels with joined parasitic n+ diffusions and readout circuits in closer proximity were designed in an attempt to improve the sensitivity matching of the readout circuits in a DAPS. To join the parasitic n+ diffusions of a pixel, the area of the diffusion had to be increased.

The output waveforms of the DAPS designs were captured at several levels of illumination. The output waveforms showed that the transfer rate of the DAPS-opposite design was slow, likely caused by the increased capacitance of the parasitic n+ diffusion.

When comparing the output characteristics of different DAPS designs, it was clear that there was another effect of increasing the size of the parasitic n+ diffusion. There was a range of low illumination levels where each of the DAPS designs had little or no sensitivity. This is undesirable behaviour as it limits the range of input illumination levels the sensor is sensitive to. The reason for this effect is charge cannot be transferred to the FD until the parasitic n+ diffusion well is partially filled. Recall that during reset the parasitic n+ diffusion is filled with positive charges. During transfer, electrons (negative charges) are moved through the parasitic n+ diffusion. However, some positive charges recombine with the electrons before the

electrons can be transferred to the FD. To minimize the range of low illuminations where the pixel is unresponsive, the parasitic n+ diffusions should be minimized.

CDS was performed on the output waveforms and this data was used to plot each pixel's output characteristics. A piecewise linear fit of the output characteristics was calculated to determine the sensitivity of each pixel. After comparing the matching % of each DAPS design, the DAPS-separate design clearly had the best matching. Based on this analysis and the other undesirable effects of increasing the parasitic n+ diffusion area, it is concluded that joining the parasitic n+ diffusions of a DAPS device does not improve sensitivity matching and causes other undesirable behaviour. Future DAPS designs should minimize the parasitic n+ diffusion area.

DAPS devices fabricated in the future should minimize the area of the parasitic n+ diffusion for the best readout circuit sensitivity matching. Removing the parasitic n+ diffusion altogether using a double poly process is ideal, however this also introduces other complications as adequate step coverage of the poly-2 layer must be maintained. In fact, while the 0.35µm process used to fabricate these DAPS devices has a poly-2 layer, design rules prevented a photogate APS design with no parasitic n+ diffusion. The design rule is most likely in place because of step coverage issues between poly-1 and poly-2.

DAPS devices should also focus on matching components in the layout. All diffusions and transistors in the layouts should be matched as best as possible, particularly the FD and the amp transistor as they affect the sensitivity of the pixel the most. Increasing the area of the pixel and reducing its FF may be needed to implement these layout modifications.

Since the FD area plays a crucial role in the sensitivity matching of a pixel, its area could be increased to reduce the effect of process variations on its size. However, increasing the FD area will also decrease the sensitivity of the DAPS, so optimization of the FD area may be required to obtain the best overall performance of sensitivity and sensitivity matching.

6.4. Duo-Output Active Pixel Sensor Background Subtraction Testing

Once the DAPS-separate design was identified as the pixel with the best sensitivity matching, its background subtraction capabilities were tested. The first goal of the background subtraction testing was to determine the background subtraction sensitivity of the DAPS. The second goal was to observe how the background illumination level affects the sensitivity of the DAPS.

The control signals were modified from those used in the DAPS sensitivity testing so that two exposures were done in a single reset cycle. In the first exposure, background illumination and additional illumination from a simulated modulated light source is captured and in the second exposure only the background illumination was captured. By taking the difference of the outputs of Channel 1 and Channel 2, the output due to the background illumination should be removed.

To test the performance of the background subtraction, the output of both DAPS channels was captured while incrementally increasing the modulated light source illumination for several background levels. The output of both channels was plotted versus the modulated light source energy density. Then the sensitivity of both DAPS channels to the modulated light source was determined. The channel that is exposed to the modulated light source is referred to as the "in-phase" channel" and the

channel only exposed to background light is referred to as the "out-of-phase channel". Ideally, only the in-phase channel would have a significant sensitivity. The out-of-phase channel should have negligible sensitivity. As well, several background levels were tested to determine whether the sensitivity of each channel was dependent on the background light.

6.4.1. Background Subtraction Control Signal Timing

The control signals for the background subtraction testing differed from the testing done previously. In a single cycle for background subtraction, the DAPS was reset once, but two exposures were taken. One exposure was captured Channel 1 and the other was captured on Channel 2. Since the output of one channel must be stored while the other channel is exposed, the reset cannot be held high until just before readout as in previous photogate APS testing. Thus, DS was used instead of CDS to determine the pixel output. Furthermore, due to the complexity of the control signal timing, the parasitic n+ diffusions were not reset.

By controlling the voltage of the LEDs in the test setup, a modulated light source and background illumination were simulated. For the majority of the exposure, the LED voltage was set to the background illumination level. To simulate a modulated light source, the LED voltage was increased during the in-phase exposure. The control signal timing for DAPS background subtraction when Channel 1 was in-phase is illustrated in Figure 63.

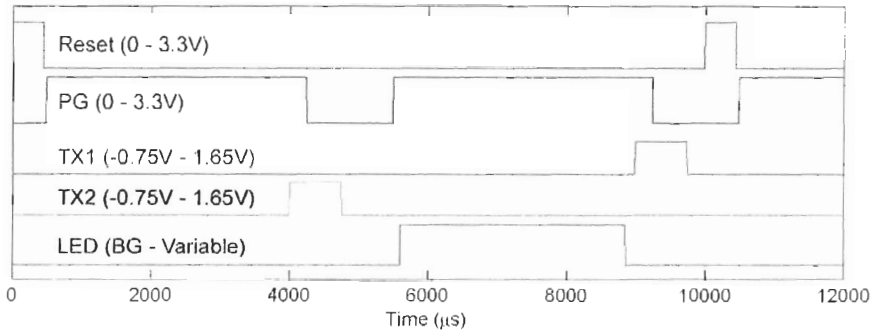

Figure 63: DAPS background subtraction testing control signal timing, Channel 1 in-phase

A single cycle where Channel 1 is in-phase follows these steps:

1. The pixel is reset. When the Reset control line goes low, the reset level is sampled for both channels.
2. The photogate is turned on to capture an exposure with only the background light.
3. Charge captured under the photogate is transferred to Channel 2.
4. The photogate is turned on and the LED voltage is increased to simulate a modulated light source. This exposure captures both background light and light from the modulated source.
5. Charge captured under the photogate is transferred to Channel1.
6. When the transfer to Channel 1 concludes, the readout level is sampled for both channels.

The only difference in the control signal timing when Channel 2 is in-phase is the LED voltage is increased during the first exposure instead of the second.

6.4.2. Duo-Output Active Pixel Sensor Background Subtraction Test Results

The background subtraction performance of six DAPS-separate devices were tested for five background illumination levels. The background levels tested were 0.083fW/μm^2, 5.42 fW/μm^2, 12.0 fW/μm^2, 18.8 fW/μm^2, and 26.4 fW/μm^2

corresponding to LED voltages of 0V, 0.5V, 1.0V, 1.5V, and 2.0V respectively. Compared to the saturation output of the DAPS, the background levels were approximately 0% saturation, 12.5% saturation, 25% saturation, 37.5% saturation and 50% saturation.

For each background level, the modulated light source was simulated by increasing the LED voltage from the background LED voltage to 7V in 0.25V increments. This set of testing was performed twice, once with Channel 1 in-phase and once with Channel 2 in-phase. The background subtraction DAPS-separate output waveforms with Channel 1 in-phase is shown in Figure 64. Each waveform is for a different modulated light source illumination level and the dashed lines indicate the reset and readout times.

As in the previous DAPS testing, the output waveform was captured ten times for each illumination level. The output was obtained by taking the difference of the readout value and reset value using DS. The average DS output of both DAPS-separate channels was plotted versus the modulated light source illumination energy density. A sample plot of the output characteristics for background subtraction is given in Figure 65. Channel 1 was in-phase and the background illumination power density was negligible (0.083fW/μm^2).

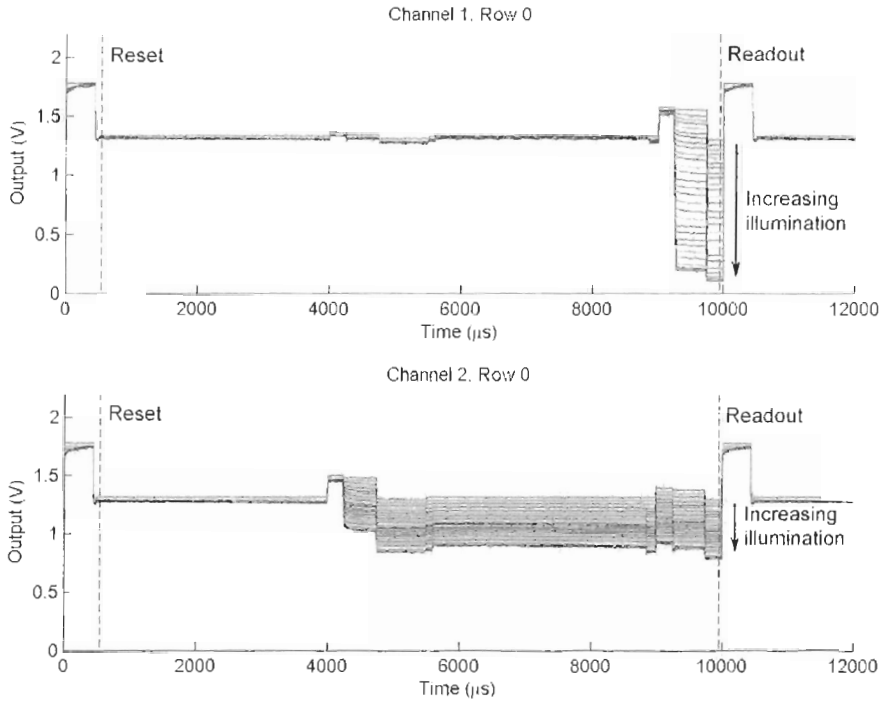

Figure 64: Sample DAPS-separate output waveforms for background subtraction, Channel 1 in-phase

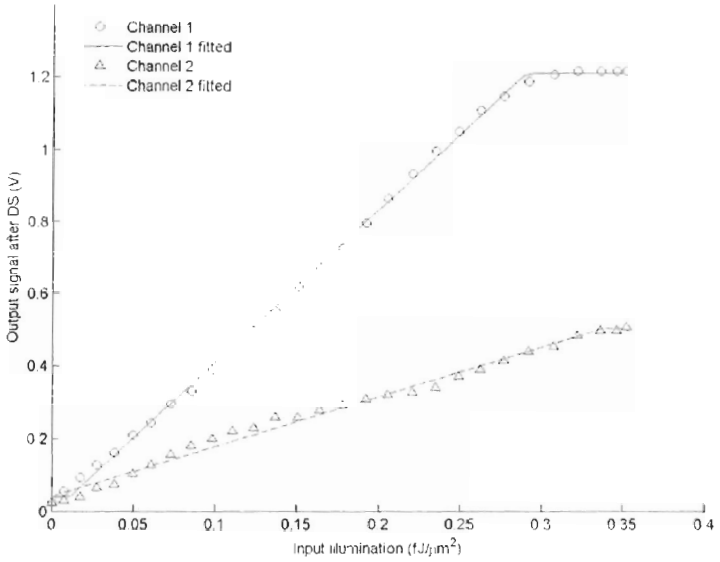

Figure 65: Sample background subtraction DAPS-separate output characteristics (Channel 1 in-phase, background = 0.083fW/μm^2)

From Figure 65, there is clearly a significant amount of crosstalk since Channel 2 responds to the modulated light even though it is only exposed to background

illumination. As stated previously, crosstalk degrades the background subtraction performance of the DAPS so this constitutes a serious problem for the background subtraction capabilities of the DAPS. When Channel 2 was in-phase, crosstalk was again observed as illustrated in Figure 66. The "crosstalk sensitivity" of the DAPS-separate will be analyzed in detail later in this section.

An objectives of the background subtraction testing was to test if the sensitivity of each channel was dependent on the background illumination level. Testing showed that when the background illumination level was increased, the sensitivity of both DAPS-separate channels, i.e. the slope of the pixel response, stayed fairly constant. Figure 67 shows the output characteristics of a DAPS-separate with a background illumination of 12.0fW/μm^2.

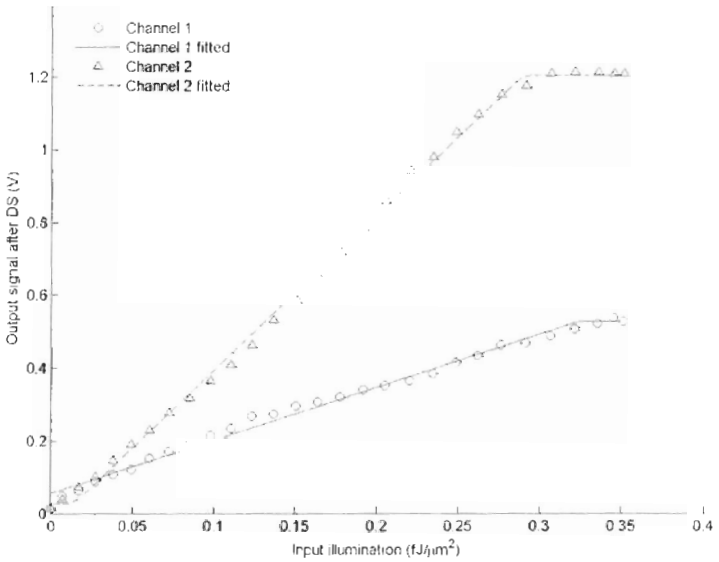

Figure 66: Sample background subtraction DAPS-separate output characteristics (Channel 2 in-phase, background = 0.083fW/μm^2)

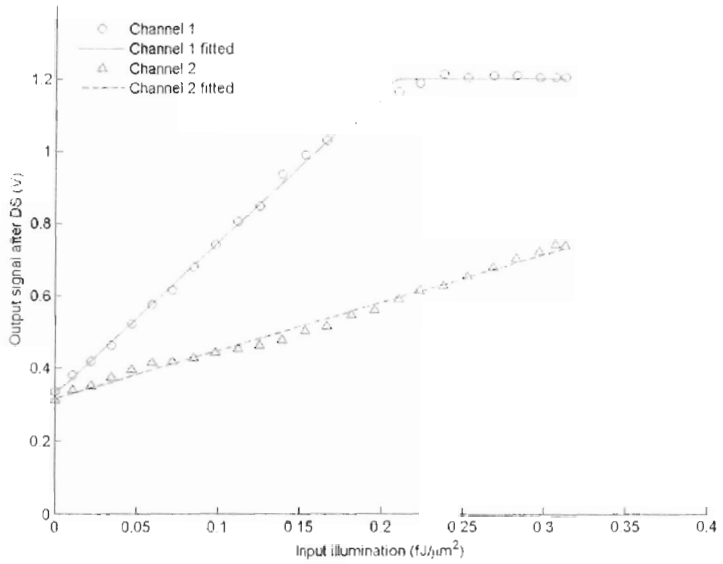

Figure 67: Sample background subtraction DAPS-separate output characteristics (Channel 1 in-phase, background = 12.0fW/μm^2)

Before the background subtraction test data is analyzed, three terms are defined. The "in-phase sensitivity" is the sensitivity of the in-phase channel, the "crosstalk sensitivity" is the sensitivity of the out-of-phase channel, and the "background subtraction sensitivity" is the sensitivity of the DAPS after performing background subtraction.

The output of the DAPS after performing background subtraction is the difference of the in-phase output and the out-of-phase output. Thus, the DAPS background subtraction sensitivity is the difference of the in-phase sensitivity and the crosstalk sensitivity. It should be clear that to maximize the background subtraction sensitivity the in-phase sensitivity should be maximized and the crosstalk sensitivity should be minimized.

The in-phase sensitivity and the crosstalk sensitivity were found for each background illumination level and the average and maximum sensitivity variation of each was calculated. The maximum sensitivity variation is defined as

$$Maximum\ Sensitivity\ Variation = \frac{\max(Sens) - \min(Sens)}{\min(Sens)} \times 100\% . \qquad (51)$$

The data from the DAPS-separate background subtraction testing is summarized in Table 18.

Several points should be made from the data in Table 18. As was first observed in the output characteristics, the crosstalk sensitivity was quite significant. On average, the crosstalk sensitivity was 33.9% of the in-phase sensitivity. Thus, the crosstalk seriously degrades the background subtraction sensitivity of the DAPS.

Table 18: Summary of DAPS-separate background subtraction testing results

	Pixel	In-phase Sensitivity		Crosstalk Sensitivity	
		Average ($V/fJ/\mu m^2$)	Variation (%)	Average ($V/fJ/\mu m^2$)	Variation (%)
Channel 1 In-phase	1	4.09	13.2	1.43	23.7
	2	4.07	5.7	1.24	99.0
	3	3.71	6.7	1.11	17.9
	4	3.66	6.9	1.13	17.5
	5	3.61	10.6	1.25	42.8
	6	3.66	2.4	1.14	27.8
Channel 2 In-phase	1	4.19	10.7	1.37	8.5
	2	3.71	27.8	1.41	36.9
	3	3.56	13.3	1.38	11.4
	4	3.60	15.6	1.36	8.8
	5	3.80	3.0	1.20	21.3
	6	3.59	6.5	1.28	9.4

Comparing the in-phase sensitivities in Table 18 to the DAPS-separate sensitivities in Table 17, the in-phase sensitivities are noticeably smaller than the DAPS-separate sensitivities. The average in-phase sensitivity is $3.77V/fJ/\mu m^2$ and the average DAPS-separate sensitivity is $4.61V/fJ/\mu m^2$, a difference of 22.2%. Since the DAPS-

separate design is used for both sets of tests, it is interesting that the sensitivities in the tests differ. The cause could simply be a result of the different control signal timing that was used in the tests. However, future work should investigate this issue as it could be the result of crosstalk.

From the data on the maximum sensitivity variation, it is evident that the crosstalk sensitivity varies quite a bit. The pixel with 99.0% crosstalk sensitivity variation is likely an outlier since the variation of other pixels is much lower. More importantly, the in-phase sensitivity is not affected by the background illumination greatly. However, care must be taken to avoid excessively high background illuminations. At high background illuminations the pixel is near or at saturation which will decrease the sensitivity of the pixel. In fact, if the sensitivity for the highest background level ($26.4fW/\mu m^2$) is ignored, the maximum in-phase sensitivity variation is less than 10% for all pixels. Thus, it can be concluded that the background illumination level has very little effect on the in-phase sensitivity.

To summarize the analysis for the background subtraction testing, background subtraction is possible with the DAPS. Unfortunately, it suffers from significant crosstalk which degrades the background subtraction sensitivity. The sensitivity of the DAPS in the background subtraction experiments is lower than the sensitivity that was measured during the sensitivity experiments. The likely cause of the decrease in sensitivity is the again crosstalk, but further experimentation is needed to confirm this. Lastly, background illumination level does not significantly affect the in-phase sensitivity. Only at high background levels does the in-phase sensitivity change significantly.

6.4.3. Background Subtraction Testing Conclusion

There were two objectives of the background subtraction testing. The first was to determine the background subtraction performance of the DAPS and the second was to observe the effect of background illumination on the sensitivity of the DAPS. The control signal timing was altered so that the DAPS was only reset once every two. During the in-phase exposure, the LED voltage was increased to simulate the light from a modulated light source. The background subtraction experiment was performed for five background illumination levels and the output was sampled with DS. A set of experiments was run with Channel 1 in-phase and another set was run with Channel 2 in-phase.

After analyzing the data from the background subtraction testing, three key points were made. First, the DAPS can be used for background subtraction, however the crosstalk sensitivity significantly degrades the background subtraction sensitivity. On average, the crosstalk sensitivity was 33.9% of the in-phase sensitivity.

Secondly, the average in-phase sensitivity of the DAPS-separate design was 22.2% less than the average sensitivity measured in the DAPS sensitivity testing. While it is likely that the cause of this effect is the difference in control signal timing or crosstalk, further work is needed to confirm this.

Lastly, the in-phase sensitivity of the DAPS-separate was not significantly affected by the background illumination level. Only at high illuminations where the DAPS-separate output was near saturation did the background illumination become affect the in-phase sensitivity. If only the four lower background levels were considered, the in-phase sensitivity varied by less than 10% for all pixels.

From the background subtraction testing, a serious problem was identified. Since the crosstalk sensitivity of the DAPS-separate was very high, the DAPS background subtraction performance suffers. As a result, the goal of the next set of experiments was to identify the primary source of crosstalk for the DAPS.

6.5. Duo-Output Active Pixel Sensor Crosstalk Testing

The main objective of the crosstalk testing was to identify the main source of crosstalk for the DAPS. Crosstalk is a much more serious problem than a readout circuitry sensitivity mismatch as it is more difficult to correct for it. The most likely source of crosstalk was identified and an experiment was designed to determine the validity of this hypothesis.

6.5.1. Crosstalk Source

From past experience testing the DAPS, the parasitic n+ diffusions were considered the most likely source of crosstalk. Preliminary tests on DAPS photodiode designs by J. Dudas indicated that the metal shielding did not adequately shield the FD from light in the visible spectrum [39]. The layout of the DAPS photodiode is slightly different from the DAPS photogate as the FD is closer to the photosensitive area in the photodiode design. However, the parasitic n+ diffusions in the DAPS photogate are very close to the photosensitive area. Therefore, it is likely that the parasitic n+ diffusions are exposed to illumination. Figure 68 shows the DAPS-separate layout with shading to indicate the location of the metal shielding. Notice how close the parasitic n+ diffusion is to the edge of the metal shielding.

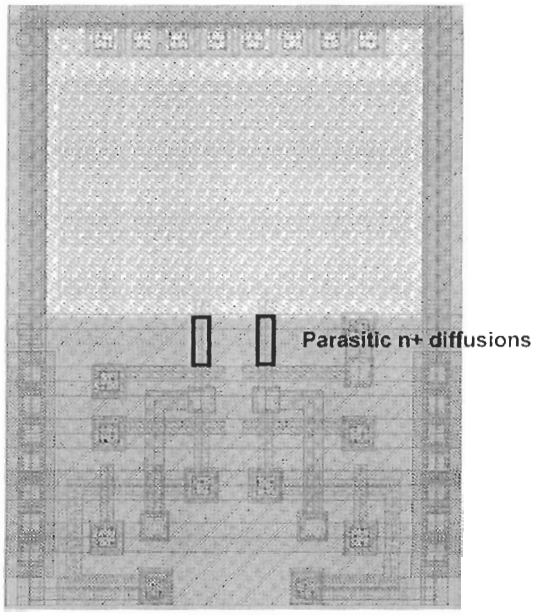

Figure 68: DAPS-separate layout with shading to indicate location of metal shielding

It was hypothesized that despite metal shielding on the DAPS designed to allow only the photogate to be illuminated, areas around the photogate were also illuminated. As well, charge that is generated near the parasitic n+ diffusion could diffuse to it and be collected. Charge would build up in the parasitic n+ diffusion as it would behave as a photodiode. During transfer, the charge in the parasitic n+ diffusion would be transferred to the FD, affecting the output of the pixel. During background subtraction testing, the modulated light source would affect the parasitic n+ diffusions of both channels. Therefore, both channels would be sensitive to the modulated light source, resulting in the crosstalk that was observed.

6.5.2. Crosstalk Testing Experimental Setup

The goal of the crosstalk experiments was to determine if the parasitic n+ diffusions collected photo-generated charge. If so, the source of crosstalk would be confirmed. The DAPS crosstalk testing used exactly the same experimental setup and control signal timing as in the background subtraction testing (see Section 6.4.1) except for one key difference. The PG control line was never turned on so that no charge was

collected under the photogate. Any output response would be the result of charge collected by the parasitic n+ diffusions. As stated previously, charges diffusing from under the photogate or exposure to light due to inadequate shielding could cause the parasitic n+ diffusions to collect charge.

The experiment was run with no background illumination and the modulated light source was varied from 0-7V in 0.25V increments, as in previous testing. Two experimental runs were performed on the same six DAPS-separate devices tested previously, once with Channel 1 in-phase and once with Channel 2 in-phase.

6.5.3. Crosstalk Testing Results

Using the same methodology as previous analyses, reset and readout levels of each output waveform were sampled for each illumination level. As with the background subtraction testing, DS was employed and the output versus input illumination was plotted as the output characteristics of the pixel. Figure 69 and Figure 70 show the DAPS-separate crosstalk testing output characteristics of a DAPS device with Channel 1 in-phase and Channel 2 in-phase.

From these figures, the output characteristics of the DAPS for crosstalk testing look very similar to the characteristics found in previous testing. However, the sensitivity and saturation level of the DAPS in this testing was, not surprisingly, much lower. This was expected as the parasitic n+ diffusion is much smaller than the photogate and the metal shielding likely partially blocks some of the illumination. The pixel should saturate when the parasitic n+ diffusion well is "filled", however it is interesting that the in-phase channel (Channel 1 for Figure 69, Channel 2 for Figure 70) has a higher saturation level than the out-of-phase channel. This behaviour will be discussed in detail later in this section.

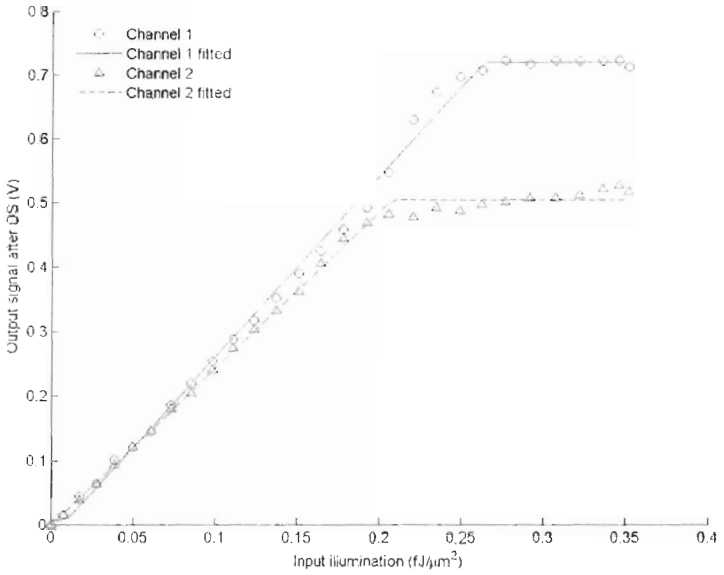

Figure 69: DAPS-separate crosstalk testing output characteristics (Channel 1 in-phase)

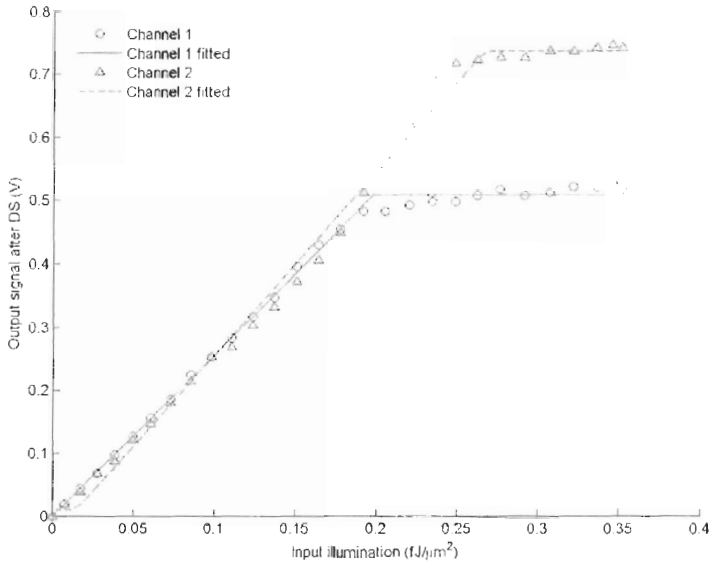

Figure 70: DAPS-separate crosstalk testing output characteristics (Channel 2 in-phase)

The sensitivity of both channels appears to be well-matched. Table 19 summarizes the sensitivities of the DAPS-separate for crosstalk testing.

Table 19: Summary of DAPS-separate crosstalk testing sensitivities

	Channel 1 In-phase		Channel 2 In-phase	
Pixel	**Channel 1 Sensitivity (V/fJ/μm²)**	**Channel 2 Sensitivity (V/fJ/μm²)**	**Channel 1 Sensitivity (V/fJ/μm²)**	**Channel 2 Sensitivity (V/fJ/μm²)**
1	2.81	2.44	2.57	2.89
2	3.00	2.87	2.17	2.60
3	2.53	2.37	2.17	2.58
4	2.54	2.39	2.13	2.54
5	2.48	2.03	2.50	2.75
6	2.55	2.41	2.10	2.48
Average	2.65	2.42	2.27	2.64

A few things should be noted from the data in Table 19. First, it is clear that charge is collected by the parasitic n+ diffusions as a result of illumination on or near the parasitic diffusion. The average sensitivities given in this table are approximately half of the sensitivities determined from DAPS sensitivity testing (Table 17). Thus, the contribution of the parasitic n+ diffusions to the DAPS-separate design sensitivity is significant.

Secondly, the average sensitivities in Table 19 are approximately twice as large as the crosstalk sensitivities found during background subtraction testing (Table 18). Thus, when a field is applied by the photogate, many of the charges that would otherwise be collected by the parasitic n+ diffusion are instead collected by the photogate.

Lastly, the average sensitivity of the in-phase channel is slightly higher than for the out-of-phase channel. This effect is linked to the reason why the saturation level is different for the in-phase and out-of-phase channel. Looking carefully at Figure 69 and Figure 70, note the slope of the in-phase channel output when it goes above the

saturation level of the out-of-phase channel. The slope increases slightly forming a "knee" in the curve. Figure 71 shows the crosstalk testing output characteristics of a DAPS-separate where the knee is obvious.

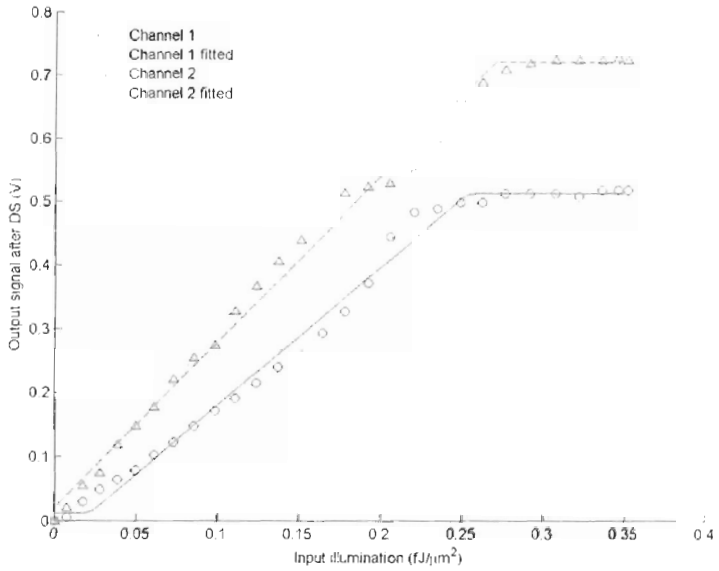

Figure 71: DAPS-separate crosstalk testing output characteristics with obvious knee (Channel 2 in-phase)

Since the fitted line does not take into account this change in slope, the calculated sensitivity of the in-phase channel is higher due to the higher sensitivity near saturation. In reality, the sensitivity of the in-phase and out-of-phase channels for the lower illumination levels is even better matched than is indicated by Table 19.

The reason for the difference in saturation levels is a result of when the transfer of charge is done. Since the out-of-phase channel begins its transfer well after the LEDs turn off, nearly all photo-generated carriers that have not been collected by a capacitive element have recombined. This is not the case for the in-phase channel. Since the LEDs have just turned off when the in-phase channel begins its transfer, photo-generated carriers are still available to be collected. Thus, as charge is

transferred out of the parasitic n+ diffusion, additional carriers are collected and transferred which increases saturation level.

To summarize the crosstalk testing results, three key points are noted. The crosstalk experiment confirmed that the parasitic n+ diffusions collect photo-generated carriers and account for a significant portion of a DAPS-separate's sensitivity. However, the effect of the parasitic n+ diffusions is not as bad as the sensitivities in Table 19 might indicate. When the photogate is operating normally, it collects many carriers that would otherwise diffuse to the parasitic n+ diffusion. Lastly, the in-phase channel has a higher saturation level than the out-of-phase channel as a result of additional photo-generated carriers that are collected during transfer. When the out-of-phase channel performs its transfer, most photo-generated charge has recombined.

6.5.4. Crosstalk Testing Conclusion

The goal of the crosstalk testing was to determine the source of crosstalk in the DAPS. From previous experience, the parasitic n+ diffusions were the most likely mechanism of crosstalk. Preliminary testing indicated that areas near the photosensitive area could also collect photo-generated charge despite the implementation of metal shielding. As the parasitic n+ diffusions are situated close to the photogate, it was likely that they also collected photo-generated charge.

The crosstalk experiment was designed to confirm that the parasitic n+ diffusions could collect photo-generated charge. The background subtraction setup and control signal timing was used with one important difference: the PG control line was never turned on. Any output resulting from illumination would be the result of charge collected by the parasitic n+ diffusions.

Once the output waveforms were collected, the data was processed and analyzed similarly to previous testing. The sensitivity of the DAPS-separate in the crosstalk experiments was significant, confirming that the parasitic n+ diffusions collect photo-generated charge. However, when the photogate is active it collects many of the charges that would otherwise be collected by the parasitic n+ diffusions. Thus, the DAPS-separate sensitivity due to the parasitic n+ diffusions is not as high as is indicated by the crosstalk testing. Finally, the in-phase channel had a higher saturation level than the out-of-phase channel as it can collect photo-generated charge during transfer. When the out-of-phase channel performs its transfer nearly all of the photo-generated charge has recombined if it has not been collected already.

Having confirmed that the parasitic n+ diffusions in this design cause the crosstalk observed in the background subtraction testing, it is recommended that future DAPS layouts be modified to provide greater shielding for the parasitic n+ diffusions and other in-pixel circuitry. A metal shield at one of the lower metal levels (metal-1 or metal-2) is a possible solution. As well, moving the parasitic n+ diffusion away from the main sensing area is advised to reduce the likelihood that charge will be collected by the diffusion.

6.6. Duo-Output Active Pixel Sensor Testing Summary

Three new DAPS pixels were fabricated in 0.35µm technology that attempted to improve their readout circuit sensitivity matching. Two suggestions were implemented in these pixel designs. To reduce the effect of process variations, the DAPS-separate design and DAPS-joined design had readout circuits on the same side of the pixel in close proximity. To eliminate the need to match the size of the

parasitic n+ diffusions, the diffusions were joined in the DAPS-joined design and DAPS-opposite design. To join the diffusions, the overall parasitic n+ diffusion area had to be larger.

Three experiments were performed on the DAPS. The objective of the sensitivity testing was to determine which DAPS design had the best readout circuit sensitivity matching. From analyzing the DAPS sensitivity testing results, the size of the parasitic n+ diffusion was found to be a critical factor. All of the key findings of this testing involved the parasitic n+ diffusion. The DAPS-separate design had the best readout circuit sensitivity matching of the three DAPS designs. Thus, to have the best sensitivity matching the parasitic n+ diffusions should be minimized. Larger parasitic n+ diffusions also caused other problems for the DAPS. A longer transfer time was needed to transfer charge from the photogate to the FD. As well, the parasitic n+ diffusion well must be partially filled before it can transfer charge. Thus, at low illuminations the output does not respond to light until there is enough charge to partially fill the parasitic n+ diffusion. This is undesirable behaviour as it limits the range of input illuminations that the pixel will respond to. Therefore, minimizing the parasitic n+ diffusion areas is also necessary to minimize transfer time and maximize the range of usable input illuminations.

The second experiment focused on the background subtraction performance of the DAPS. The DAPS-separate design was tested so that two exposures were taken in a single cycle. The in-phase exposure captured modulated light source and background light and the out-of-phase exposure only captured background light. The difference of the in-phase channel output and out-of-phase channel output should remove the effect of the background light from the DAPS output. After analyzing the data from the background subtraction testing, three key points were made. First, the crosstalk

sensitivity was very significant as it was 33.9% of the in-phase sensitivity, on average. Since the crosstalk sensitivity is effectively a "noise" when background subtraction is performed, the crosstalk constitutes a serious problem for the DAPS design. Due to this result, another experiment was run to determine the source of crosstalk.

Secondly, the in-phase sensitivity of the DAPS-separate in background subtraction testing was 22.2% smaller than the DAPS-separate in sensitivity testing. While these sensitivities should be matched, it is likely this discrepancy is the result of crosstalk. Further work is needed to explain this behaviour. Lastly, the in-phase sensitivity of the pixel was not significantly dependent on the background illumination, except for high background illuminations where the pixel was almost in or in saturation. For the four lower background illumination levels tested, the variation of the DAPS-separate in-phase sensitivity was less than 10%.

Due to the significant DAPS crosstalk sensitivity, another experiment was performed to identify the source of crosstalk. Based on preliminary testing, it was hypothesized that photo-generated charge collected by the parasitic n+ diffusions was the cause of crosstalk. An experiment similar to the background subtraction testing was devised, however the PG control line was never turned on. Thus, any output response would be the result of photo-generated charge stored by the parasitic n+ diffusions.

Once the data from the crosstalk testing was analyzed, several key points were made. The parasitic n+ diffusions were clearly able to collect photo-generated charge which led to the crosstalk observed during the background subtraction testing. However, activating the photogate seemed to reduce the number of charges that would be collected by the parasitic n+ diffusion. As well, the in-phase channel had a

higher saturation level than the out-of-phase channel because the in-phase channel was able to collect photo-generated charges that had not yet recombined during transfer.

6.7. Duo-Output Active Pixel Sensor Future Work

Future work on DAPS devices should consider a few issues. First, readout circuit sensitivity matching is extremely important for the DAPS. Any mismatch in sensitivity will act as a "noise" when performing background subtraction. Minimizing or removing the parasitic n+ diffusion will reduce mismatches in sensitivity. As well, the components in a DAPS should be matched to minimize the effect of process variations. In particular, the FD and amp transistor are most critical in determining the sensitivity of the pixel. Enlarging the FD to reduce the effect of process variations at the cost of sensitivity is also a possibility. Note that all of these suggestions may require an increase in pixel area or FF.

The other major issue for the DAPS is crosstalk when performing background subtraction. Since the parasitic n+ diffusions have been identified as the source of crosstalk, care should be taken to shield it as well as possible. A specific shield for the parasitic n+ diffusions in one of the lower metal levels is a possibility. Another recommendation is situate the parasitic n+ diffusion farther from the photogate to reduce the likelihood that charge will be collected by the diffusion.

7. Conclusion

Digital imagers have drastically affected the field of imaging in the last decade. The ease with which digital images can be stored and manipulated has given digital cameras an advantage over film cameras that has allowed them to compete with film in many applications. The focus of this thesis was to investigate two designs of digital image sensors: a fault tolerant image sensor that can recover from point defects and an image sensor with built-in background subtraction capability.

7.1. Fault Tolerant Active Pixel Sensor Conclusion

The performance of the FTAPS was tested in two ways: experiments were performed to examine the behaviour of the FTAPS and the noise of a FTAPS was compared to the noise of a standard APS. The experiments involved testing the FTAPS in defect conditions, comparing the sensitivity of the FTAPS to standard pixels, and comparing the sensitivity of pixels fabricated in 0.35μm technology with those fabricated in 0.18μm technology. For the FTAPS noise analysis, the total noise of the FTAPS and standard APS was calculated by considering shot noise, thermal noise, and flicker noise in each circuit.

7.1.1. Fault Tolerant Active Pixel Sensor Testing Conclusion

Like all other integrated electronics, image sensors are susceptible to defects during manufacturing and in the field. While factory calibration is commonly used to correct defects that occur during manufacturing, defects that occur in the field are often much harder to identify and correct for. Using hardware redundancy, the FTAPS is designed to recover from point defects that would otherwise render a pixel unusable.

Fault tolerant photodiode and photogate APS devices were designed and fabricated in 0.35µm technology. Some pixels were designed with intentional defects to test the behaviour of the FTAPS for various defect states.

The FTAPS was tested in three experiments. The objective of the first experiment was to test the behaviour of the FTAPS in various defect states. All FTAPS devices behaved as expected except for the photodiode FTAPS with a half stuck high defect. During reset, the half stuck high photodiode FTAPS drew a high current and several of them were laid out in close proximity which exacerbated the current issue. Thus, a race condition occurred during reset which reduced the performance of the pixel. It is believed that the half stuck high photodiode FTAPS would behave as expected if they were not situated as closely together.

Previous testing on an older design of the FTAPS had indicated that it had higher sensitivity than a standard APS. It was suggested that the two halves of the FTAPS operating in parallel was akin to having a standard APS with double width amp and row transistors. The sensitivity of a standard APS, DW APS, and FTAPS were compared to better understand why the FTAPS exhibits higher sensitivity. As expected, the DW APS had greater sensitivity than a standard APS because the transconductance of the amp and row transistors is higher. The photodiode FTAPS also exhibited higher sensitivity than a standard photodiode APS as its charge conversion gain is higher. Conversely, the charge conversion gain of the photogate FTAPS is the same as a standard photogate APS so their sensitivities were similar. However, the photogate FTAPS did have an enhanced output swing which is a result of its increased FD area.

In the third experiment, photodiode pixels fabricated in 0.18µm technology were tested to compare their sensitivity with pixels fabricated in 0.35µm technology. The 0.35µm pixels were approximately twice as sensitive as the 0.18µm pixels, which confirms previous analysis by other authors that technology scaling adversely affects pixel sensitivity of imagers fabricated in standard CMOS processes.

In summary, the FTAPS behaved mostly as expected in the presence of defects and the photodiode design had enhanced sensitivity due to a higher conversion gain. As well, pixels fabricated in 0.35µm technology were more sensitive than 0.18µm pixels as was suggested by other authors.

7.1.2. Fault Tolerant Active Pixel Sensor Noise Analysis Conclusion

While the benefits of the FTAPS have been investigated in detail, the cost of incorporating fault tolerance were not as clear. While it was obvious that the FF of a FTAPS would be reduced, other costs had not been explored. A paper by K. Salama et el suggested that additional noise would degrade the sensor's performance, particularly at low illuminations [19]. A re-analysis of noise was calculated for this thesis to compare the noise of a standard APS with that of a FTAPS.

Each source of noise in a photodiode APS was identified and equations were derived for the shot noise, thermal noise, and flicker noise of each component, i.e. the photodiode, transistors, and column amplifier. Each source of noise was output referred and an expression for the total output noise was determined. To calculate the noise, HSpice simulations, component datasheets, and experimental data were used to quantify the parameter values.

Three illumination conditions were considered in the analysis: dark, average, and saturation. The dominant source of noise in this analysis of the standard APS and FTAPS was the transistor flicker noise for all illumination conditions. When one of the transistor noises is dominant, as in this case, the noise of the FTAPS is the square root of two times greater than the noise of a standard APS. The worse-case scenario is when one of the photodiode noises is dominant. In the worst-case situation, the noise of the FTAPS is twice as large as the noise of a standard APS.

The superior sensitivity of the FTAPS offsets the additional noise of the fault tolerant design. Since the sensitivity of the photodiode FTAPS is twice as large as a photodiode standard APS, the overall SNR of a FTAPS is at least as good as the SNR of a standard APS. In the worst-case scenario where the noise of a FTAPS is twice that of a standard APS, the FTAPS SNR is similar to the standard APS SNR. However, in this noise analysis the transistor flicker noise was dominant, thus the FTAPS SNR is better than the standard APS SNR as the noise only the square root of two times larger. To summarize the photodiode FTAPS noise analysis, the FTAPS had greater noise than a standard APS; however its SNR is as good or better than the SNR of a standard APS due to its increased sensitivity.

7.1.3. Duo-Output Active Pixel Sensor Conclusion

In optical triangulation systems for 3-D scanning, a modulated light source is used to scan an object. Background light increases the difficulty of scanning and increasing the power of the modulated light source to compensate is not always desirable. The DAPS was designed to remove the effect of background illumination with background subtraction.

Previous DAPS designs suffered from mismatched readout circuitry sensitivity. The sensitivity mismatch in a DAPS behaves like a noise source when background subtraction is performed. The DAPS-separate, DAPS-joined, and DAPS-opposite layouts were fabricated in an attempt to improve the sensitivity matching of the readout circuit.

The DAPS was tested in three experiments. The objective of the first DAPS experiment was to determine which DAPS design had the best sensitivity matching. After analyzing the results of the DAPS sensitivity testing, the DAPS-separate design with separate parasitic n+ diffusions and readout circuits on the same side of the pixel was determined to have the best readout circuit sensitivity matching. Increasing the parasitic n+ diffusion area created several problems. Along with poorer sensitivity matching, the increased capacitance of a larger parasitic n+ diffusion caused charge transfer to be much slower. As well, the parasitic n+ diffusion well must be partially filled before it will transfer charge. The larger parasitic n+ diffusions required more charge to fill them which created a significant range of low illuminations where the DAPS output was unresponsive. Thus, minimizing the parasitic n+ diffusion is necessary to maximize sensitivity matching, to improve charge transfer, and to reduce the range of low illuminations where the pixel is unresponsive.

The second DAPS experiment tested the background subtraction performance of the DAPS-separate design. The results of the testing indicated that the DAPS-separate suffered from significant crosstalk when performing background subtraction. Since this is a serious problem, further testing would investigate the issue of crosstalk. Another result of the background subtraction testing was that the in-phase sensitivity was smaller than the DAPS-separate sensitivity measured in previous testing. The

most likely explanations for the reduction in sensitivity is crosstalk. Lastly, the in-phase sensitivity did not very significantly when the background illumination level was changed, except when the illumination was high enough that the pixel was in or near saturation.

The goal of the last DAPS experiment was to identify the source of crosstalk in the DAPS-separate design. Testing showed that the parasitic n+ diffusions were collecting photo-generated charge which caused the crosstalk observed in the background subtraction testing. Also, the results suggested that activating the photogate reduces the number of charges that are collected by the parasitic n+ diffusion.

Thus, a DAPS design with good readout circuit sensitivity matching was identified, but crosstalk hampered its background subtraction performance. Collection of charge by the parasitic n+ diffusions was the cause of crosstalk. The results of the DAPS testing will allow further improvements in future DAPS designs.

7.2. Future Work

Recent developments and the results of this thesis have suggested several possibilities for future work for the FTAPS and DAPS. New information on defects that develop in the field has suggested that stuck defects do not commonly occur. Hot pixel defects were found to be most common, thus the behaviour of the FTAPS with a hot defect should be examined. It is possible that the fault tolerant architecture could recovery the pixel output in the presence of a hot defect. If this work is fruitful, the noise analysis of a FTAPS with a hot defect could be explored as well.

For the DAPS, future designs should focus on optimizing the sensitivity matching of the design and reducing crosstalk. The parasitic n+ diffusion areas should be minimized and all of the readout circuit components should be matched, particularly the FD and amp transistor as they affect the circuit's sensitivity the most. Enlarging the FD is also a possible method of reducing the effect of process variations at the cost of sensitivity.

Crosstalk should be reduced by preventing photo-generated charge from being collected by the parasitic n+ diffusion. The parasitic n+ diffusion should be moved away from the photogate and shielding in a lower metal level could be implemented just above the diffusion.

Lastly, background subtraction for the DAPS using multiple exposures should be tested. However, this should done on a new DAPS design which has solved the crosstalk problem.

7.3. Summary

A fault tolerant image sensor and an image sensor with built-in background subtraction have been designed, fabricated, and tested. The FTAPS was found to behave mostly as expected with and without defects. As well, the issues of sensitivity and noise were investigated. For the DAPS, the issues of readout circuit sensitivity matching and crosstalk were examined. Although further work on these sensors is still needed, this thesis has accomplished its objectives and provides a stepping stone for further improvements.

Reference List

[1] Richard Hornsey, *Short Course Notes*, <URL> = "http://www.cs.yorku.ca/~visor/", accessed May 2006.

[2] Camera & Imaging Products Association, [Online Document], <URL> = "http://www.cipa.jp/english/index.html", accessed Aug. 2006.

[3] Karim S. Karim, ENSC 895 Course Notes, <URL> = "http://www.sfu.ca/~kkarim/Karim_1.pdf", accessed Aug. 2006.

[4] Eric R. Fossum, "CMOS Image Sensors: Electronic Camera On A Chip," *International Electron Devices Meeting*, pp. 17-25, 1995.

[5] Gene P. Weckler, "Operation of p-n Junction Photodetectors in a Photon Flux Integrating Mode," *IEEE Journal of Solid-State Circuits*, vol. SC-2, pp. 65-73, 1967.

[6] Rudolph H. Dyck and Gene P. Weckler, "Integrated Arrays of Silicon Photodetectors for Image Sensing," *IEEE Trans. Electron Devices*, vol. ED-15, no. 4, pp. 196-201, 1968.

[7] Peter J. W. Noble, "Self-Scanned Silicon Image Detector Arrays," *IEEE Trans. Electron Devices*, vol. ED-15, no. 4, pp. 202-219, 1968.

[8] Savvas G. Chamberlain, "Photosensitivity and Scanning of Silicon Image Detector Arrays," *IEEE Journal of Solid-State Circuits*, vol. SC-4, no. 6, pp. 333-342, 1969.

[9] Peter W. Fry, Peter J. W. Noble, and Robert J. Rycroft, "Fixed-Pattern Noise in Photomatrices," *IEEE Journal of Solid-State Circuits*, vol. SC-5, no. 5, pp. 250-254, 1970.

[10] Willard S. Boyle and George E. Smith, "Charge Coupled Semiconductor Devices," *Bell Syst. Tech. J.*, vol. 49, pp. 587-593, 1970.

[11] Sunetra K. Mendis, Sabrina E. Kemeny, and Eric R. Fossum, "A 128×128 CMOS Active Pixel Sensor for Highly Integrated Imaging Systems," *IEEE IEDM Tech. Dig.*, pp. 583-586, 1993.

[12] Jozsef Dudas, Linda M. Wu, Cory Jung, Glenn H. Chapman, Zahava Koren, Israel Koren, "Identification of in-field defect development in digital image sensors," *Proc. SPIE*, vol. 6502, 2007.

[13] Glenn Chapman and Yves Audet, "Creating 35 mm Camera Active Pixel Sensors," *Proc. IEEE Intl. Symposium on Defect and Fault Tolerance in VLSI Systems*, pp. 22-30, 1999.

[14] Yves Audet and Glenn H. Chapman, "Design of a Self-Correcting Active Pixel Sensor," *Proc. IEEE Intl. Symposium on Defect and Fault Tolerance in VLSI Systems*, pp. 18-27, 2001.

[15] Israel Koren, Glenn Chapman, and Zahava Koren, "A Self-Correcting Active Pixel Camera," *Proc. IEEE Intl. Symposium on Defect and Fault Tolerance in VLSI Systems*, pp. 56-64, 2000.

[16] Sunjaya Djaja, Glenn H. Chapman, Desmond Y. H. Cheung, and Yves Audet, "Implementation and Testing of Fault-Tolerant Photodiode-based Active Pixel Sensors," *Proc. IEEE Intl. Symposium on Defect and Fault Tolerance in VLSI Systems*, pp. 53-60, 2003.

[17] Desmond Y. H. Cheung, Glenn H. Chapman, Sunjaya Djaja, Yves Audet, Bob Wai, and Cory Jung, "Fault Tolerant Active Pixel Sensors for Large Area Digital Imaging Systems," *Proc. SPIE*, vol. 5356, pp. 142-153, 2004.

[18] Michelle L. La Haye, Glenn H. Chapman, Cory Jung, Desmond Y. H. Cheung, S. Djaja, Benjamin Wang, Gary Liaw, and Yves Audet, "Characteristics of Fault-Tolerant Photodiode and Photogate Active Pixel Sensor (APS)," *Proc. IEEE Intl. Symposium on Defect and Fault Tolerance in VLSI Systems*, pp. 58-66, 2004.

[19] Kalama Salama and Ahmad Al-Yamani, "Analysis of Self-Correcting Active Pixel Sensors," *Proc. SPIE*, vol. 5668, pp. 262-269, 2005.

[20] Hon-Sum Wong, "Technology and Device Scaling Considerations for CMOS Imagers," *IEEE Trans. Electron Devices*, vol. 43, no. 12, pp. 2131-2142, 1996.

[21] Se B. Oh, Kyung-Chan Kim, Soo H. Kim, Yoon K. Kwak, "Resolution enhancement using a diffraction grating for optical triangulation displacement sensor," *Proc. SPIE*, vol. 4285, pp. 102-108, 2001.

[22] Koji Yamamoto, Keiichiro Kagawa, Jun Ohta, Masahiro Nunoshita, "Demonstration of a Frequency-Demodulation CMOS Image Sensor," *Proc. SPIE*, vol. 5017, pp. 24-29, 2003.

[23] S. Burak Gokturk, Hakan Yalcin, Cyrus Bamji, "A Time-of-Flight Depth Sensor – System Description, Issues and Solution," *Proc. IEEE Computer Vision and Pattern Recognition Workshops*, pp. 35-43, 2004.

[24] M. Kawakita, T. Kurita, H. Kikuchi, S. Inoue, "HDTV Axi-Vision Camera," *Proc. of International Broadcasting Convention*, pp. 397-404, 2003.

[25] Desmond Y. H. Cheung, "CMOS Active Pixel Sensor Designs for Fault Tolerance and Background Illumination Subtraction," *MASc thesis*, Simon Fraser University, 2005.

[26] Sunjaya Djaja, "CMOS Active Pixel Sensors That Incorporate Concepts of Fault Tolerance and Active Background Illumination Discrimination," *MASc thesis*, Simon Fraser University, 2007.

[27] Jun Ohta, Koji Yamamoto, Takao Hirai, Keiichiro Kagawa, Masahiro Nunoshita, Masashi Yamada, Yasushi Yamasaki, Shozo Sugishita, Kunihiro Watanabe, "An Image Sensor With an In-Pixel Demodulation Function for Detecting the Intensity of a Modulated Light Signal," *IEEE Trans. Electron Devices*, vol. 50, no. 1, pp. 166-171, 2003.

[28] Koji Yamamoto, Yu Oya, Keiichiro Kagawa, Masahiro Nunoshita, Jun Ohta, and Kunihiro Watanabe, "A 128 × 128 Pixel Complementary Metal Oxide Semiconductor Image Sensor with an Improved Pixel Architecture for Detecting Modulated Light Signals," *Optical Review*, vol. 13, no. 2, pp. 64-68, 2006.

[29] Simon M. Sze, *Physics of Semiconductor Devices*, New York: Wiley, 1981.

[30] Karim S. Karim, *ENSC 895 Course Notes*, <URL> = "http://www.sfu.ca/~kkarim/", accessed Sept. 2006.

[31] Harry Nyquist, "Thermal Agitation of Electric Charge in Conductors," *Physical Review*, vol. 32, pp. 110-113, 1928.

[32] Yap-Peng Tan and Tinku Acharya, "A robust sequential approach for the detection of defective pixel in an image sensor," *IEEE Intl. Conf. Acoustics, Speech and Signal Processing*, vol. 4, pp. 2239-2242, 1999.

[33] B. Jin, Nohpill Park, K. M. George, Minsu Choi, and M. B. Yeary, "Modeling and Analysis of Soft-Test/Repair for CCD-Based Digital X-Ray Systems," *IEEE Trans. Instrumentation and Measurement*, vol. 52, no. 6, pp. 1713-1721, 2003.

[34] Glenn H. Chapman, Israel Koren, Zahava Koren, Jozsef Dudas, Cory Jung, "On-Line Identification of Faults in Fault-Tolerant Imagers," *Proc. IEEE Intl. Symposium on Defect and Fault Tolerance in VLSI Systems*, pp. 149-157, 2005.

[35] Jozsef Dudas, Cory Jung, Glenn H. Chapman, Zahava Koren, Israel Koren, "Robust detection of defects in imaging arrays," *Proc. SPIE*, vol. 6059, 2006.

[36] Cory Jung, Mohammed H. Izadi, Michelle L. La Haye, Glenn H. Chapman, Karim S. Karim, "Noise Analysis of Fault Tolerant Active Pixel Sensors," *Proc. IEEE Intl. Symposium on Defect and Fault Tolerance in VLSI Systems*, pp. 140-148, 2005.

[37] Yavuz Dağerli, Francis Lavernhe, Pierre Magnan, Jean A. Farré, "Analysis and Reduction of Signal Readout Circuitry Temporal Noise in CMOS Image Sensors for Low-Light Levels," *IEEE Trans. on Electron Devices*, vol. 47, no. 5, pp. 949-962, 2000.

[38] Igor Shcherback, Alexander Belenky, Orly Yadid-Pecht, "Empirical dark current modelling for complementary metal oxide semiconductor active pixel sensor," *Optical Engineering*, vol. 41(6), pp. 1216-1219, 2002.

[39] Jozsef Dudas, "Characterization of a Dual-Output Photodiode Active Pixel Sensor," report for ENSC 895 – Electronics for Digital Imaging, Simon Fraser University, 2006.